NEUROMODULATION OF SPINAL AUTONOMIC REGULATION

A Dissertation
Presented to
The Academic Faculty

by

Amanda L. Zimmerman

In Partial Fulfillment
of the Requirements for the Degree
Doctor of Philosophy in the
School of Biomedical Engineering

Georgia Institute of Technology
December 2011

NEUROMODULATION OF SPINAL AUTONOMIC REGULATION

Approved by:

Dr. Shawn Hochman, Advisor
Department of Physiology
Emory University School of Medicine

Dr. Lawrence Schramm
Departments of Biomedical Engineering and Neuroscience
John's Hopkins University

Dr. T. Richard Nichols
School of Applied Physiology
Georgia Institute of Technology

Dr. Minoru Shinohara
School of Applied Physiology
Georgia Institute of Technology

Dr. Keith Tansey
Departments of Physiology and Neurology
Emory University School of Medicine

Date Approved: August 9, 2011

ACKNOWLEDGEMENTS

I would like to thank the many people that have encouraged me throughout this process and helped me reach this point. While I walk away with a new title and diploma, this would not have been possible without the help and support of lab mates, family, and friends.

First and foremost, to my advisor, Shawn Hochman, thank you for welcoming me into the lab despite the differences in our stated scientific goals and helping me develop as a scientist. Thank you for encouraging me to pursue my scientific interests, for fostering my creativity and professional confidence, for encouraging me to keep going, and for all your patience troubleshooting when I was about to give up. Thank you for your patience, your questions, and your motivation in pushing me to strive for the best.

Thanks also to the rest of my lab (past and present) for your help and encouragement. Mike Sawchuk, thank you for your expertise in all things immuno and never-ending eagerness to help troubleshoot. JoAnna, Heather, Jacob, Lisa, and Katie, thank you for brainstorming ideas, troubleshooting matlab and coreldraw, sharing electrode making and surgery techniques, and overall making the Hochman lab a great place to spend the last 6 years.

To my committee, Keith Tansey, Richard Nichols, Minoru Shinohara, and Larry Schramm, thank you for your guidance along the way, for your feedback during this process, and for encouraging me to think about the big picture. Larry, thank you also for letting me pick your brain at countless conferences and your never-ending wealth of knowledge about the autonomic nervous system.

To my family and Atlanta pseudo-family, thank you for your support and encouragement throughout this process. Mom and Dad, thank you for teaching me to question everything, to believe in myself, and for cheering me on every step of the way. Michelle, thank you for teaching me how to explain myself without the scientific jargon, and for all your support. To my Atlanta friends, thanks for putting life in perspective, encouraging me to finish, and overall being such a wonderful support network. Jeff, thank you for your kind words of encouragement, your patience and caring in the past year of crazy traveling, and for not letting me run-away every time I got the urge. I don't know what I would've done without you all!

TABLE OF CONTENTS

Page

LIST OF TABLES

Page

LIST OF FIGURES

Page

LIST OF ABBREVIATIONS

ANS	autonomic nervous system
SNS	sympathetic nervous system
PNS	parasympathetic nervous system
T, L, S	thoracic (T), lumbar (L), and sacral (S) spinal segments
SPNs	sympathetic preganglionic neurons
ILf	pars funicularis
ILp	pars principalis
IC	intercalatus spinalis
ICpe	intercalatus spinalis pars paraependymalis
IML	intermediolateral column
TTX	tetrodotoxin
AHP	afterhyperpolarization
4-AP	4-aminopyridine
TEA	tetraethylammonium
DRG	dorsal root ganglia
PSI	Presynaptic inhibition
GABA	γ-amino-butyric acid
PAD	primary afferent depolarization
DRP	dorsal root potential
NE	norepinephrine, noradrenaline
5HT	Serotonin, 5-hydroxytryptamine

DA	dopamine
MAs	Monoamines
LC	locus coeruleus
NMDA	N-methyl-D-aspartate
EPSPs	excitatory postsynaptic potentials
IPSPs	inhibitory postsynaptic potentials
eGFP	enhanced green fluorescent protein
DIC	differential-interference contrast optics
V_m	membrane potential
τ_m	membrane time constant
L	equivalent cylinder electrotonic length
I-V	Current-voltage
R_{in}	input resistance
C_m	Membrane capacitance
V_{th}	threshold voltage
f-I	frequency-current
PAM	Partition Around Medoids method
V_{rest}	resting potential
I_{peak}	peak inward current
AP	action potential
V_m	membrane potential
PIC	persistent inward current
SFA	spike frequency adaptation

(s)ACSF	(sucrose) artificial cerebrospinal fluid
mM	millimolar
VRP	ventral root potential
EFP	extracellular field potential

SUMMARY

The central nervous system is largely responsible for receiving sensory information from the environment and determining motor output. Yet, centrally-derived behavior and sensation depends on the optimal maintenance of the cells, tissues, and organs that feed and support these functions. Homeostasis, or maintaining a stable internal environment in the face of changing external conditions, is largely obtained through the function of our visceral organs and blood vessels. Most of visceral regulation occurs without conscious oversight, making the spinal cord a key site for integration and control. How the spinal cord modulates output to our organs, or sensory information from them, is poorly understood.

The overall aim of this dissertation was to better understand spinal processing of both visceral sensory information to and sympathetic output from the spinal cord. To do this, I first established and validated a HB9-GFP transgenic mouse model that unambiguously identified sympathetic preganglionic neurons (SPNs), the spinal output neurons for the sympathetic nervous system. Transitioning to the mouse model opens the study of the autonomic nervous system to powerful transgenic technologies currently being developed, allowing characterization of circuit operation in ways that would otherwise be impossible. Using this model, I investigated the electrophysiological similarities and diversity of SPNs, and compared their active and passive membrane properties to those described in other animal models. I hypothesized that SPNs would exhibit similar properties as seen in other species, yet would not be homogeneous in function. My results indicate that while many of the same characteristics are shared, SPNs are a

heterogeneous group that can be differentiated based on their electrophysiological properties.

Since descending monoaminergic pathways have particularly dense projections to areas in the spinal cord that SPNs are found, I next examined the modulatory role that the monoamines have on spinal sympathetic output. While each neuromodulator tested had a unique signature of action, serotonin and norepinephrine appeared to increase the excitability of individual SPNs, while dopamine had more mixed actions. Given the electrophysiological diversity of SPNs determined in aim 1, I sought to characterize the actions of the monoamines on the population of SPNs. Additionally, since many autonomic reflexes are integrated by the spinal cord, I questioned whether these reflexes would be similarly modulated. I therefore developed a novel *in vitro* spinal cord and sympathetic chain preparation, which allowed me to investigate visceral afferent mediated reflexes and their neuromodulation by monoamines, by recording population responses of SPNs and motor neurons in the ventral roots. This preparation exposed a dichotomy of action, where sympathetic and somatic motor output is generally enhanced by the monoamines, but reflexes mediated by visceral input are depressed.

Utilizing the spinal cord and sympathetic chain preparation, I also investigated how the spinal cord modulates visceral sensory information. One of the most powerful means of selectively inhibiting afferent information from reaching the spinal cord is presynaptic inhibition. My results demonstrated that activity in multiple visceral afferents in the splanchnic nerve and sympathetic chain can lead to presynaptic inhibition of afferents. Additionally, I hypothesized that descending monoamine systems would depress synaptic transmission of visceral afferents to the spinal cord, resulting in decreased visceral

reflexes. My results showed that in addition to depressing synaptic transmission to the spinal cord, the monoamines also depress the intrinsic circuitry that generates presynaptic inhibition of related afferents.

Taken together, my results indicate that descending monoaminergic pathways shift the state of the autonomic nervous system. When strongly active, the monoamines act to limit the amount of visceral sensory information reaching the central nervous system and increase sympathetic output, resulting in an uncoupling of output from visceral sensory input and transitioning to a feed-forward, sympathetically dominant control strategy. On the other hand, when descending monoaminergic release is low, the central nervous system becomes more receptive to visceral sensory information and sympathetic tone is decreased, likely resulting in a parasympathetic dominant output state. This combination offers complex modulatory strategies for descending systems.

CHAPTER 1

INTRODUCTION

The central nervous system is largely responsible for receiving sensory information from the environment and determining motor output. Yet, centrally-derived behavior and sensation depends on the optimal maintenance of the cells, tissues, and organs that feed and support these functions. Homeostasis, or maintaining a stable internal environment in the face of changing external conditions, is largely obtained through the function of our visceral organs and blood vessels. This includes digesting and absorbing nutrients (gastrointestinal), exchanging O_2 and CO_2 with the environment (respiratory), waste excretion (kidney, urinary tract), and transporting blood and nutrients throughout the body (cardiovascular) [114]. The spinal cord is a major integration and control center for both output from the central nervous system to the various organs and sensory information from them. Yet, exactly how the spinal cord regulates this bidirectional flow of information is not well understood.

The focus of this dissertation, therefore, is how the spinal cord generates motor output to the viscera and regulates sensory information from them. Below, I begin with an overview of the body's "involuntary" nervous system, the autonomic nervous system. I then present more detailed background on the spinal control of this system, focusing separately on the spinal output to the viscera, input from the viscera to the spinal cord, and their modulation by known descending monoamine systems from the brain. Lastly, I discuss the benefits of shifting to a transgenic mouse model, before concluding with the objective and aims of this thesis.

1.1 ORGANIZATION OF THE AUTONOMIC NERVOUS SYSTEM

The visceral motor system is known as the autonomic nervous system (**ANS**), and is called so because its regulation is largely independent of voluntary control and conscious sensation. There are three major divisions of the ANS: sympathetic, parasympathetic, and the enteric nervous system. The enteric nervous system regulates gastrointestinal function through local motor neurons, sensory neurons, and interneurons with relatively little oversight from the central nervous system. The sympathetic and parasympathetic branches are dependent on activation from the central nervous system, with largely antagonistic actions. The sympathetic nervous system (**SNS**) is most commonly associated with the fight-or-flight reaction to stress, where the body shunts blood to skeletal muscles, increases heart rate, increases sweating, dilates pupils, and shuts down digestion. On the other hand, the parasympathetic nervous system (**PNS**) is better known for enabling the "rest-and-digest" functions under non-stressful conditions, such as maintaining resting heart-rate and metabolism [125].

While the SNS and PNS are not as simply differentiated as described above, both systems work to maintain ongoing homeostatic activity (e.g. heart rate, respiration, and metabolism) and respond to an emergency (e.g. extreme, heat cold, or danger). Each branch exerts opposing actions on multiple target tissues (**Figure 1.1**). The balance of these two systems shifts depending on circumstances: exercise and stress causes the SNS to dominate, while PNS is predominant during relaxing conditions, allowing the body to focus on food breakdown and storage [169]. Yet, some body functions require the cooperation of both branches. Such is the case with micturition, which requires sympathetic activation and parasympathetic inhibition for bladder filling, and

parasympathetic activation and somatic motor neuron inhibition for bladder emptying [125]. Importantly, autonomic circuits have the ability to evoke both target-specific responses (e.g. bladder contraction) well as system-wide activation (e.g. fight-or-flight response).

1.1.1 Efferent Pathways

As opposed to the somatic nervous system, where motor neurons project directly from the spinal cord to skeletal muscles, autonomic efferent pathways are disynaptic. Preganglionic neurons, whose cell bodies lie within the spinal cord or brainstem, synapse onto postganglionic neurons within autonomic ganglia in the periphery. Unlike the innervation of skeletal muscle by somatic nerve fibers, autonomic postganglionic fibers lack both presynaptic specializations and specialized postsynaptic regions; rather, they have highly branched axon terminals with several nerve endings, allowing for diffuse activation. Efferent pathways for both the SNS and PNS are anatomically distinct, with preganglionic neurons exiting different locations of the central nervous system and travelling different distances to their postganglionic targets ([125]; see also **Figure 1.1**). Some end targets, such as vascular smooth muscle and sweat glands, receive only sympathetic innervation.

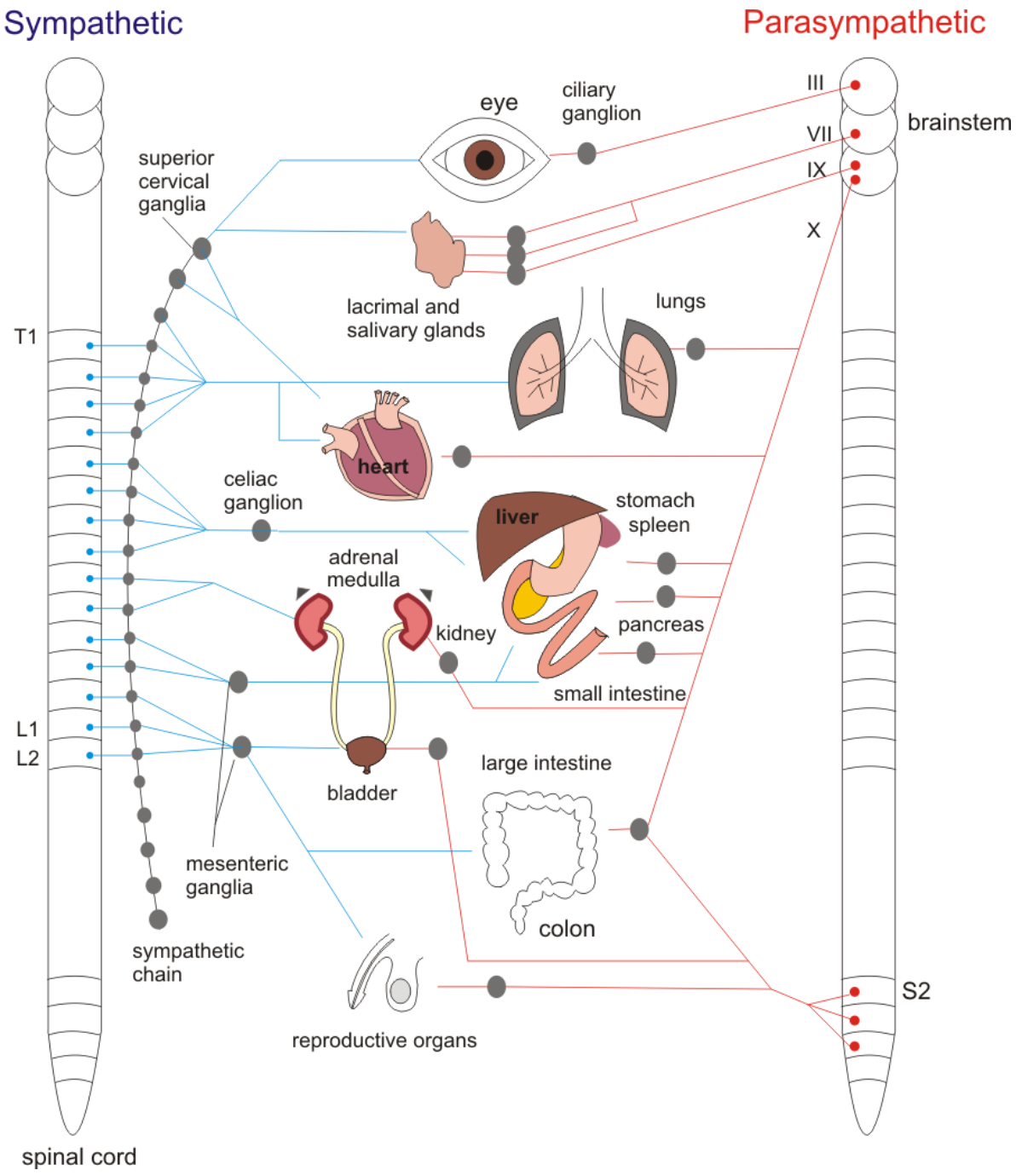

Figure 1.1 General organization of the efferent projections of the autonomic nervous system.

Autonomic efferent pathways synapse in autonomic ganglia before reaching their end targets. Sympathetic preganglionic neurons have cell bodies in the thoracolumbar spinal cord, while parasympathetic preganglionic neurons have cell bodies in the brainstem and sacral spinal cord. Sympathetic ganglia lie close to the spinal cord while parasympathetic ganglia are adjacent to their end targets. Most target organs receive dual sympathetic and parasympathetic innervation. Figure and information based on text and figures in [113, 125, 169]

1.1.1.1 Sympathetic Efferents

Preganglionic neurons of the sympathetic division have cell bodies in the thoracic (**T**) and upper lumbar (**L**) regions of the spinal cord (T1-L2). Most sympathetic preganglionic axons are short, synapsing in autonomic ganglia adjacent to the spinal cord, the paravertebral ganglia. The paravertebral ganglia form a chain, with preganglionic axons often travelling multiple segments rostrally and/or caudally (see **Figure 1.2**). Other preganglionic neurons pass through the sympathetic chain and synapse on postganglionic neurons in more distal, pre-vertebral ganglia (e.g. celiac ganglion and the

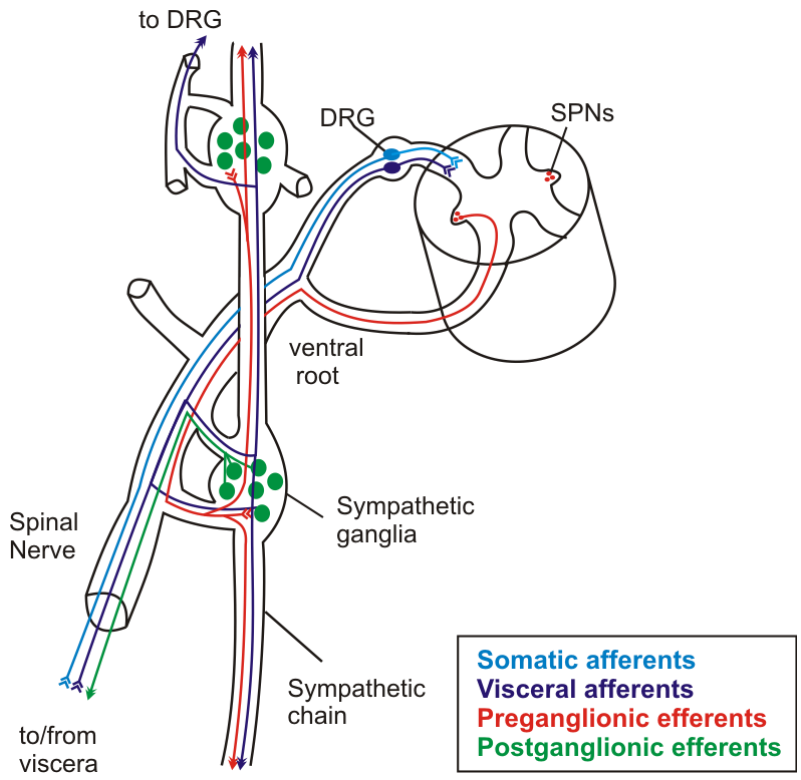

Figure 1.2. Schematic of spinal segmental organization associated with the sympathetic nervous system.

Shown are two segmental ganglia as part of the paravertebral sympathetic chain and their relation to afferent input and efferent output from the spinal cord.

inferior and superior mesenteric ganglia) or on cells in the adrenal medulla.

1.1.1.2 Parasympathetic Efferents

Preganglionic neurons of the PNS have cell bodies in the brainstem (nuclei associated with cranial nerves III, VII, IX, and X) and in the sacral spinal cord (S_2-S_4). In contrast to the SNS, PNS ganglia are much closer (and sometimes in) the target tissue, resulting in longer preganglionic and shorter postganglionic axons. 75% of all parasympathetic fibers lie in the vagus nerve (X), which innervates the thoracic and abdominal viscera (e.g. heart, lungs, stomach, and pancreas). The PNS also has much less divergence than the SNS, with the average preganglionic to postganglionic ratio 1:3 (compared to the average SNS ratio of 1:10), allowing for more targeted tissue stimulation [169].

1.1.2 Visceral Afferent Pathways

Neurons that send sensory information from the visceral organs (e.g. stomach, bladder, colon, and blood vessels) to the central nervous system are called visceral afferent neurons. These afferents are involved in regulation of specific organs, multi-organ reflexes, general neuroendocrine regulation, visceral sensation (including pain), and likely influence emotional feeling [112]. Except in cases of potential organ danger and bladder control, visceral afferent-mediated reflexes are generally not under voluntary control, and are regulated by circuits in the brainstem, hypothalamus, and spinal cord [125]. While an integral part of determining output from the ANS, visceral afferents are not classified as sympathetic or parasympathetic since they are functionally associated with both branches.

Of great clinical concern is the generation of visceral pain. In contrast to somatic pain, which is caused by insult to the tissue and is relatively well localized, visceral pain is not necessarily linked to visceral injury, is difficult to localize, and is often referred to nearby somatic regions [39]. These substantial differences in processing visceral sensory information make it imperative to study visceral pain and afferent modulation specifically, and not make assumptions based on somatic afferent processing.

This dissertation will focus on spinal regulation of the autonomic nervous system. Below I will outline in greater detailed the research completed to date on the following: (1) the sympathetic output neurons from the spinal cord, (2) visceral afferent processing in the spinal cord, and (3) modulation of these by descending monoamine systems.

1.2 Sympathetic Preganglionic Neurons

Within the sympathetic division, the cells responsible for integrating the descending control and sensory input and determining the final central output from the spinal cord are the sympathetic preganglionic neurons (**SPNs**).

1.2.1 Sympathetic Preganglionic Neuron Organization and Anatomy

There are at least 4 populations of SPNs; pars funicularis (**ILf**), pars principalis (**ILp**), intercalatus spinalis (**IC**) and, intercalatus spinalis pars paraependymalis (**ICpe**). The ILp (also known as the intermediolateral column, or **IML**) has the largest number and density of SPNs [194], and within this region SPN somas are found in distinct clusters in each spinal segment, forming a ladder-like distribution symmetric around the central canal [6] (see also **Figure 1.3**). Their dendrites are mainly oriented rostrocaudally within the lateral funiculus and to a lesser extent medially within the grey matter toward the central

autonomic area [220]. While location does not predict their end targets, SPNs are segmentally organized and exhibit a rostrocaudal and mediolateral gradient of projections [77].

1.2.2 Intrinsic Membrane Properties of SPNs.

There are comparatively few studies on SPN intrinsic properties, and all in rat and cat models. Earlier reports suggest SPNs are not intrinsically active, but rather driven by synaptic inputs [197]. However, intrinsic firing and strong electrical interactions have been observed in neonatal rat spinal slices [151] and isolated spinal cord preparations [170]. Spontaneous activity in a subpopulation of SPNs is often rhythmic, and can be induced by monoaminergic application in otherwise quiescent neurons [231, 276].

While there are at least 4 subpopulations of neurons along the mediolateral axis, only those located in the IML have been targeted electrophysiologically [108, 197, 220, 236]. Resting membrane potentials range between -40 and -80 mV and linear current-voltage relations have been reported. Action potentials comprise tetrodotoxin (**TTX**)–sensitive and kinetically-slower Ca^{2+}-sensitive/TTX-insensitive components resulting in a strikingly long spike duration and long afterhyperpolarization (**AHP**). Other *in vitro* conductances observed include: a fast 4-aminopyridine (**4-AP**)-sensitive and slower Ba^{2+}-sensitive outward rectifier (A and D type respectively), and an atypical K^+- mediated sustained outward rectifier with insensitivity to Cs^+ and tetraethylammonium (**TEA**) [180, 270].

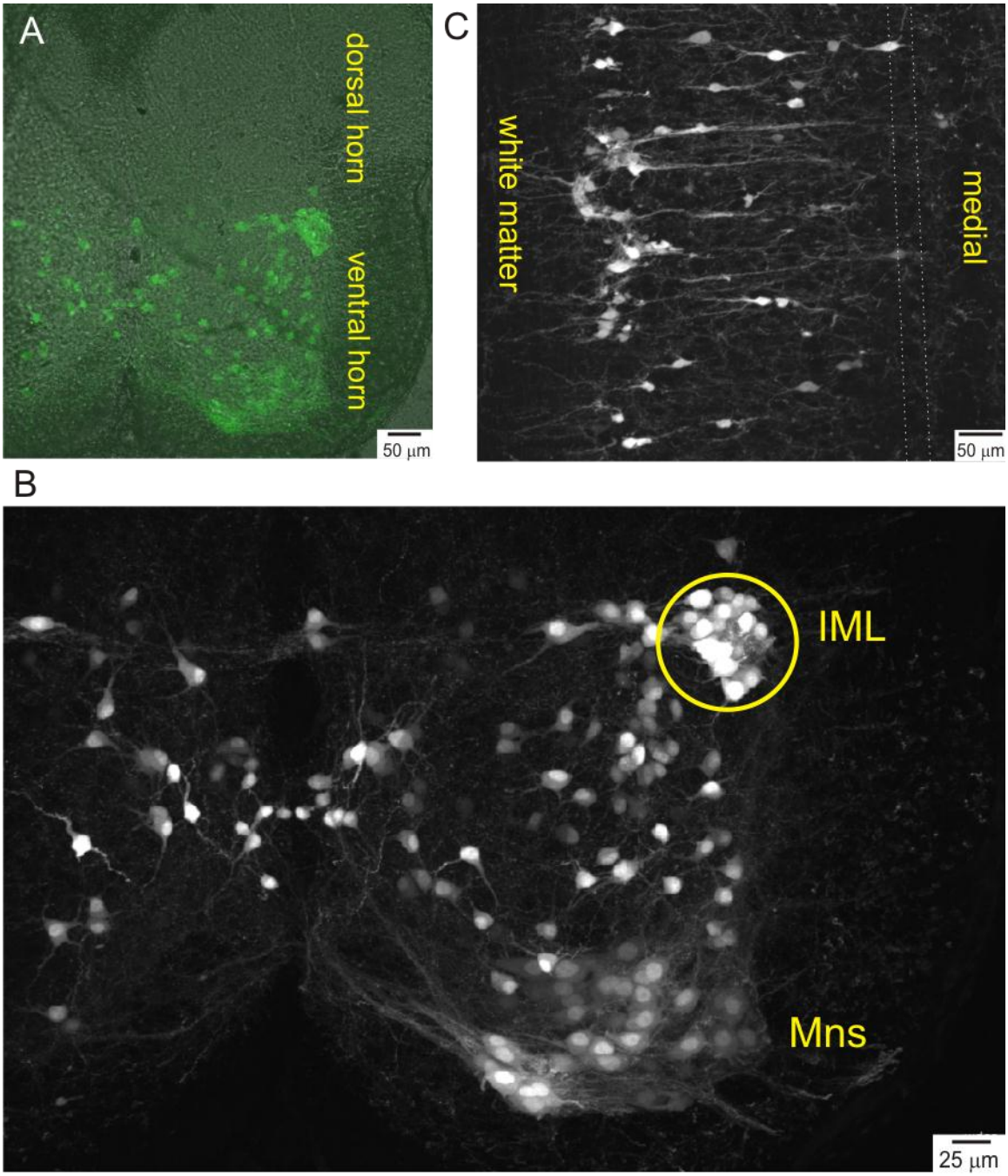

Figure 1.3. Sympathetic preganglionic neuron organization

A. Confocal stacks of HB9-GFP labeling in a thoracic cord transverse section of a p3 mouse, shown as an overlay of spinal cord darkfield images (stack of 70; each slice is 1.3 μm thick, for a total depth of 91 μm shown). Note complete absence of label in dorsal horn. **B**. Same HB9-GFP image as in A in grayscale with dorsal horn omitted. **C**. Horizontal section at central canal level shows SPNs in the IML and additional SPNs and their projection in the mediolateral plane (confocal stack z-stack of 25 sections, each 1.0 μm optical thickness, for a total depth of 25 μm). Dotted line identifies midline region just dorsal to the central canal. Abbreviations are: IML, intermediolateral nucleus; Mns, motor neurons.

Currently, aside from our work, there have been no studies on the functional properties of SPNs in mouse, yet many properties have been conserved across species (including cat, rat, and guinea pig). Due to the versatility of transgenics (see section 1.5), I believe the mouse will quickly become the species of choice to detail membrane properties of SPNs.

1.3 VISCERAL AFFERENTS

The central nervous systems receives sensory information from the internal organs through two paths: the vagus nerve, which projects to the nucleus of the solitary tract and then on to 2nd order neurons in the brainstem and other subcortical regions [112]; and through sympathetic and pelvic parasympathetic nerves, which pass through prevertebral and/or paravertebral ganglia to the thoracolumbar and sacral spinal cord [13, 17, 229]. It is commonly thought that nociceptive signals travel predominantly through the latter path [36], yet little is understood of the spinal processing of visceral afferent signals.

1.3.1 Anatomy and Organization

Apart from afferents of the enteric nervous system (which have their cell bodies in the walls of the gastrointestinal tract and function largely outside the regulation of the CNS), visceral afferents that project to the spinal cord have cells bodies that lie in the dorsal root ganglia (DRG), with distal processes that often travel with the sympathetic nerves (**Figure 1.1**, see also [36, 187]). Spinal projections of visceral afferents are segmentally organized in 'viscerotomes' [112, 187], with the greater splanchnic nerve carrying most of the sensory information from abdominal viscera [134, 188]. Horseradish peroxidase studies of the projections of neurons within this nerve have been investigated in the rat, cat, and guinea pig [37, 38, 188, 247], with consistent results of projections in the spinal cord and the

location of cell bodies in the DRG. Ipsilateral DRG neurons were labeled in many thoracic segments, with the greatest density in the T8-T12 range in the rat [188]. Even with this large rostral-caudal distribution, only about 5-6% of afferents in the cat and about 10% in the rat at those DRG levels are visceral in origin. In contrast, about 80% of the fibers in the cervical vagus nerve are afferent [112].

Visceral afferents also differ from somatic afferents in their spinal projections. Visceral afferents project predominantly to lamina I and V of the dorsal horn, with sparse labeling in the intermediate laminae (III- IV) [37, 188, 247]. A few contralateral branches also follow the border between the dorsal funiculus and grey matter, to reach final destinations in lamina X or the contralateral side [188]. Terminations largely appear to skip lamina II, where most somatic C fibers terminate [246]. Thinly myelinated and unmyelinated Aδ and C-fibers make up the vast majority of visceral afferent fibers [2, 3, 78, 134, 188]. While most somatic C fibers terminate almost exclusively in the superficial dorsal horn in dense terminal plexuses, visceral C fibers have more diffuse projections, with processes extending 2-3 segments in both the rostral and caudal directions in the dorsal funiculus or Lissauer's tract [246-248]. Collateral branches from visceral afferents also transverse lamina II-IV to reach terminal destinations near laminae V and X, sometimes even on the contralateral side.

In summary, while innervation of viscera is much less dense than innervation of skeletal muscle and skin, projections to the spinal cord are much more diffuse in terms of laminar and rostrocaudal termination. This is often hypothesized to be one of the reasons visceral sensations are difficult to localize yet have widespread action [112, 187].

1.3.2 Presynaptic Inhibition

At any time, the spinal cord receives an overabundance of input from afferent and supraspinal sources. One can imagine the need to suppress some of this information to maximize intrinsic processing capabilities. Since the time of Sir John Eccles, it has been noted that presynaptically inhibiting afferent inflow is one of the most powerful forms of inhibition, more powerful than postsynaptic inhibition at blocking information from a variety of afferents, and that this mechanism is widespread throughout the spinal cord [67]. Presynaptic inhibition (**PSI**) is longer lasting than postsynaptic inhibition, lasting for hundreds of milliseconds compared to tens of milliseconds [68]. Additionally, by blocking sensory inflow without influencing the cellular properties of the postsynaptic cell and acting directly on primary afferents, it allows for selective inhibition of particular afferent subclasses or even specific collaterals from the same afferents [69].

PSI of primary afferents is traditionally thought to be mediated by trisynaptic circuitry with last order γ-amino-butyric acid (**GABA**)ergic interneurons [102, 219]. Activation of $GABA_A$ receptors on primary afferent terminals causes an efflux of Cl^- ions, since the chloride gradient in primary afferents is higher inside the neuron than in the extracellular space. This leads to a depolarization of primary afferents (primary afferent depolarization, or **PAD**). A summation of PAD in multiple afferents can be measured by electrodes on the dorsal roots of the spinal cord, as a slow dorsal root potential (**DRP**). This depolarization is thought to prevent action potentials from reaching the afferent terminals or reducing their amplitude (e.g. [67, 68, 263], for review see [219]). A schematic summarizing the mechanisms producing PAD and the resulting DRP is shown in **Figure 1.4**.

PSI can be elicited by afferents of the same origin as well as by functionally distinct afferents. While PAD was elicited in and across subsets of group I and II muscle and cutaneous afferents and has been relatively well characterized (e.g. [27, 28, 121, 213]), PSI in visceral afferents has been explored in much less detail. PSI has been shown in vagal afferents mediating lung stretch, but not vagal afferents involved in blood pressure regulation [212, 217]. More targeted PSI appears to be present on autonomic circuits involved in micturition [9]. Only one group has looked at the occurrence of PAD in non-vagal visceral afferents. Early work by Selzer and Spencer in the anesthetized and acute spinalized cat has demonstrated that PAD can be evoked in response to splanchnic nerve and sympathetic chain stimulation [228]. Unfortunately, no subsequent research has sought to investigate the conditions and extent of PSI, or how descending systems may modulate it. To investigate this, I developed an *in vitro* model for assessing spinal visceral afferent evoked PAD (see Chapter 4 for more detail).

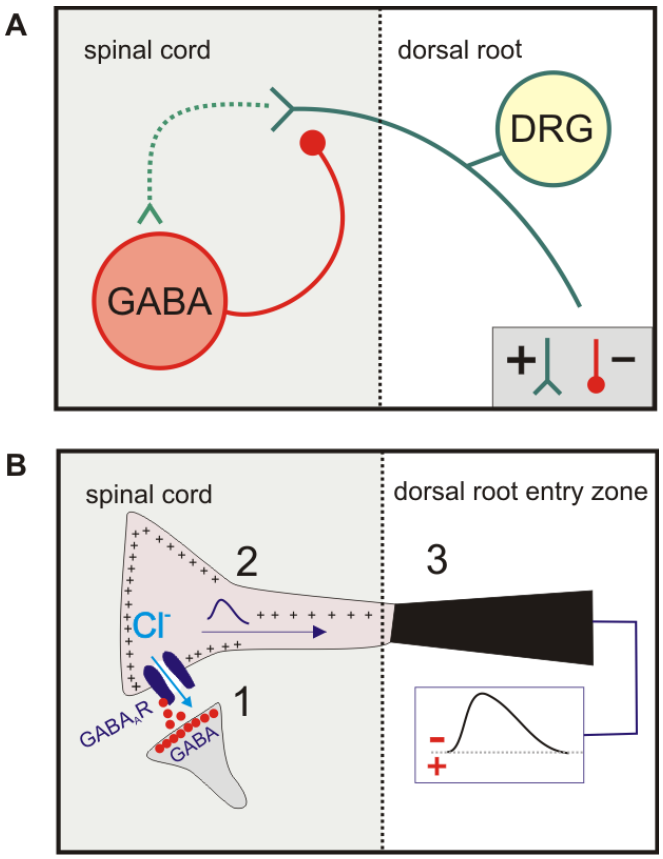

Figure 1.4. Circuitry and proposed mechanisms producing primary afferent presynaptic inhibition via depolarization of their afferent terminals.

A. Simplified schematic and predominant circuitry proposed to produce presynaptic inhibition of primary afferents. It is thought that GABAergic axo-axonic synapses activate postsynaptic $GABA_A$ receptors which leads to a chloride efflux down its concentration gradient and consequent depolarization of primary afferent terminals. **B**. Events leading to recording PAD as a DRP. 1. Afferent stimulation-evoked $GABA_A$ receptor activation. 2. Primary afferent depolarization (PAD). 3. The dorsal root potential (DRP) is the summed back-propagated electrical recording of PAD from a population of axons.

1.3.3 Visceral Reflexes

As described above, autonomic preganglionic neurons synapse in para- and pre-vertebral ganglia on postganglionic neurons, which then innervate the viscera. Individual preganglionic neurons project to many postganglionic neurons (approximately 1:15 ratio in rodents[203] and 1:100 ratio in human [66]), which tend to receive only one or two

strong synaptically connected inputs [172]. Visceral spinal afferents can influence efferent activity by way of both extra-spinal and spinal reflexes.

1.3.3.1 Extraspinal Reflexes

Extraspinal reflexes are mediated by visceral afferent collaterals directly synapsing on postganglionic neurons in prevertebral (such as intestino-intestine reflexes in the inferior mesenteric ganglia [130] or direct connections in the stellate ganglia [208]). Yet no such direct connections have been found in the paravertebral ganglia [114, 117]. These connections are likely mediated by peptidergic synapses [58, 94].

1.3.3.2 Spinal Reflexes

Similar to the somatic nervous system, visceral afferents can evoke a wide variety of reflex responses, both somatic and autonomic in nature. Electrical stimulation of the visceral afferent nerves has been found to cause motor [64, 272], respiratory [4, 181], and cardiovascular responses [1, 33]. Mechanical and chemical stimuli to viscera have also elicited similar results but are less consistent for quantification purposes [187]. Visceral afferents are believed to connect to efferent pathways through disynaptic pathways [32, 260].

1.4 DESCENDING MONOAMINES

The monoaminergic systems of the brainstem and hypothalamus are best described as neuromodulators. That is to say they modulate the general excitability of the systems to which they project. Activation of each is associated with varying degrees of wakefulness and stress. Noradrenergic centers are associated with vigilance and responsiveness, with noradrenaline (**NE**) release lowest during sleep [141] and increased during acute stress [183].

Serotonergic centers are associated with arousal, mood, thermoregulation, sexual behavior [87, 255], and the generation of movement, and serotonin (**5HT**) is released during arousal and stress [40]. Dopaminergic centers are involved in movement initiation, reinforcement, and emotion; dopamine (**DA**) is released during stress, locomotion, and after rewarding behavior [87, 125]. Overall, the monoaminergic systems are state-dependently active.

1.4.1 Descending Monoaminergic Projections to the Spinal Cord

The monoamines (MAs) have profound actions on both sensory and motor spinal circuits, yet there are no known spinal origins. 5HT, NE, and DA all project from supraspinal centers into the spinal cord, with the densest concentration of terminals often in autonomic spinal nuclei [73, 103, 173, 266].

1.4.1.1 Serotonin.

5HT projections to spinal cord arise from nuclei in the pons and medulla, more specifically the nucleus raphe obscurus, nucleus raphe pallidus, and nucleus raphe magnus, with the densest terminations in the IML, ventral horn, dorsal horn lamina I & II, and lamina X [26]. Raphe pallidus and raphe obscurus projections terminate only in the IML and ventral horn [150], while raphe magnus projects predominantly to the dorsal horn [22]. The vast majority of 5HT terminals in the IML end as classical synapses rather than acting by volume transmission [202], yet there is virtually no evidence for direct contact with primary afferent terminals [175]. This anatomical dichotomy between direct 5HT projections to SPNs and indirect projections near primary afferents likely reflects differential effects on autonomic efferents and afferents, respectively.

1.4.1.2 Norepinephrine and Epinephrine.

The spinal cord receives noradrenergic projections from all pontine noradrenergic nuclei, including the locus coeruleus (**LC**), A5 and A7 cell groups [44-46, 73, 82, 266]. These cells project through the dorsolateral and ventral funiculi and terminate throughout the spinal grey matter, with particularly dense projections in the superficial dorsal horn, around motoneurons in the ventral horn, and in the IML and other autonomic regions [44-46, 173, 266]. Projections from the brainstem nuclei appear anatomically distinct, with A5 and A7 nuclei predominantly terminating in the ventral horn and IML while LC axons heavily project to the dorsal horn [82].

Adrenergic projections to the IML originate in the C1 cell group of the ventrolateral medulla. Adrenergic projections to the spinal cord terminate almost exclusively in the IML (and adjacent in the lateral funiculus), around the central canal, and in a thin region connecting these two areas [177, 216]. The concentration of adrenergic terminals is estimated to be much smaller than noradrenergic terminals [73]

1.4.1.3 Dopamine.

Presumed dopaminergic projections to the spinal cord arise in the dorsal hypothalamus and caudal thalamus, exclusively from A11 nucleus in the rat and predominantly the A11 (with some A10 projections) in the mouse [19, 205]. The highest density of DA terminals are found in the IML and around the central canal in the thoracic and upper lumbar cord [148], yet strong DA labeling was seen in all regions of the spinal cord, excluding the substantia gelatinosa [105]. Like 5HT, the vast majority of DA terminals in the IML end as classical synapses. However, in the thoracic dorsal horn, over 75% of the projections did

not [214], supporting actions by volume transmission in this region. This again suggests differential activation of afferents and efferents by DA.

Surprisingly, recent evidence questions the DA-composition of the A11 nucleus. A11 neurons are tyrosine hydroxylase-positive but DOPA-decarboxylase and DA-transporter negative [14], suggesting that these projections are not actually dopaminergic but rather L-DOPAergic. While this needs to be explored further, this pathway and/or spinal dopaminergic receptors are implicated in both anti-nociception [74] and modulation of spinal reflexes [47].

1.4.2 Effects of Monoamines on Sympathetic Preganglionic Neurons

Monoamine projections to the spinal cord often mimic the ladder-like distribution of SPNs [73]. The monoamines have complex modulatory actions on neurons, often based on the receptors activated. They can affect neuronal excitability by both modulating ion channels directly as well as by activating common signal transduction pathways that then modulate voltage- and ligand gated ion channels (monoamine receptor subtypes, their common signal transduction pathways, and potential actions are summarized in **Figure 1.5**). While the monoamines clearly project strongly to the IML, their modulatory actions on SPNs have been subject to debate over the last couple of decades. The following is a summary of their presumed actions.

A

	Gs	Gq	Gi
Transmitter	↑ AC	↑ PLC	↓ AC
Serotonin	$5HT_{4,6,\&7}$	$5HT_{2A-C}$	$5HT_{1A,B,D,E,F}$
Norepinephrine	β_{1-3}	$\alpha_{1A,B,D}$	α_{2A-D}
Dopamine	D_{1-5}		$D_{2,3,4}$

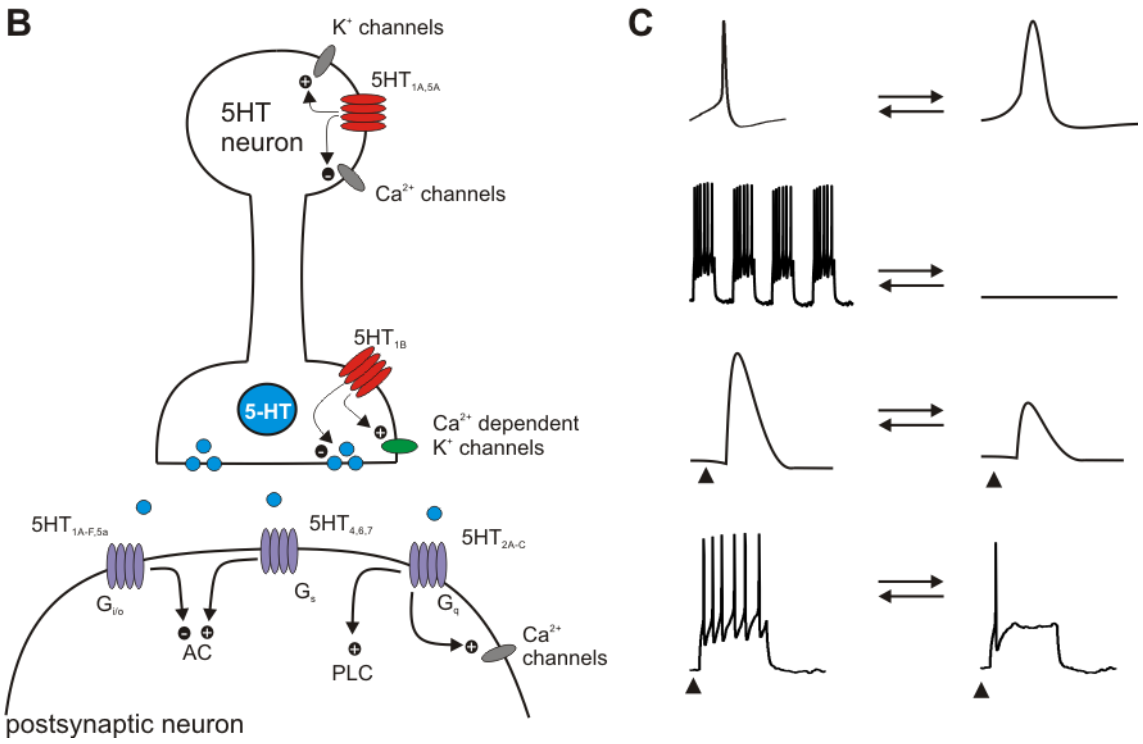

Figure 1.5 Mechanisms of neuromodulation.

A. Table of common signal transduction pathways and monoamine receptor subtypes coupled to them. Note serotonin, norepinephrine, and dopamine all have common actions on adenylyl cyclase (AC) and phospholipase-C (PLC) depending on receptor subtype activated. **B**. Example of potential sites of neuromodulation and receptor subtypes activated, here with a serotonergic neuron. Presynaptic G_i-coupled receptors have been shown to have facilitatory actions on voltage-gated and Ca^{2+}-dependent K^+ channels while inhibiting Ca^{2+} channels and neurotransmitter release. Postsynaptic receptors positively or negatively couple to AC and PLC, as well as to voltage and ligand gated ion channels, resulting in changed properties of the postsynaptic neuron. Not all neurons have all types/locations of receptors. **C.** Examples of neuromodulation: neuromodulators can have actions on (i) action potential shape, (ii) state transitions to include rhythmic activity, (iii) changes in synaptic transmission (excitatory postsynaptic potential evoked by synaptic activation at arrow), and (iv) changes in response to synaptic input (at arrow). Images based on reviews in [62, 124, 176, 178].

1.4.2.1 Serotonin.

Serotonin (5HT) strongly and directly depolarizes the majority of SPNs (90%) in spinal cord slices, presumably by activation of $5HT_2$-like receptors that are localized to the IML region [145]. Similar 5HT actions have been observed in rat *in vivo* and spinal 5HT promotes sympathetic activity in renal, cardiovascular and bladder afferents, also presumably via $5HT_2$ receptor activation [144, 168]. Interestingly, the depolarizations were slow in onset, long lasting (longer than 10 minutes) and often irreversible, suggesting a long term and slow-acting neuromodulatory regulation of SPN function. Methysergide and metergoline ($5HT_{2C}$ and $5HT_{1B/D}$ receptor antagonists) also decreased spontaneous SPN discharge in intact but not spinally transected rats in vivo, suggesting tonic descending serotonergic activation [168]. 5HT has also been shown to induce rhythmicity in SPNs recorded in vitro [198, 199] and to restore tail sympathetic rhythms when delivered intrathecally in the rat [163]. Lastly, 5HT potentiated sympathetic responses to N-methyl-D-aspartate (**NMDA**) in the IML [43].

1.4.2.2 Norepinephrine

NE (norepinephrine) has been more extensively studied, with contrasting responses of SPNs. Superfusion of NE onto spinal cord slices of the adult cat depolarized (30%), hyperpolarized (40%), or had mixed (14%) responses [273, 277, 278]. In the neonatal rat, only depolarizing responses were seen [220]. Similarly, excitatory postsynaptic potentials (**EPSPs**) and inhibitory postsynaptic potentials (**IPSPs**) could be evoked by stimulating the dorsolateral funiculus [220, 277, 278], the presumed descending noradrenergic tract [31]. Both NE and stimulation evoked depolarizations were mediated by α_1 receptors and

associated with a decreased K_{Ca} conductance, while hyperpolarizations were mediated by α_2 receptors and associated with an increased non-Ca^{2+} mediated K^+ conductance [109]. In vivo iontophoretically applied NE inhibited SPN firing in the adult cat and pigeon [53, 95]. NE was also found to suppress the characteristic slow afterhyperpolarization following the action potential and often produced a spike afterdepolarization [274, 275]. Additionally, NE was also able to induce rhythmic oscillations in previously quiescent cells and increase discharges of spontaneously active SPNs [276].

Interestingly, biphasic responses to NE were observed in the adult cat and adrenaline was able to evoke hyperpolarizing responses in the rat [179]. Similarly, eliminating the slow IPSP or EPSP often unmasked the other, suggesting coexistence of both α_1 and α_2 adrenoceptors.

1.4.2.3 Dopamine.

Few studies have examined the actions of DA in the spinal cord. Although dopaminergic neurons from the A11 hypothalamic region project to the IML, little is understood of its modulatory potential in SPNs.

One study examined the effects of exogenously applied DA on unidentified but presumed SPNs in transverse slices. The actions of DA were slow and long-lasting and were inhibitory (46%), excitatory (28%) or mixed (23%). The DA-induced depolarization was reported to be synaptically-mediated via D_2-like actions, and the hyperpolarization directly acting via D_1-like receptor-mediated actions [90]. However, the DA ligands used were at concentrations (up to 100 μM) that make interpretations of receptor selective actions uncertain. Further confounding the issue, *in vivo* microiontophoretic studies

suggest DA actions are inhibitory in the adult cat [53] while excitatory in the adult rat [144]. Similarly, spinal application of DA excited rat renal sympathetic nerve activity [232], yet D_2- like agonists block thermogenesis in response to cold in brown adipose tissue [191].

In summary, given the multiplicity of MA receptors and their differential actions on signal transduction pathways, it is difficult to speculate too strongly on function. Overall, the conflicting reports on whether 5HT, DA, and NE actions are excitatory or inhibitory may be due to differences in spatial location, dose, selectivity of ligands, and experimental condition. Thus, there is a need for more controlled pharmacological and experimental methods to determine the functionally relevant actions of these neuromodulators on SPNs. This dissertation will further investigate and clarify the role of MAs in modulating SPN excitability, and compare actions in the mouse to the species described above.

1.4.3 Monoaminergic Modulation of Visceral Afferents

Not only do the MAs densely project to the IML, they also project more diffusely throughout the dorsal horn (see [148] for DA; [166] for NE; and [26] for 5HT). Preliminary studies suggest all three systems can influence visceral afferents, yet our knowledge of the modulatory actions of these descending systems is rudimentary at best. 5HT activates both peripheral and spinal colonic afferents, at least partially through $5HT_3$ receptors [101]. NE inhibits viscero-motor and pressor responses to colorectal distension, acting via α_2 receptors [55, 186]. Lastly, DA has inhibitory like actions on the spinal pelvic-urethral reflex [271].

Given that spinal visceral afferents are thought to predominantly convey pain information to the CNS, some insight into the actions of descending monoamines may be inferred by what is known about their influence on spinal nociceptive processing. NE generally inhibits nociception acting on presynaptic α_2 receptors on primary afferent terminals [175]. 5HT, acting on $5HT_{1B/D}$ receptors, acts to presynaptically inhibit nociceptive afferents, while $5HT_2$ and $5HT_3$ receptors actions appear to mediate pro-nociceptive actions [16]. Similarly, DA can have both anti-nociceptive and pro-nociceptive actions, acting on $D_{2\text{-like}}$ and $D_{1\text{-like}}$ receptors respectively [175]. However, DA actions may be dose sensitive, with low concentrations leading to anti-nociception and high concentrations leading to pro-nociceptive effects [192].

While the monoamines are traditionally thought to inhibit nociception, more complex neuromodulation is often the case, depending on the site of action and receptor subtype(s) activated.

1.4.3.1 Monoaminergic Modulation of Visceral Afferent Presynaptic Inhibition

While monoaminergic modulation of PAD has been shown in group II muscle afferents [24, 233], and both high and low-threshold cutaneous afferents [75, 129, 206], the modulatory actions of the descending monoamines on presynaptic inhibition in visceral afferents is currently unknown [219]. The second part of this dissertation will therefore address whether or not changes in the body's general state of arousal influences the magnitude of visceral afferent input received by the CNS.

1.5 USE OF TRANSGENIC MOUSE MODELS IN STUDIES ON CNS FUNCTION AND DYSFUNCTION

Given the relative scarcity of studies on spinal autonomic function, the work detailed above was done in various animal models, including cat, rat, and guinea pig. Yet mouse models are rapidly becoming the preferred model for many areas of biology, due to the increasing number of powerful transgenic approaches being developed. Transgenic technologies are particularly well suited to the study of the central nervous system, allowing characterization of circuit operation in ways that were otherwise impossible. This includes expression-based neuron identification, which was used in the present work to unambiguously identify SPNs in the IML.

Recently, several groups have utilized genetic markers to identify and study subpopulations of spinal neurons and initiated an exciting trend towards characterizing the properties of these molecularly-identified neurons, based on their early expression with transcription factors (e.g. [138]). In this case, the homeodomain transcription factor Hb9 is expressed by embryonic motoneurons and SPNs [11, 252, 267]. HB9-GFP mice were generated that demonstrate strong green fluorescent protein (GFP) fluorescence detectable in SPN axons, dendrites, and somas from embryonic day 9.5 to adult [269]. I used this mouse model to visualize SPNs for whole-cell patch clamp recordings (Chapter 3), immunohistochemistry of receptor subtypes present on SPNs (Chapter 3), and identification of SPN axons in the periphery (Chapter 4).

Additional advantages for transgenic mouse models lay in the possibilities ahead for the study of spinal autonomic function. Transgenic and molecular approaches amenable to

studies on spinal autonomic function include: conditional neuronal knockout/silencing of molecularly distinct cell populations [92], optogenetics, [61, 96], and selective retrograde tracing of monosynaptically connected neurons [242]. Together with well-established electrophysiology and neuroanatomical techniques, elegant studies can be undertaken to define functional organization and alterations by disease or injury. Particularly in the case of the autonomic nervous system, these approaches can help more rapidly investigate this understudied area.

1.6 SUMMARY AND GOALS

The autonomic nervous system is thought to function largely without conscious control or sensation. However, our knowledge about the spinal circuits that both control sympathetic output and modulate visceral input is limited. The monoamines, acting as general modulators of spinal excitability, have generally opposing actions on somatic afferent and efferent spinal sites: largely inhibiting afferent activity while increasing the excitability of motor circuits. Yet their actions on autonomic circuits are less known.

Transgenic approaches have revolutionized and hastened our understanding of mammalian CNS circuit function in many areas, and have the ability to similarly increase our knowledge of spinal autonomic function. The first major goal of this thesis, therefore, was to establish the mouse as an animal model for the study of spinal sympathetic function. Using this model system, this dissertation sought to (i) characterize the CNS sympathetic 'final common output' by determining the recruitment properties of spinal SPNs [Chapter 2], (ii) characterize the actions of three prominent monoamine transmitters (5HT, NE, and DA) on SPN excitability [Chapter 3], (iii)

provide an anatomical appraisal of putative receptor subtypes involved in altering SPN excitability using immunohistochemistry [Chapter 3], and (iv) integrate these findings with the studies of monoamine transmitter modulation of visceral afferent inputs by examining actions on primary afferent depolarization (presynaptic inhibition) and visceral afferent-evoked reflexes [Chapter 4]. Through this research and subsequent analysis, I aimed to gain a better understanding of how these descending modulatory systems effect spinal control of the autonomic nervous system as a whole.

SYMPATHETIC PREGANGLIONIC NEURON INTRINSIC PROPERTIES

The work in this chapter is published in the Journal of Neurophysiology in 2010 (103:490-8) and titled: Heterogeneity of membrane properties in sympathetic preganglionic neurons of neonatal mice: evidence of four subpopulations in the intermediolateral nucleus (**doi: 10.1152/jn.00622.2009)**.

2.1 ABSTRACT

Spinal cord sympathetic preganglionic neurons integrate activity from descending and sensory systems to determine the final central output of the sympathetic nervous system. The intermediolateral column has the highest number and density of SPNs and, within this region, SPN somas are found in distinct clusters within thoracic and upper lumbar spinal segments. Whereas SPNs exhibit a rostrocaudal gradient of end-target projections, individual clusters contain SPNs with diverse functional roles. Here we explored diversity in the electrophysiological properties observed in Hb9-eGFP-identified SPNs in the IML of neonatal mice. Overall, mouse SPN intrinsic membrane properties were comparable with those seen in other species. A wide range of values was obtained for all measured properties (up to a 10-fold difference), suggesting that IML neurons are highly differentiated. Using linear regression we found strong correlations between many cellular properties, including input resistance, rheobase, time constant, action potential shape, and degree of spike accommodation. The best predictor of cell function was rheobase, which correlated well with firing frequency-injected current (f-I) slopes as well as other passive and active membrane properties. The range in rheobase suggests that

IML neurons have a recruitment order with stronger synaptic drives required for maximal recruitment. Using cluster analysis, we identified at least four subpopulations of SPNs, including one with a long time constant, low rheobase, and high f-I gain. We thus propose that the IML contains populations of neurons that are differentiable by their membrane properties and hypothesize they represent diverse functional classes.

2.2 INTRODUCTION

Sympathetic preganglionic neurons (**SPNs**) integrate activity from descending and sensory systems to determine the final central output of the sympathetic nervous system. The ILp (also known as the intermediolateral column or nucleus (**IML**)) has the highest number and density of SPNs [194, 210], and within this region SPN somas are found in distinct clusters in each spinal segment. Their dendrites are mainly oriented rostrocaudally within the lateral funiculus and to a lesser extent medially within the grey matter toward the central autonomic area in lamina X, thus forming a ladder-like distribution symmetric around the central canal [7, 220]. SPNs are segmentally organized and exhibit a rostrocaudal gradient of end-target projections, yet individual clusters contain SPNs with diverse functional roles [77].

The cellular physiological properties of SPNs that lie in the IML have been investigated in rats, guinea pigs, and cats to some extent [59, 89, 108, 197, 220, 236], largely using thick transverse (400-500 μm) slices in vitro. Action potentials are notable for long afterhyperpolarizations mediated largely by Ca^{2+} dependent transient- and sustained K^+ conductances. Other conductances observed include: a fast 4-AP-sensitive and slower Ba^{2+}-sensitive transient outward rectifier (A- and D- type respectively), an atypical K^+-

mediated sustained outward rectifier with insensitivity to Cs^+ and TEA, an anomalous inward rectifier, and a low-voltage activated T-type Ca^{2+} conductance [180, 220, 270]. While IML SPNs are traditionally treated as a homogenous group, there are some notable electrophysiological differences. Spontaneous activity has been observed in a subset of SPNs in the neonatal rat and adult guinea pig, and is sometimes rhythmic [235]. Additionally, strong electrical interactions have been observed in a subpopulation of SPNs, resulting in a low input resistance in these neurons [151]. Lastly, a number of investigators report mixed actions of the monoamines on SPNs [89, 90, 273, 277, 278], suggesting different populations may have different receptor configurations.

Recently, an enhanced green fluorescent protein (**eGFP**) labeled transgenic mouse (JAX laboratories) has been generated that identifies SPNs based on coupled expression to the HB9 homeodomain protein [269], greatly facilitating ease of identification for electrophysiological and histochemical analyses (see Figure 2.1). The current study represents the first characterization of membrane properties of SPNs in this mouse model, and provides the first detailed appraisal of SPN repetitive firing properties. Lastly, we propose a novel classification scheme to differentiate SPN populations based on their electrophysiological properties.

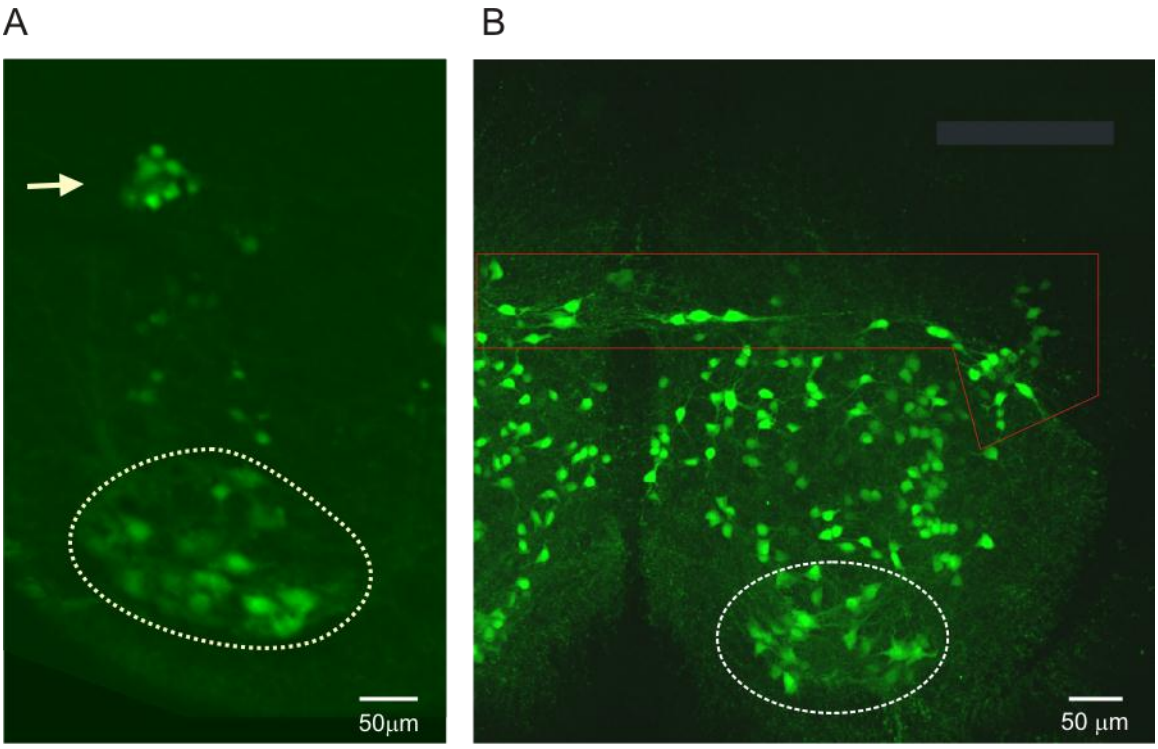

Figure 2.1 HB9-GFP fluorescence in transverse slice permits selective targeting of SPNs in the IML.

A. Typical transverse slice showing GFP+ SPNs in the IML (arrow) as well as additional neurons including motoneurons (circled). B. A similar transverse section of a 250 μm slice that was subsequently immersed in fixative and mounted on a slide for confocal z-stack of 32 images (1.33 mm optical section thickness, or 42.56 mm total section thickness) imaging of overall distribution of GFP+ neurons and morphological integrity. Note the abundance of SPNs in autonomic regions compared to motoneurons in the ventral horn. Additionally labeled neurons may be HB9 interneurons or ectopic GFP expression [54, 269] or additional SPNs whose identity would require retrograde labeling for verification.

2.3 Materials and Methods

All procedures described here comply with the principles of The Care and Use of Animals outlined by the American Physiological Society and were approved by the Emory University Institutional Animal Care and Use Committee.

2.3.1 Electrophysiology and Slice Preparation

All experiments were performed in transgenic mice expressing HB9-eGFP (JAX laboratories; known to label SPNs), postnatal day 3-9. Animals over age p6 were anesthetized with 10% urethane (2mg/kg ip) and placed on ice to slow the heart rate. All animals were decapitated, eviscerated, and the spinal cords removed. The T8-L2 section of the spinal cord was isolated and sliced into thick transverse (400μm) and thin horizontal (200 μm) sections using a vibrating blade microtome (Leica VT1000 S). Initial removal of the spinal cord and slicing were performed in cooled (4 °C), oxygenated (95% O_2, 5% CO_2) solution containing (in mM) 250 sucrose, 2.5 KCl, 2 $CaCl_2$, 1 $MgCl_2$, 25 glucose, 1.25 NaH_2PO_4, and 26 $NaHCO_3$, pH 7.4. Slices were left to recover for at least 1 hour.

The recording chamber was continuously perfused with oxygenated King's ACSF (in mM: 128 NaCl, 1.9 KCl, 2.4 $CaCl_2$, 1.3 $MgSO_4$, 10 D-glucose, 1.2 KH_2PO_4, and 26 $NaHCO_3$; pH 7.4) at a rate of ~2ml/ minute. Patch clamp recordings were made from fluorescently-identified SPNs with patch pipettes of resistance 4-8 MΩ. The standard intracellular recording solution contained (in mM): 140 K-gluconate; 11 EGTA; 10 HEPES; 1 $CaCl_2$, 35 KOH, 4 Mg-ATP; 1 tris-GTP; pH, 7.3. GTP and ATP were included in pipettes to prevent rundown of evoked currents. When assessing the effects of intracellular Cs^+, the intracellular solutions contained 140 CsF, 11 EGTA, 35 KOH, 10 HEPES, 1 $CaCl_2$, pH 7.3.

Whole cell patch-clamp recordings were undertaken at room temperature using the Multiclamp amplifier (Molecular Devices, Sunnyvale, CA). $eGFP^+$ SPNs were identified

in the intermediolateral column using epifluorescent illumination (Figure 2.1) with cell location further verified with differential-interference contrast optics (**DIC**). Voltage- and current-clamp data were acquired on the computer using pClamp 10 acquisition software (Molecular Devices).

2.3.2 Quantification of Membrane Properties

Immediately after rupture of the cell membrane (in voltage clamp at –90 mV), the current-clamp recording configuration was used to determine resting membrane potential. Junction potential was corrected for after recording, experimentally derived previously to be 10mV [158]. In current clamp configuration, electrode resistance was compensated for, and ranged from 8-15 MΩ. Unless otherwise noted, cells were brought to -70 mV membrane potential ($\mathbf{V_m}$) by injecting bias current, and a series of hyperpolarizing and depolarizing current steps 1 second in duration were applied. The membrane time constant ($\boldsymbol{\tau_m}$) was found by fitting the first 500ms of the membrane charging response to small hyperpolarizing current steps with one or two exponentials. In cases where the data was better fit with two exponentials, the longest exponential was used as τ_m as suggested by Rall [209] and previously calculated in SPNs [197, 270]. Additionally in these cases, the equivalent cylinder electrotonic length (**L**) was estimated using the formula: $L = \pi (\tau_0/\tau_1 - 1)^{-1/2}$, where τ_0 is τ_m and τ_1 refers to the first equalizing time constant [209]. τ_m was averaged for hyperpolarizing current steps causing a change in membrane potential less than 20mV. Current-voltage (**I-V**) plots were generated from voltage clamp recordings. Electrode series resistance was uncompensated in voltage clamp recordings but was subtracted in current clamp recordings. Series resistance values ranged between 15-38 MΩ. As these values are one to two orders of magnitude less that measured membrane

resistance, the uncompensated voltage drop across the electrode should not introduce significant error. In voltage clamp, cells were held at -90 mV and a series of voltage steps (-140 mV to 0 mV, 500 ms duration) were applied. The input resistance ($\mathbf{R_{in}}$) was calculated by fitting a portion of the steady state I-V curve slightly negative to resting membrane potential (-70 to -90mV) with a straight line. Membrane capacitance ($\mathbf{C_m}$) was determined from Multiclamp Commander automatically, by fitting the capacitive transient to a brief 10mV voltage step and using the formula: $\tau_m = R_{in} \times C_m$. Peak inward current was measured as the maximal transient inward current obtained following voltage steps.

Active properties were averaged for all spikes at the lowest spike triggering current step. The threshold voltage ($\mathbf{V_{th}}$) was determined by detecting the maximum 2nd derivative in phase space (dVm/dt versus V_m) for each spike [226]. The spike amplitude and afterhyperpolarization (**AHP**) magnitude was taken from this voltage threshold, and the spike overshoot calculated as the portion of the spike above zero mV. Duration of the action potential was measured as the time above one-third of the amplitude [270]. Duration of the AHP was measured as the time below one-tenth of the AHP magnitude. Rheobase was the minimum current injection required to elicit a spike. For frequency-current (***f*-I**) analyses, both mean frequency and instantaneous frequency (based on the interspike interval between the first two spikes) were found. Data from neurons not showing electrode compensation in current clamp were discarded.

2.3.3 Statistical Analysis

All parameter values are reported as mean ± S.D. Matlab software was used to compute correlation coefficients between membrane properties, and to determine p-values for each correlation. Unless otherwise noted, only those with $p<0.05$ were used. For some parameters with statistically significant correlations, linear regression with a least-squares fit was computed for either a straight line, $y=mx+b$, or logarithmic line, $y=bm^x$.

Cluster analysis was performed using a Partition Around Medoids (**PAM**) method [128] from Libra: a MATLAB Library for Robust Analysis. In short, the PAM method minimizes the sum of dissimilarities between data points, to partition data into k clusters. This algorithm was run on k=2-10 clusters, with each parameter normalized and centered. Both the Calinski-Harabasz [34] and Silhouette [128] indices were calculated for each cluster number, each giving a weighted comparison between intra- and inter-cluster differences. These indices were maximized to determine the optimal number of data clusters.

2.4 RESULTS

2.4.1 General Membrane Properties

No significant difference in membrane properties was seen between thin horizontal and thick transverse slices, therefore the data were combined. Data were obtained from 39 neurons and membrane properties quantified as described in the methods section. Their properties are summarized in Table 1. The mean resting potential ($\mathbf{V_{rest}}$) was -60 ± 7 mV, ranging between -44 and -85 mV. The input resistance (R_{in}) was 1.1 ± 0.6 GΩ, ranging from 260 MΩ to 2.6 GΩ with an approximately normal distribution but with a greater spread in high resistance values (not shown). The mean membrane time constant (τ_m) was 92 ± 44ms, ranging between 36 to 184 ms, with an apparent bimodal distribution (not shown). Frequently, voltage responses to large current pulses were well fit with single exponentials, yet smaller current steps were better fit with double exponentials, also seen in the neonatal rat [197]. For those charging curves where double exponential fits were easily distinguished, electrotonic length L was estimated to be 1.83 ± 0.27 (n=17). R_{in} correlated well with both τ_m (ρ= 0.65, p=0.001) and C_m (ρ= -0.50, p= 0.01) indicating that variations in both membrane resistivity and cell size account for much of the range of resistances seen.

The relationships among and between active and passive membrane properties were quantified (**Figure 2.2**). A color-coded correlation matrix compared significance of correlations among the membrane properties measured. The best predictor of cell function was rheobase, which accounted for 10.5% of the variance seen. Rheobase was positively correlated with threshold voltage (V_{th}), negatively correlated with R_{in}, τ_m, and

peak inward current (**I_{peak}**), and weakly negatively correlated with both mean and instantaneous firing frequency – injected current (*f*-I) slopes, which fell just shy of statistical significance (ρ=-0.33, p=0.08 for both). The early peak inward current (presumably Na^+ dominated) contributed greatly to the cell's active properties, as I_{peak} was inversely correlated to both V_{th} and rheobase. Additionally, action potential (**AP**) height was inversely correlated to AP width and directly correlated to V_{th}, further highlighting the important role of Na^+ channel kinetics in SPN behavior. Lastly, the pronounced AHP magnitude was directly correlated to both mean and instantaneous *f*-I slopes, suggesting a strong modulatory role of the underlying currents on SPN excitability.

While not shown in the figure, age of mouse used was also a factor, showing a strong positive correlation with I_{peak} (ρ=0.73, p=$3e^{-5}$), a weaker positive correlation with AHP magnitude (ρ=0.43, p=0.05), and a negative correlation with τ_m (ρ=–0.40, p=0.03). This would suggest that as the mouse ages, the density of voltage gated Na^+ and K^+ channels

Table 2.1: Summary of membrane properties

Property	mean	±	S.D.	*n*
Resting membrane potential (mV)	-59.8	±	7.4	38
Input resistance (GΩ)	1.14	±	0.60	38
Time constant (ms)	92.4	±	43.7	30
Capacitance (pF)	32.8	±	14.1	25
Action potential amplitude (mV)	57.1	±	8.9	30
Action potential overshoot (mV)	11.8	±	9.6	30
Action potential duration (ms)	6.3	±	1.4	30
Threshold voltage (mV)	-45.3	±	5.8	30
Rheobase (pA)	32.7	±	21.4	30
Afterhyperpolarization magnitude (mV)	15.2	±	3.6	30
Afterhyperpolarization duration (ms)	253.3	±	124.5	23

increases and membrane resistivity decreases, a pattern supported by motoneuron research [190, 261].

2.4.2 Anomalous Inward Rectification

We next examined evidence of voltage-gated channels observed in these neurons compared to those reported previously in guinea pig and rat. In current clamp mode, a number of SPNs exhibited an inward rectification or a fall in input resistance in response to larger hyperpolarizing current steps. This rectification was further explored and quantified in voltage clamp. In response to 500 ms voltage steps (-130 to 0 mV, 10 mV steps), 24/38 SPNs (63%) exhibited an increased conductance (mean change 492 pS) at membrane potentials less than -80mV (**Figure 2.3B**). This conductance was instantaneous and sustained, and consistent with that seen in the neonatal rat [270].

2.4.3 Transient Outward Rectification

As seen in the guinea pig and rat [108, 180, 270], all neurons displayed a transient outward rectification. This could be seen in current clamp as either a delayed return to resting membrane potential from hyperpolarizing current steps (10-40pA, 1 s duration; **Figure 2.3Ai**), or as a delay in time to fire the first action potential with depolarizing current steps from a hyperpolarized membrane potential of -90 mV (Fig 2Aii). This was further investigated in voltage clamp configuration, where voltage steps (500 ms, 10 mV steps) were applied from a hyperpolarized holding potential (-90 mV). An outward transient current was observed with mean onset of -50.0 ± 6.7 mV, and always with a lower threshold than the sodium spike (**Figure 2.3B**). Decay was best fit by double exponentials, with the longest tau at onset of 160 ± 52 ms (**Figure 2.3C**). At least a

portion of this transient outward current noticeably persisted when Cs^+ replaced K^+ in the intracellular solution (n=6; inset **Fig 2.3B**).

2.4.4 Repetitive Firing

In current clamp from a -70mV holding potential, 90% (39/43) of SPNs fired repetitively over a wide range of current injections, with the remaining 4 displaying an initial burst or single spike phenotype. Frequency-current (*f*-I) relationships were measured for both instantaneous and mean firing frequency at each current step. SPN *f*-I instantaneous slopes had a mean value of 0.228 ± 0.125 Hz/pA with lower values for mean *f*-I slope (0.196 ± 0.106 Hz/pA). Peak firing frequencies in individual neurons reached up to 28 Hz before depolarization block occurred.

Of SPNs firing repetitively, 70% (21/30) displayed spike frequency adaptation (**SFA**), or a slowing of the firing rate with long current steps (**Figure 2.4A**). SFA was best fit by a logarithmic linear regression (**Figure 2.4B**) and only cells with established SFA are shown (fits significantly different from no correlation, $p<0.05$). The averaged slope (m) of the logarithmic fit at each current step had a mean value of 0.95 ± .02. This slope was inversely correlated with input resistance, i.e. the greater R_{in}, the more rapidly spike frequency declined (**Figure 2.4C**).

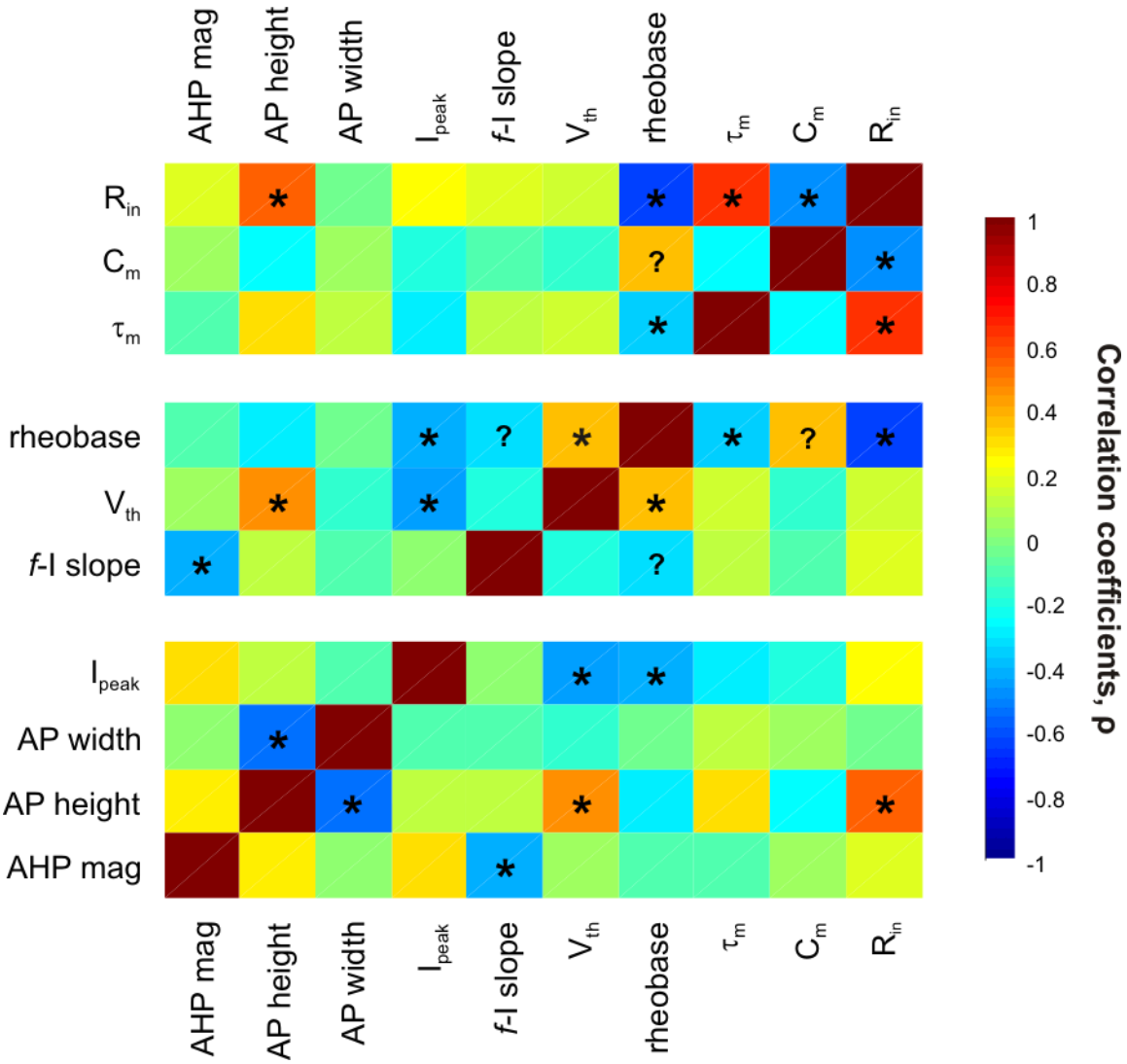

Figure 2.2 Membrane property correlations.

Figure shows correlation coefficients between membrane properties, with values close to 1 showing strong positive relationships and values close to -1 showing strong negative relationships. The firing frequency–injected current (*f*–I) slope refers to instantaneous firing frequency. Asterisks (*) denote statistically significant correlations ($P < 0.05$) and "?" denotes correlations with $0.05 < P < 0.1$.

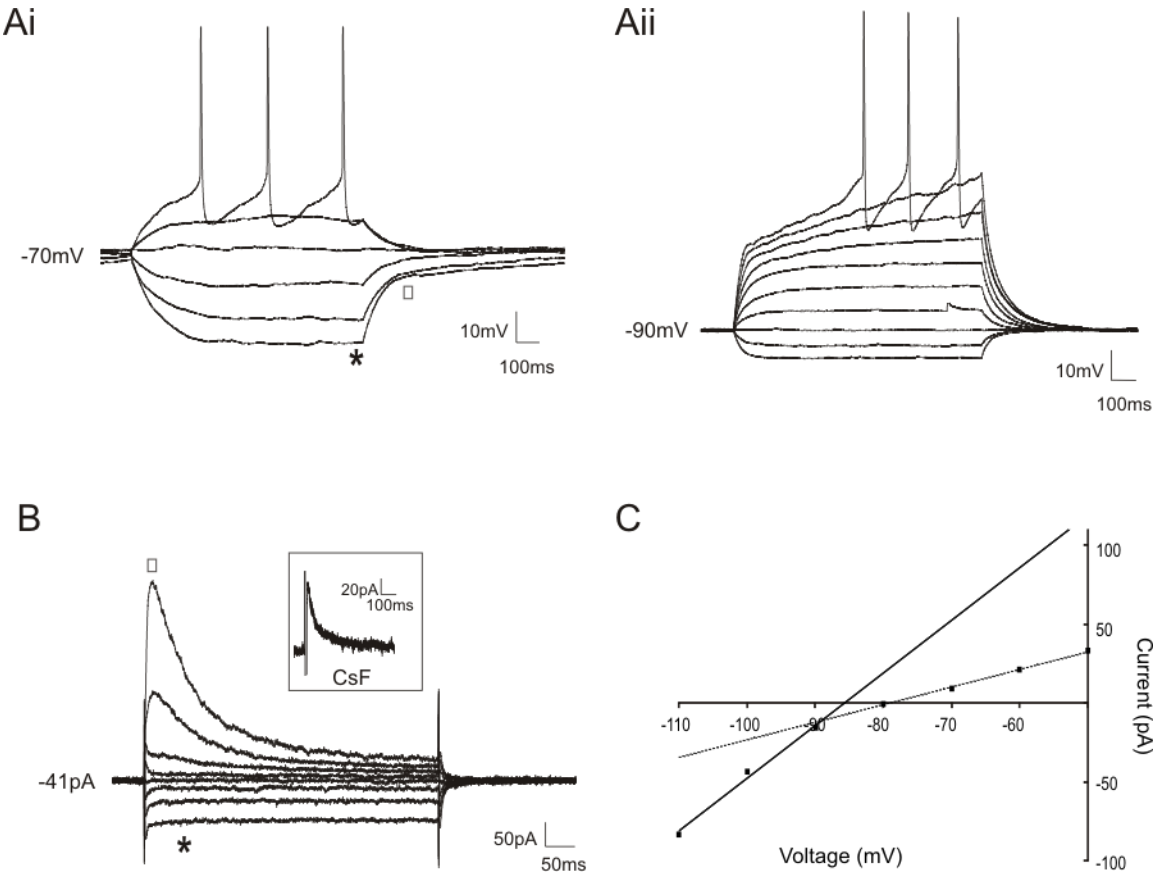

Figure 2.3 Transient outward and anomalous rectification.

Ai. sample membrane response to a series of current steps (1 s duration, 15 to 10 pA, 5-pA steps), holding current 12.6 pA. Asterisk (*) indicates anomalous inward rectification;□ indicates transient outward rectification, seen as a much longer repolarization time to hyperpolarizing current steps. **Aii**. Sample voltage response to a series of injected current pulses (1 s duration,10-pA steps) from a hyperpolarized holding potential. Note delay to first spike, due to transient outward conductance. **B**. Sample current response to a series of voltage-clamp steps (30 to 40 mV, 10-mVsteps) from a hyperpolarized holding potential of 90 mV. Asterisk (*) indicates instantaneous increased conductance at hyperpolarized membrane potentials; □ indicates transient outward conductance, here activated at 70 mV and more pronounced at 60 and 50 mV. Next voltage step (40 mV) produced an inward action current (not shown). Inset shows sample current response of a different cell to a 50 mV voltage step, when Cs replaced intracellular K. Note the presence of the transient outward conductance. **C.** Sample current–voltage plot of steady-state currents obtained during voltage-clamp recordings, revealing inward rectification at potentials less than about 80 mV.

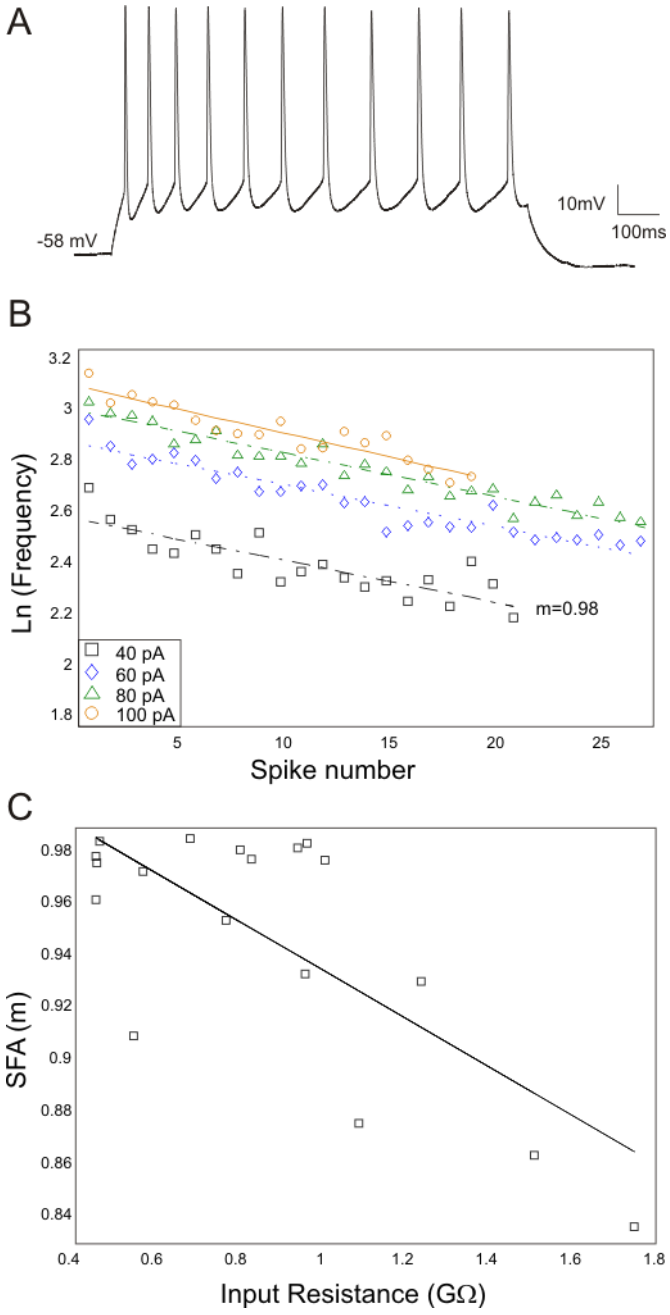

Figure 2.4. Repetitive firing properties.

A. Sample response to 20-pA current injection (1-s duration). Note the slowing of the firing rate with each spike. **B.** Frequency response of a typical sympathetic preganglionic neuron (SPN) showing spike-frequency adaptation (SFA) to multiple current injections, logarithmic scale. *m* was the natural log of the slopes of the lines shown. **C.** Correlation between input resistance (R_{in}) and SFA slope *m*, averaged for each cell. Only cells with statistically significant SFA are shown.

2.4.5 Persistent Inward Current

When intracellular K^+ was replaced with Cs^+ to block most voltage-gated K^+ conductances, the steady state current-voltage plot revealed a region of negative slope conductance (**Figure 2.5A**). This negative slope region indicates the presence of a persistent inward current (**PIC**) [99]. Net inwards currents were absent in several neurons at least partly due to the presence of an outward leak conductance, but could be easily calculated as a deviation from linear leak slope (see **Figure 2.5B**). The persistent inward current in the presence of Cs^+ had an average onset of -76 ± 5 mV and peak magnitude 21.6 ±13.5 pA (n=8). In comparison, with K-gluconate intracellular solution, the effects of the PIC were largely hidden by the dominating contribution of activated outward currents during voltage steps, but could be detected during a slow voltage ramp (8mV/s), as a slight deviation from the linear leak slope (**Figure 2.5C**, n=2/2).

2.4.6 Cluster Analysis

Given the wide range of membrane properties recorded, we wondered whether SPNs could be classified into electrophysiological clusters. Using cluster analysis of the parameters measured for each cell and the maximum of the silhouette and Calinski-Harabasz indices, data was best sorted into four clusters (**Figure 2.6A**). A one-way ANOVA was performed on each parameter, resulting in statistically significant differences between clusters in τ, rheobase, *f*-I slopes, AP width, and I_{peak} (**Figure 2.6B**). The mean values are summarized in Table 2. The four groups are as follows: Group 2 and 3 SPNs are recruited first (have lower rheobases), have relatively long τ_ms and mid-range I_{peak} values. Group 2 neurons have lower *f*-I gains and longer AP durations, while Group

3 SPNs have higher *f*-I gains and shorter AP durations. Group 1 and 4 SPNs are then sequentially recruited, with group 1 SPNs having the largest and group 4 having the smallest I_{peak} values of all groups.

Table 2.2 Comparison of statistically significant parameter differences between clusters

Group	τ_m (ms)	Rheobase (pA)	*f*-I slope (Hz/pA)
1	56.7 ± 23.1[3]	36.3 ± 13.8[3,4]	0.15 ± 0.07[3]
2	112.9 ± 53.1	20.0 ± 0.0[4]	0.17 ± 0.03[3]
3	115.5 ± 43.8[1]	17.9 ± 8.5[1]	0.36 ± 0.13[1,2,4]
4	83.1 ± 28.2	63.3 ± 23.4[1,2]	0.19 ± 0.08[3]

Group	I_{peak} (pA)	AP width (ms)	n
1	2157.8 ± 270.3[2,3,4]	5.3 ± 0.7[2]	8
2	1553.9 ± 363.4[1,4]	8.1 ± 1.6[3,1]	6
3	1608.0 ± 473.7[1,4]	5.9 ± 1[2]	9
4	837.3 ± 426.8[1,2,3]	6.7 ± 0.6	6

Note: superscripted numbers indicate statistically significant differences ($p<0.05$) from group noted.

2.4.7 Properties in Juvenile Mice

In order to understand some of the physiological developmental changes, 7 SPNs were recorded from 3 juvenile mice, postnatal day 21-28. Juvenile SPN recordings showed the anomalous rectification and transient outward currents described above for neonatal mice. Juvenile SPNs exhibited shorter action potentials (3.6 ± 0.5 ms in juvenile versus 6.3 ± 1.4 ms in the neonate, $p=5e^{-5}$), larger spike overshoots (44.5 ± 14.6 mV in juvenile versus 21.9 ± 8.9 mV in the neonate, $p=0.04$) , and larger peak inward currents (4.2 ± 1.7 nA in juvenile versus 1.6 ± .6 nA in the neonate, $p=0.02$; **Figure 2.7A**). Juveniles also had larger steady-state inward and outward currents during voltage clamp. (**Figure 2.7B**).

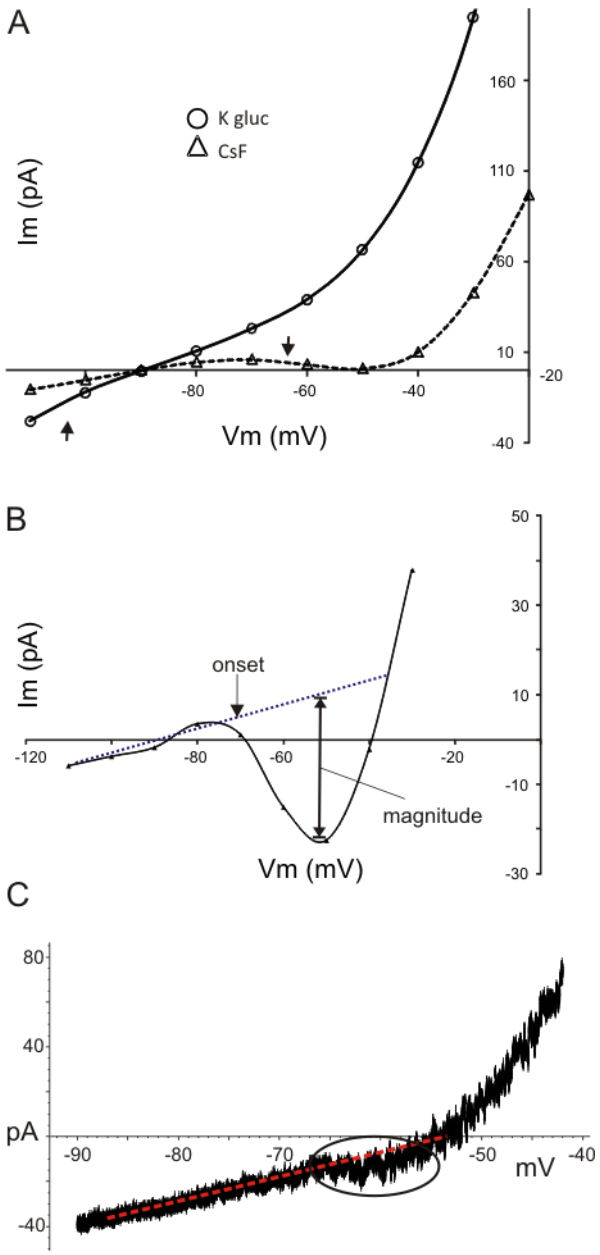

Figure 2.5 Persistent inward currents (PICs).

A: average steady-state current response to a series of 500-ms voltage steps with a CsF- and K-gluconate–based intracellular solution. Arrows denote the absence of anomalous rectifier and onset of negative slope conductance in CsF. B: sample neuron with a PIC resulting in negative conductance value, CsF-based intracellular solution. Arrows denote PIC onset and peak magnitude. C: PICs were largely masked by K conductances in K-gluconate– containing patch electrodes, but could be seen as small deviations from linear conductance during a slow voltage ramp (8 mV/s).

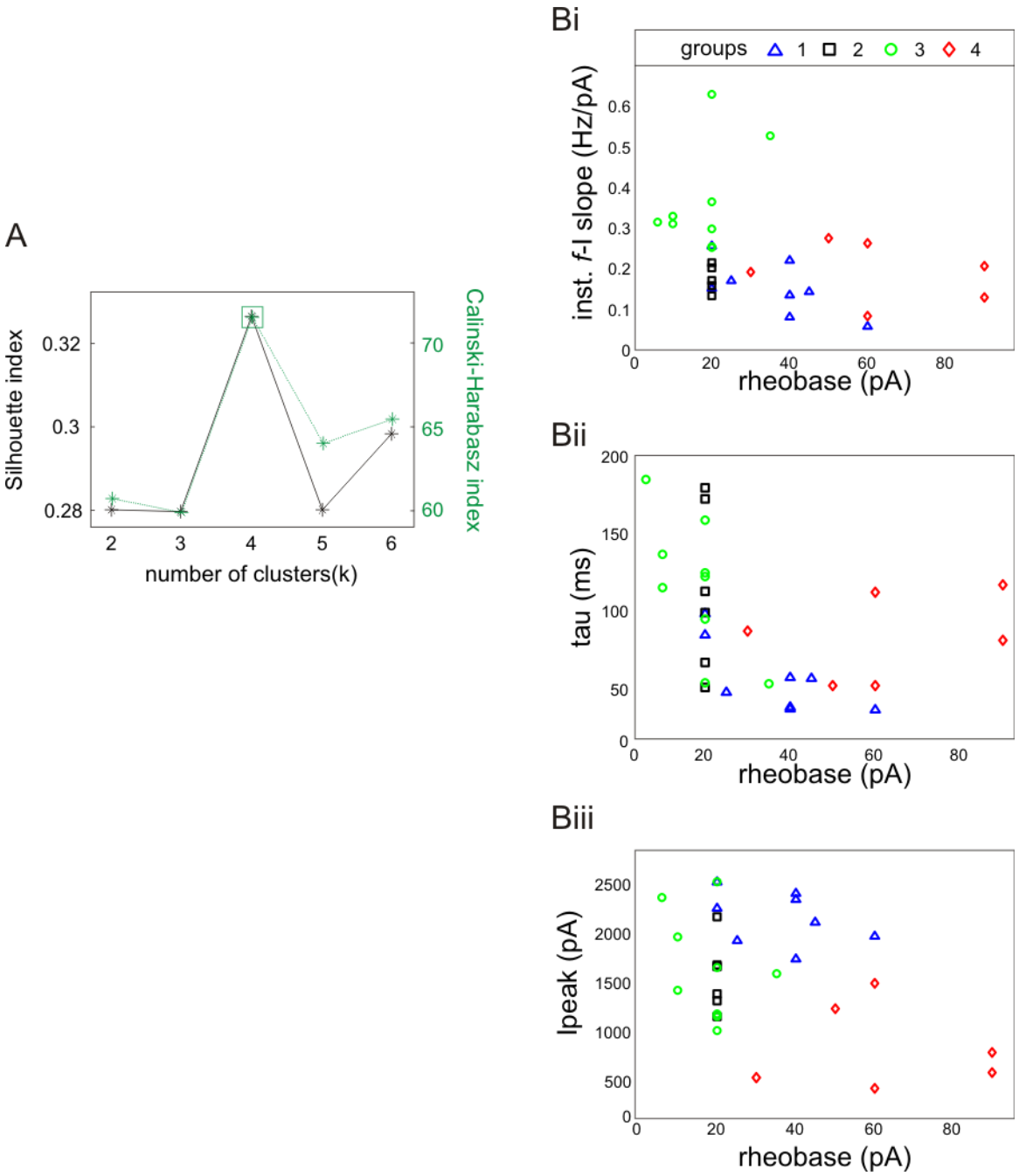

Figure 2.6 Cluster analysis.

A. Analysis of cluster validity, using 2 different indices. Both indices peak at 4 clusters, signifying best fit for the data set. **B.** Distribution of cluster membrane properties as a function of rheobase. **Bi**. Groups 2 and 3 have low rheobase values, with group 3 having larger f–I gains. Groups 1 and 4 are sequentially recruited and can be largely distinguished by rheobase values. **Bii.** Group 3 neurons have statistically larger m values than those of group 1 neurons. **Biii**. Group 1 neurons display statistically larger I_{peak} values than those of both group 2 and group 3 SPNs and all have larger values than those of group 4 SPNs.

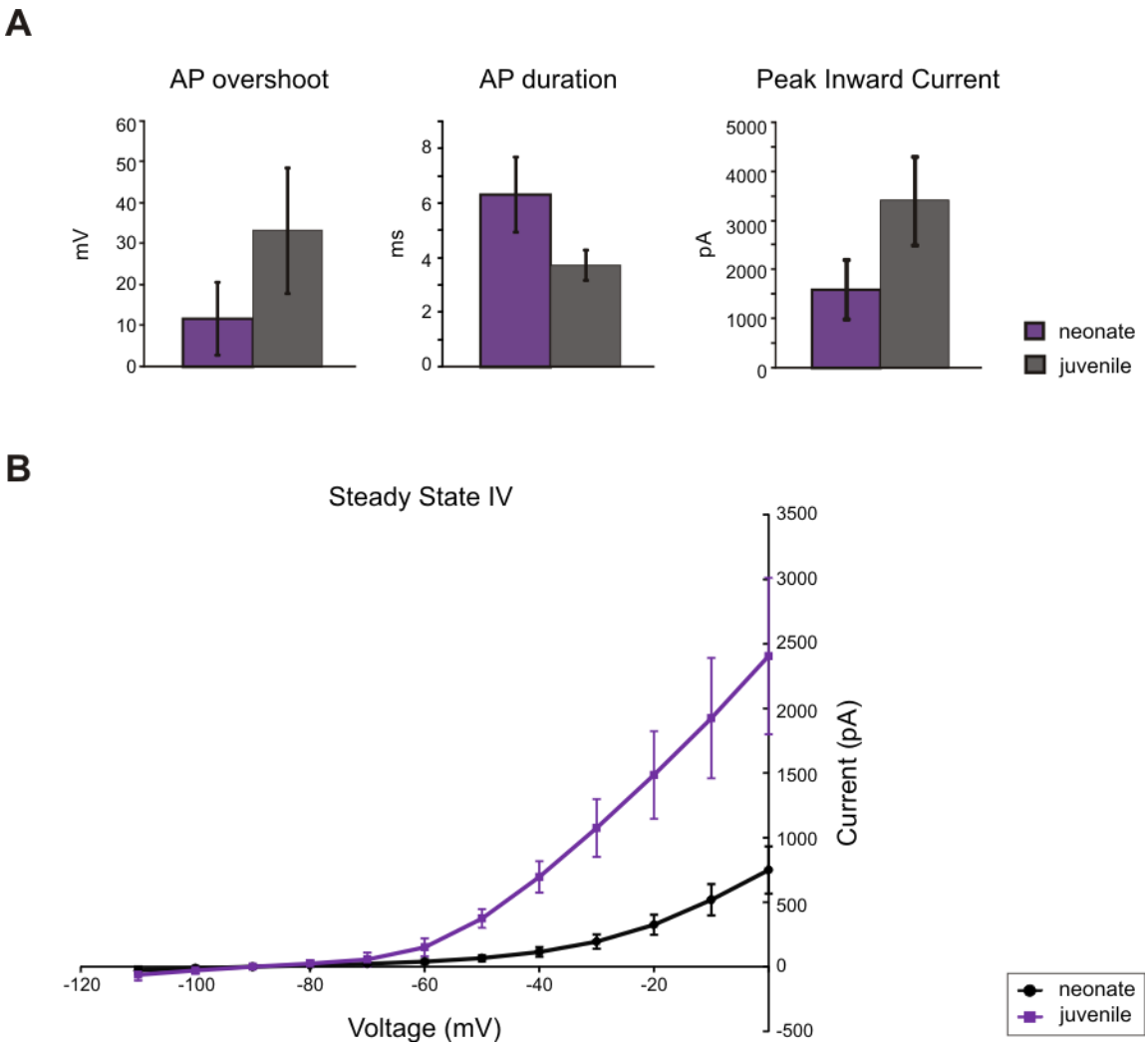

Figure 2.7 Neonatal and juvenile mice comparison.

A. Juvenile mice exhibit larger action potentials of shorter duration than neonatal mice. The also generate larger sodium currents, as seen by comparison of peak inward current during voltage clamp protocols. **B**. Steady state I-V relationship. Steady state values for outward currents during voltage clamp also show increased magnitude for juveniles. Overall this implies greater current flow for multiple ion types.

2.5 DISCUSSION

Using eGFP-HB9-transgenics the present study undertook the first characterization of membrane electrical properties of sympathetic preganglionic neurons in the thoracolumbar intermediolateral nucleus of mouse. Studies were undertaken in either thicker transverse or thinner horizontal slices and membrane properties in these populations were indistinguishable. Given the strong rostrocaudal and mediolateral orientation of SPN IML dendrites, horizontal sections would be predicted to provide neurons with largely intact architecture. However, while mediolateral dendrites are strongly present in utero [196], rostrocaudal projections have a relatively later maturation, (2 weeks postnatal; [72, 164]), perhaps minimizing the level of dendrotomy in transverse slices at this age. Consequently, it is likely that the SPNs recorded in transverse sections retained considerable rostrocaudal dendrites.

A correlation matrix was used to identify relationships between active and passive membrane properties. One important observation was that rheobase - the amount of current required to recruit a neuron - was the best predictor of cell group and correlated with several other membrane properties. Given the obvious importance of SPN membrane excitability as the 'final common CNS output' of sympathetic neural activity, we also undertook a detailed examination of their firing properties. SPNs consistently demonstrated spike-frequency adaptation. In addition, the relation of firing frequencies to magnitude of current injection (*f*-I relations) generated slopes that varied considerably across the SPN population, indicating that SPNs represent a highly differentiated class of neurons. Indeed, cluster analysis subdivided this nucleus into four subpopulations. The

rostrocaudal range (T_8-L_2) sampled from potentially includes SPNs with five different end-target innervations [244]. While outside the scope of the current study, it is possible this electrophysiological classification is influenced by end target differentiation, and warrants further investigation. Regardless, the overall conclusion is that this population of output neurons constitutes a heterogeneous population, differentiated by their electrophysiological properties, with complex recruitment properties.

2.5.1 Comparison to Membrane Properties Reported in Other Species

Membrane properties measured here compare well with those reported previously in other mammalian species. Resting membrane potential values were similar to those reported in the neonatal rat, guinea pig, and adult cat [60, 108, 197, 273]. Since impalement-induced leak conductance with sharp microelectrodes alters passive membrane properties [237], our whole-cell patch recordings can only be compared to patch-clamp recordings as reported in the neonatal rat [180, 197, 270]. Similar input resistance (R_{in}), membrane capacitance (C_m), and membrane time constant (τ_m) values were observed [[180, 197, 270]; but see [270] for temperature-dependent differences in R_{in}]. The presence of multiple exponentials in the membrane charging curves in a number of neurons here was also reported in the neonatal rat [197, 270]. Multiple exponential responses are indicative of initial non-uniform distribution of membrane potential, likely due to a complex dendritic tree. Values obtained for L are much greater than those found in patch-clamp recordings from CA3 pyramidal neurons [162] and even somatic motoneurons [253], known to have a very extensive dendritic arbor [211]. This suggests SPNs are not as electrically compact and their ability to integrate synaptic input from distal dendrites may be comparatively weak. The functional consequences of this are currently unknown.

The use of neonatal animals in the current study may be subject to criticism, as the sympathetic nervous system of rodents is still maturing at this young age [20]. While end-target responses to central sympathetic activation are not present until after the first week postnatal, level of tonic SPN activity and response to asphyxia and hypoglycemia in the neonate (1-2 days postnatal) were comparable to those in the adult rat [234]. Additionally in the rat, as early as embryonic day 14.5 SPNs are already positioned in the IML, central autonomic region, and areas in between [133, 196]. At birth, SPNs in the IML have the characteristic ladder-like rostrocaudal and mediolateral projecting dendritic arbor, with the rostrocaudal dendrites elongating and cluster separation increasing during the first two weeks [72, 164, 195]. Since biochemical markers of synaptic activity and synaptic connections in sympathetic ganglia in the mouse greatly increase during this period [21], electrophysiological differentiation may play a role in forming appropriate synaptic connections. Interestingly, the similarity of the above mentioned electrophysiological properties in the neonatal mouse to juvenile mice in our study, and adult cats and more mature rats in the work of others suggests that while development may affect the size of SPNs and magnitude of conductances, the overall functional aspects of SPNs are largely in place in the neonate. Indeed, while the neonatal work in this study used animals with an overlapping age range as undertaken in rat (as young as P7), we also include even younger animals (P3) to demonstrate that SPN membrane properties are specified at a very early age. Moreover, cluster analysis was able to separate the IML neurons into at least 4 discrete groups irrespective of age. This is consistent with anatomical findings that morphology is also highly differentiated at birth [195, 204], supporting an early maturation of the IML SPN neuronal phenotype.

2.5.2 Active Conductances

A transient outward rectification was present in virtually all SPNs as seen previously [60, 108, 180, 197, 220, 270]. This transient conductance was partially insensitive to intracellular Cs^+, inactive at resting membrane potential, and only released from inactivation with membrane hyperpolarization. In voltage clamp, decay was best fit with double exponential decay, consistent with the dual component A-type K^+ conductances noted by Wilson et al [270]. In neonatal rat SPNs this current acts to regulate firing frequency and contributes to spike repolarization and the afterhyperpolarization [180]. Hyperpolarizations from resting membrane potential evoked inward rectification in most SPNs, and were sensitive to intracellular Cs^+. The conductance is similar to the anomalous rectification recorded in other SPNs [108, 180, 197], and may act to return SPNs to an excitable membrane potential after large inhibitory input.

Blockade of most K^+ conductances with Cs^+ revealed the presence of a persistent inward current (PIC). In somatic motoneurons, PICs are thought to be responsible for repetitive firing and membrane bistability [135, 139]. In our acute spinalized mouse SPNs, the PIC magnitude was usually small enough to be largely masked by outward K^+ conductances with a K-gluconate based intracellular solution. This may be due to the loss of descending monoaminergic input, which greatly facilitates PICs in motoneurons [107, 140]. Given the strong descending monoaminergic projections to the IML, it is therefore possible that SPNs also possess the ability for bistable membrane behavior.

2.5.3 Repetitive Firing and Spike Frequency Adaptation

Neonatal mouse SPNs showed repetitive firing over a wide range of current injections. Compared to intracellular recordings in guinea pigs and cats, instantaneous firing rates and *f*-I slopes were much greater [60, 108]. This is likely at least partly due to a reduced leak conductance in patch clamp recordings as compared to conventional sharp intracellular recordings [237]. Compared to somatic motoneurons, SPN *f*-I gain exceeded that in both the primary and secondary firing range by 10 fold [29] but this is also likely a reflection of markedly increased input resistance observed with patch recordings. Indeed, in patch clamp recordings in putative mouse motoneurons in culture, *f*-I gains and variability were remarkably similar [135]. The strong correlation between the AHP magnitude and *f*-I gain found in the present study supports a functional role of the AHP (and underlying conductances) in controlling cellular excitability. Modulation of the AHP, such as that in response to noradrenaline in both the cat and rat [220, 275] and caffeine in the rat [231], could lead to direct changes in SPN response to synaptic input.

In a majority of neonatal mouse SPNs, we describe a pronounced spike frequency adaptation (SFA). SFA in SPNs has been reported previously [60, 220], but has not been rigorously explored. In contrast, the mechanisms serving SFA have been detailed in mouse motoneurons [174]. In this study, modeling and patch clamp studies suggest that slow inactivation of the fast inactivating Na^+ conductance is a key factor in SFA [174]. This work contrasts previous notions on the primary importance of the AHP (see Discussion in Miles et al. 2005). The physiological relevance of SFA in motoneurons has been interpreted in relation to initial versus sustained force generation in muscle [239]. Analogously, the relevance of SFA in SPNs may relate to the recruitment of

postganglionic neurons. In our neonatal mouse SPNs, SFA decay was inversely related to R_{in}. Thus, the smallest conductance neurons underwent the greatest SFA. Whether these neurons innervate a different population of postganglionic neurons or have differences in synaptic transmission remains to be determined.

The range of rheobase, R_{in}, and degree of SFA observed in SPNs could signify an organizational principle of recruitment with functional significance. For example, somatic motoneurons exhibit a well-defined order of recruitment via the size principle, whereby motoneurons are recruited with increasing size, conduction velocity, and motor unit fatigability [100, 211]. In fact, lumbar SPNs in the adult cat have distinct differences in conduction velocity, responses to afferent stimuli, and voltage intensity for axonal recruitment based on their end-target innervations [118].

SPNs normally fire at low frequencies [172], so it is worth questioning whether *f*-I curves are physiologically relevant at the higher range of firing frequencies. Peak firing frequencies observed here clearly exceed these steady state values, and many SPNs were not driven to their maximum firing potential. One possibility is that higher firing frequencies are reached during ischemia, drops in blood pressure and states of higher arousal such as the 'fight or flight' response. SPNs receive dense modulatory inputs from both brainstem and hypothalamic autonomic circuits [7, 19, 73, 150], many of which could greatly increase their excitability on a systematic level. Indeed, addition of norepinephrine and serotonin has been shown to increase spontaneous discharge in SPNs in the neonatal rat [145, 165, 231] and adult cat [89, 276], often in a bursting rhythm with intraburst frequencies greatly exceeding steady state values.

Individual SPNs project to many postganglionic neurons (1:15 ratio in rat and 1:200 in human) and postganglionic neurons are innervated by multiple SPNs. The existence of both convergent and divergent synaptic inputs forming the postganglionic 'autonomic motor unit' indicates the importance of synaptic integration in their recruitment. Hence as a population, SPN firing properties will be critical in the temporal and spatial summation necessary to activate postganglionics. There appear to be two populations of SPNs based on synaptic strength on postganglionics - strong and weak - with strong synapses lacking P type Ca^{2+} channels and evoking currents individually capable of recruiting postganglionics [172]. Thus, recruitment of postganglionics may only require the activity of individual SPNs. Conversely, weak inputs from multiple SPNs may also be used to recruit postganglionic neurons. The relation between synapse strength and membrane properties remains to be determined. However, the initial high frequency firing of SPNs could act to potentiate synaptic transmission of weak synaptic connections while the slower firing induced by SFA could act to maintain potentiation without neurotransmitter depletion [157].

In conclusion, the present study suggests that SPNs in the IML are comprised of multiple subtypes, easily distinguished by electrophysiological parameters. We hypothesize that generation of target- and condition- specific responses of the sympathetic nervous system is largely derived from electrophysiological differentiation. The easy visualization of SPNs afforded by their genetic labeling with Hb9-eGFP in transgenic mice allows for coupling future studies of electrophysiological results with immunohistochemistry, anatomy, and functional genomics for further exploration.

CHAPTER 3

MONOAMINERGIC MODULATION OF SPN PROPERTIES

3.1 ABSTRACT

Given the species specific and seemingly contradictory actions of the monoamines on spinal sympathetic outflow, I sought to characterize the effects of dopamine (DA), norepinephrine (NE), and serotonin (5HT) on SPN intrinsic properties in the neonatal mouse and more clearly elucidate the effects of the monoamines on SPN excitability. Additionally, I developed a novel *in vitro* spinal cord and sympathetic chain preparation, which allowed me to assess the population efferent responses to visceral afferent stimulation and their modulation by the monoamines. This included measures of spiking, synaptic potentials, and DC shifts in membrane polarity (a measure of membrane potential). Recordings were made from thoracic T_{11}-T_{12} ventral roots, which likely contain more SPN than motor axons. Lastly, I complemented physiological experiments on monoamine transmitter neuromodulation with immunohistochemical detection of putative 5HT, NE, and DA receptors underlying these effects.

Each monoamine had a unique signature of effects. 5HT's actions were the most uniform. 5HT consistently depolarized all intracellulary recorded SPNs, and increased their firing response to injected currents. In a similar fashion, 5HT depolarized the ventral root DC recordings and increased spontaneous activity. 5HT concomitantly greatly depressed visceral afferent evoked responses in the ventral root. Reflex depression and DC root depolarization occurred in a dose-dependent fashion with IC_{50} and EC_{50} values in the sub micromolar range. $5HT_{2A}$ and $5HT_7$ receptors observed in

SPN somas and processes support direct excitatory actions, while the absence of $5HT_1$ receptors tested supports inhibitory actions on reflexes somewhere else in the reflex circuit.

NE had mixed actions. NE depolarized some intracellularly recorded SPNs while hyperpolarizing others. Nonetheless, in all cases NE increased SPN firing responses to injected current. NE also depolarized ventral root DC recordings in some mice with increased spontaneous activity, but hyperpolarized DC recordings in others. Like 5HT, NE greatly attenuated visceral afferent-evoked reflexes with a sub-micromolar IC_{50}. Direct actions are likely due to both α_{1a} and α_{2a} receptors on SPNs.

Like NE, DA depolarized some while hyperpolarizing other intracellulary recorded SPNs. However, unlike NE and 5HT which increased membrane excitability, DA reduced firing responses to injected currents in some SPNs with increases in others. Interestingly, DA had dose-dependent actions on ventral root polarizations with lower doses depolarizing and higher doses leading to hyperpolarizations. In contrast DA consistently depressed visceral-afferent evoked responses, but with IC_{50} values 5-10x higher than that observed with 5HT and NE. Since I observed both $D_{1\text{-like}}$ (D_5) and $D_{2\text{-like}}$ receptors ($D_{2,3}$) on SPNs with immunohistochemistry, mixed responses were expected.

Overall, these results demonstrate that the monoamines have complex and differentiable actions on SPNs which coincide with the presence of numerous receptor subtypes expressed in SPNs. In contrast, the monoamines uniformly depress visceral afferent evoked reflexes by currently unknown receptors. Receptor selective pharmacology and additional immunolabeling studies are warranted.

3.2 INTRODUCTION

Sympathetic preganglionic neurons (SPNs) integrate activity from descending and sensory systems to determine the final central output of the sympathetic nervous system. The intermediolateral column (IML) has the highest number and density of SPNs [110], and within this region SPN somas are found in distinct clusters in each spinal segment, forming a ladder-like distribution symmetric around the central canal [31]. The monoamines dopamine (DA), norepinephrine (NE), and serotonin (5HT), all project from subcortical nuclei to the spinal cord [19, 103, 148, 266], often mimicking the ladder-like distribution of SPNs, suggesting profound neuromodulatory influence [73].

While direct and indirect modulatory actions have been reported for NE, 5HT and DA on SPNs [54, 90, 145, 277], conclusions as to the overall actions are often contradictory. 5HT strongly and directly depolarized the majority of SPNs in neonatal rat spinal cord slices *in vitro* [145, 155], and increased spontaneous firing in the adult cat *in vivo* [89]. NE evoked depolarizing, hyperpolarizing, and biphasic responses in adult cat spinal cord slices *in vitro* [275, 277, 278], while only depolarizations were reported in the neonatal rat [220]; depolarizations were mediated by α_1 receptors and hyperpolarizations mediated by α_2 receptors [109]. Reports on DA are less clear, with depolarizations, hyperpolarizations, and biphasic responses reported in the neonatal rat *in vitro* [90]. However, increases in firing in the adult rat [144] and decreases in the adult cat [53] have also been reported *in vivo*.

Recently, our lab developed an *in vitro* slice preparation recording from fluorescently-identified SPNs in a GFP+-HB9 transgenic mouse line [282]. Given the species specific

and seemingly contradictory actions of the monoamines (MAs) on SPNs, we sought to characterize the effects of 5HT, NE, and DA on SPN intrinsic properties in the neonatal mouse and more clearly elucidate the effects of the MAs on SPN excitability. Additionally, in order to assess the modulation of populations of SPN efferents and spinal reflexes evoked by visceral afferents, we developed a novel *in vitro* spinal cord and sympathetic chain preparation.

Previous work in the rat and cat has identified potential receptor substrates on which the descending monoamines could act. Immunohistochemistry in the rat identified moderate labeling of $5HT_{2a}$ receptors and weak labeling of $5HT_{5A}$ receptors near the IML [63, 240] , while in the cat $5HT_7$ and $5HT_{2A}$ receptors were identified in the IML and intermediate zone [189]. Immunohistochemistry in the rat showed α_{2A} adrenergic receptors in the IML [243], and these data are supported by autoradiographic evidence on sympathoadrenal SPNs in the rat [230]. In the mouse, real time PCR and in situ hybridization indicated the existence of all DA receptors (D_1-D_5), with the highest incidence of D_2 and D_5 receptors, diffusely distributed throughout the spinal cord [281]. Immunohistochemistry in the rat has confirmed the presence of moderate D_2 receptor labeling in the IML [256], while autoradiography in the rat has suggested the presence of both D_3 and $D_{1\text{-like}}$ receptors [91, 142]. To date, no one has investigated the location of any of the above mentioned receptors in the mouse spinal cord.

The transgenic HB9-GFP mouse, with its strong labeling of SPN somas and processes, is an ideal model in which to study potential substrates of monoaminergic modulation in the spinal cord. We therefore complemented our electrophysiological surveys with immunohistochemical techniques to identify potential receptors underlying the MA-

induced changes in SPN excitability. This three-pronged approach allowed us to more fully characterize the modulation of the descending MA systems.

3.3 EXPERIMENTAL DESIGN

All procedures described here comply with the principles of The Care and Use of Animals outlined by the American Physiological Society and were approved by the Emory University Institutional Animal Care and Use Committee.

3.3.1 Slice Electrophysiology

3.3.1.1 Dissection

All experiments were performed in transgenic mice expressing HB9-eGFP (JAX laboratories; known to label SPNs), postnatal day 3-9. Slice preparation followed the same protocols described in Chapter 2 for neonatal animals. Briefly, neonatal animals were decapitated, eviscerated, and the spinal cords removed, and a T_8-L_2 section isolated and sliced into thick transverse sections (400μm). Initial removal of the spinal cord and slicing were performed in cooled, oxygenated sucrose artificial cerebrospinal fluid (**sACSF**), containing (in millimolar [**mM]**): 250 sucrose, 2.5 KCl, 2 $CaCl_2$, 1 $MgCl_2$, 25 glucose, 1.25 NaH_2PO_4, and 26 $NaHCO_3$, pH 7.4. Slices were left to recover for at least 1 hour.

The recording chamber was continuously perfused with oxygenated artificial cerebrospinal fluid (**ACSF;** in mM: 128 NaCl, 1.9 KCl, 2.4 $CaCl_2$, 1.3 $MgSO_4$, 10 D-glucose, 1.2 KH_2PO_4, and 26 $NaHCO_3$; pH 7.4) at a rate of ~2ml/ minute. Patch clamp recordings were made from fluorescently-identified SPNs. Unless otherwise noted, cells

were brought to -70 mV holding potential by injecting bias current and recorded in gap-free mode to assess effects on membrane potential. The current and voltage clamp protocols described in chapter 2 were used to quantify changes in membrane properties as described above.

3.3.1.2 Application of Agonists

5-hydroxytryptamine HCl (5-HT), norepinephrine bitartrate (NA), and dopamine HCL (DA) were obtained from Sigma-Aldrich. The solutions were prepared from frozen stock solutions and bath applied at 10μM, a concentration believed to be below the concentration where nonspecific binding actions have been observed [42, 84, 257]. Each agonist was applied for 1-3 minutes, and a washout period of 10-20 minutes was allowed between drug applications. Drug order was random, and often only one or two agonists were used per cell, due to the time constraints of the recordings.

3.3.1.3 Quantifying Changes in Cellular Excitability

Using the current step protocols applied before and during drug application, mean firing frequency was calculated for each current step. Frequency – current plots were then fit with a logarithmic trendline using Microsoft Excel. Matlab was then used to integrate the area under the logarithmic trendline (see **Figure 3.1**), both before and during drug application. This integrated area was then used to quantify changes in cellular excitability, with statistical significance found using a paired t-test.

3.3.2 Ventral Root Potentials

In both the rodent and human thoracic spinal cord, the number of SPN axons in the ventral roots greatly exceeds those of somatic motoneurons [18, 50, 154]. Therefore in order to examine net modulatory actions on thoracic spinal efferents (where SPNs dominate), both ongoing DC changes in ventral root potential (VRP) and evoked VRP responses to visceral afferent stimulation were assessed with DC recordings. Electrical stimulation of the greater splanchnic nerves has often been used to study visceral afferent inflow (e.g. [3, 4, 64, 225, 251]), as they contain afferents of the gut, pancreas, spleen, kidneys, testis/ovaries, and pelvic organs [187], and this paradigm was used again here.

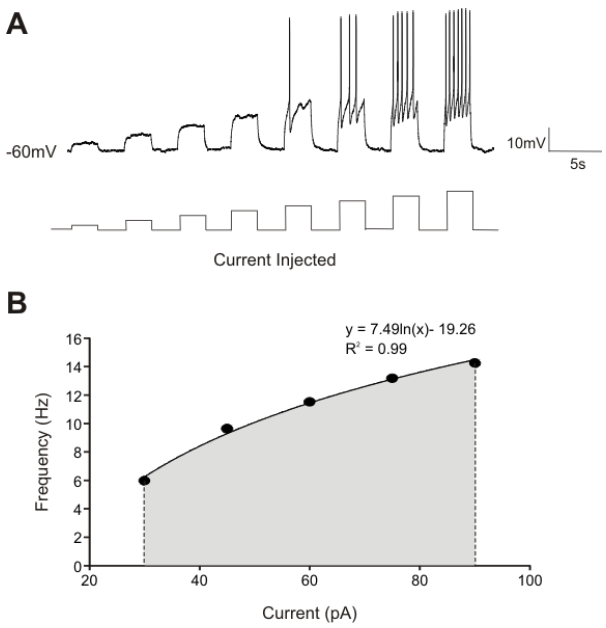

Figure 3.1 Quantifying changes in SPN excitability.

A) Response of a single neuron to increasing current steps (multiples of 5pA, 1 s duration). Bottom traces shows current steps. B) Mean firing frequency for each current step plotted. Data points are best fit with a logarithmic line (equation shown). Area under this line (shaded in grey) found by integrating line from first to last data point.

3.3.2.1 Dissection

All experiments were performed at postnatal day (P) 5-8 litter of mice crossed from transgenic hemizygote HB9-eGFP females (JAX laboratories) and inbred C57/BL6 males. Mice were either HB9-eGFP$^{+/-}$ heterozygotes or wild type. Animals over age P6 were anesthetized with 10% urethane (2mg/kg ip) before decapitation. All animals were

decapitated and eviscerated, leaving only the vertebral column, ribcage, and surrounding tissues. The preparation was then placed in a perfusion chamber filled with low-calcium, high-magnesium aCSF containing (in mM): 128 NaCl, 1.9 KCl, 1.2 KH_2PO_4, 26 $NaHCO_3$, 0.85 $CaCl_2$, 6.5 $MgSO_4$, and 10 glucose (pH of 7.4). A dorsal laminectomy and ventral vertebrectomy was performed to expose the dorsal and ventral sides of the spinal cord from the upper cervical region to the midsacral level. Care was taken to cut medial to the aorta on the left side, to preserve the connections of the dorsal and ventral roots to the sympathetic chain. The aorta was then carefully removed, and the surrounding fascia dissected away from the left sympathetic chain. The splanchnic nerve was identified branching laterally from the sympathetic chain at T13 and innervating the celiac ganglia, and cut midway between the sympathetic chain and the celiac ganglia. The perfusion solution was then switched to aCSF (composition specified above), and to limit movement of the preparation, 25 μM pancuronium bromide (Sigma-Aldrich) was added.

3.3.2.2 Recording Configuration

To both record slow potentials in spinal roots and stimulate the splanchnic nerve, bipolar glass suction electrodes (inner diameter 60-100 μm) with Teflon insulated and chlorided silver ground wires wrapped around the outside were used. This stimulating configuration both reduced ground fluctuations in the DC recordings and eliminated current spread from stimulation to the nearby intercostal muscles. Visceral afferents were activated by stimulating the splanchnic nerve or other cut regions of the sympathetic chain, at an intensity of 100μA or lower stimulus duration 100μs or less and at a rate of .0167 Hz (once every 60s).

Ventral root potentials (**VRPs**) were recorded from the ventral root, and interpreted as compound excitatory postsynaptic potentials (EPSPs) of the combined axons of somatic and sympathetic efferents. The recording configuration can be seen in figure 3.3.

Neural activity was collected on a custom built 4 channel direct current amplifier, low pass filtered at 3 kHz, and digitized at 5 kHz (Digidata 1440) and recorded in Clampex for off-line analysis (Molecular Devices).

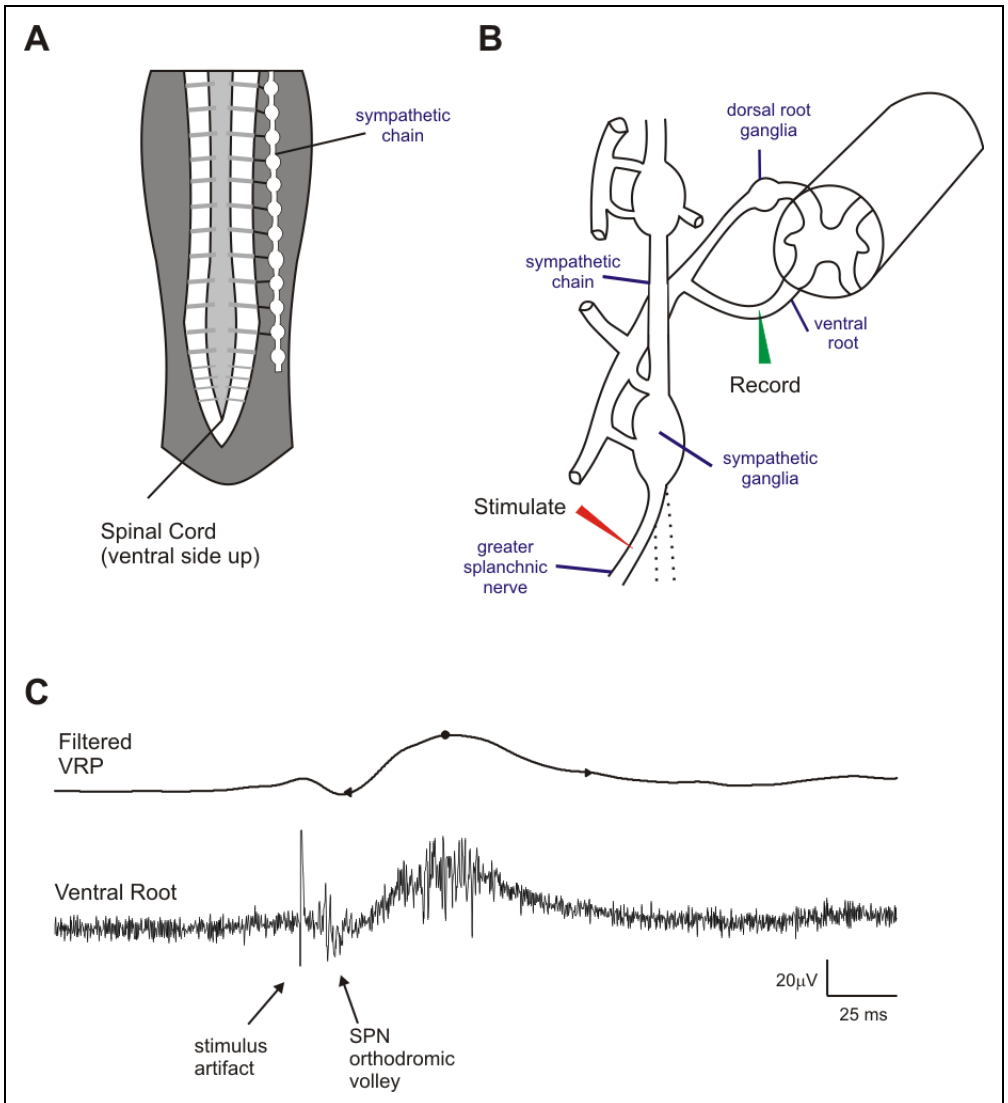

Figure 3.2. Ventral Root Potential Recording Configuration.

A. Schematic of dissection, with ventral root connections to the sympathetic chain maintained. **B**. Schematic of recording configuration. Stimulate visceral afferents in the greater splanchnic nerve, record both ongoing DC shifts and evoked responses in the ventral root. **C**. Sample trace of evoked ventral root response, mean of 5 sweeps. Upper trace shows filtering and automated analysis, onset and offsets marked by < and > respectively, peak marked with '**.**'.

3.3.2.3 Drug Application and Quantification of Drug Effects

Stock solutions of drugs (10-100 mM) were made and stored at -20 ºC until needed. All drugs were dissolved in regular ACSF and perfused through the gravity perfusion line. Increasing dosages of 5HT, NE, or DA were applied cumulatively, with 10 minutes in between each dose increment.

Changes in ventral root potentials were assessed for both the evoked responses and changes in DC resting potential. A custom built MATLAB program was used to subtract the baseline values prior to the stimulus, low-pass filter the response at 100Hz, find the onset of the compound EPSP, peak of the response, and the integral under the filtered ventral root response from onset to offset (defined as when the evoked potential decayed to 1/3 peak amplitude). This program and cutoff frequency was found to accurately capture the slow compound EPSP (see **Figure 3.2C**). Responses were averaged for the last 5 minutes of each drug dose increment for dose response curves. Changes in ventral root resting potentials were calculated using the mean baseline values for the last 5 minutes of each drug dose increment. In order to minimize effects of differences in suction, both evoked and resting ventral root potentials were normalized to baseline evoked values.

3.3.3 Immunohistochemistry

For immunohistochemistry, p7-p9 HB9-eGFP^{+} mice were anesthetized with urethane (4mg/kg ip) and perfused with 1:3 volume/body weight heparin solution (0.9%NaCl, 0.1% NaNO2, 1 unit/ml heparin) followed by equal volume/body weight of Lana's fixative (4% paraformaldehyde, 0.2% picric acid, 0.16 MPO3, pH 6.9). Spinal cords

were isolated and post fixed for 2 hours, then cyroprotected in 10% sucrose plus 0.1 M PO_3 (pH 7.4) and stored at 4º C. Spinal cord segments T_{10}-L_2 were frozen at -80º C and sectioned in 10μm thick slices on a cryostat (Leitz 1720). Both transverse as well as horizontal sections were completed to assure assessment of rostrocaudal and medio-lateral oriented dendrites. Slides were washed overnight in 0.1M PO_3 buffered saline plus 0.3% triton x-100 (PBS-T). Slides were then incubated with primary antibodies seen in Table 1 for 48 hours at 4º C, then washed three times in PBS-t for 30 minutes each at room temperature. All primary antibodies were stained with the appropriate donkey biotinylated secondary antibody (diluted 1:250, Jackson Immunoresearch) for 1.5 hours at room temperature, then washed three times for 20 minutes in PBS-t. This was followed by incubation in extravidin cy3 (diluted 1:1000, Sigma) for 1.5 hours, washed once for 20 minutes in PBS-t, followed by 2 washes for 20 minutes each in 50mM Tris-HCl. Slices were then coverslipped with Vectashield (Vector Labs) for subsequent image capture and analysis.

Low magnification images were obtained with Nikon E800 Microscope and rendered in the Neurolucida Virtual Scan Software for composite images. High magnification pictures were obtained using the Imaging Fluoview 1000 confocal microscope.

Table 3.1. Immunohistochemistry receptors and concentrations.

Receptor	Species	Concentration	Manufacturer
$5HT_{1D}$	goat	1/100	SantaCruz Biotechnology, Inc
$5HT_{2A}$	rabbit	1/250	Immunostar, Inc
$5HT_{2C}$	mouse	1/100	Affinity Bioreagants, Inc
$5HT_{7}$	rabbit	1/100	GenWay
D_{1A}	rabbit	1/100	SantaCruz Biotechnology, Inc
D_{2L}	rabbit	1/250	Millipore
D_{3}	rabbit	1/250	Millipore
D_{5}	goat	1/250	Millipore
α_{1D}	goat	1/100	Santa Cruz Biotechnology, Inc
α_{2A}	goat	1/250	Santa Cruz Biotechnology, Inc.

3.4 RESULTS

SPNs in the IML were targeted for whole-cell patch clamp recordings (see **Figure 2.1**).

3.4.1 Effects of the Monoamines on SPN Membrane Properties

3.4.1.1 Serotonin

With the membrane potential initially held at -70 mV by injecting a constant bias current, bath application of 10 μM 5HT depolarized all SPNs tested (mean 4.9 ± 2.1 mV, n=6). This depolarization was always accompanied by an increase in input resistance. When compared to baseline values, in the presence of 5HT, the frequency-current (*f*-I) plots were shifted up to the left, i.e. SPNs fired action potentials at a lower current injections and at higher rates. 5HT increases the cell's response to current injection by a mean 15.9 ± 9.2 % (**Figure 3.3**).

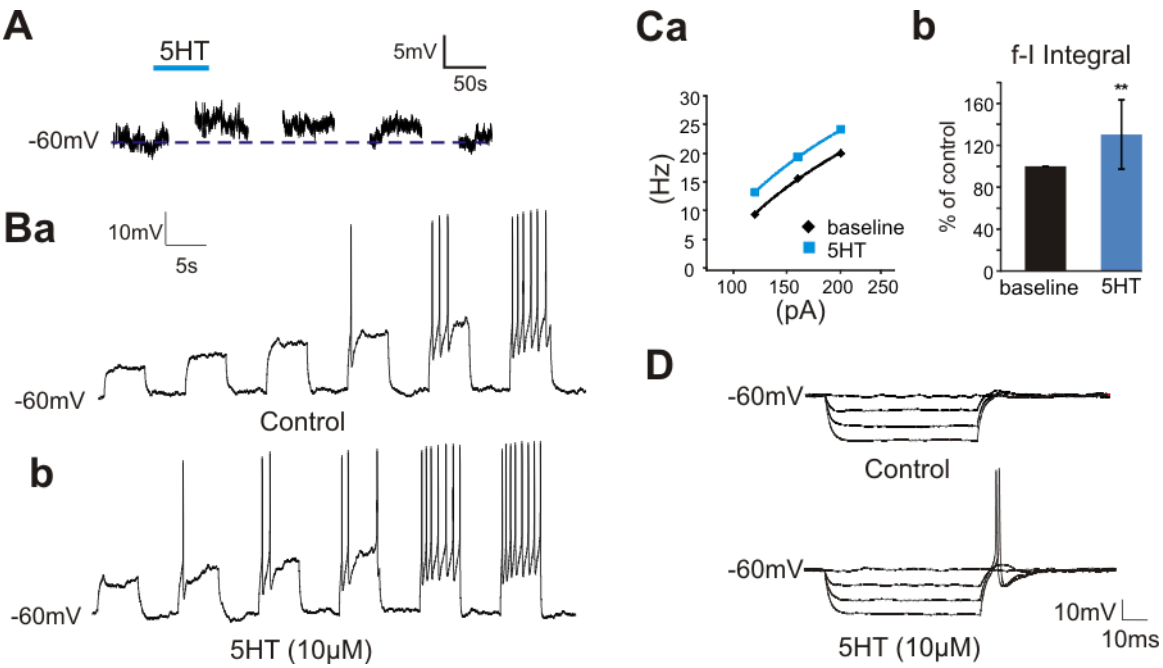

Figure 3.3. Serotonin (5HT) increases cellular excitability.

A. Sample of voltage traces recorded when 5HT (10 μM, 1min) was added to the bath. 5HT depolarized the cell membrane (mean 4.9 ± 2.1 mV) and increased input resistance (not shown) in all cells tested (n=6). **B**. Sample of voltage traces in response to series of current steps (5pA steps,1s duration) (**a**) in control and (**b**) during peak of 5HT application. **Ca.** A sample frequency-current (fI) plot calculated from mean firing frequency at each current injection. **b**. The area under the fI plot for each cell was calculated and a paired t-test performed on control and 5HT values (p=0.04, n=6). Plot shows normalized integral changes with standard deviations. **D**. On occasion, application of 5HT elicited rebound excitation to hyperpolarizing current steps.

After a hyperpolarizing current step, upon returning to baseline holding values some cells exhibited rebound spiking (**Figure 3.3D**). While only seen in a minority of cells (n=2/8), this demonstrated 5HT's ability to unmask rebound excitation.

3.4.1.2 Norepinephrine

Bath application of NE had more diverse actions on SPN excitability. NE primarily depolarized the membrane (mean 4.7 ± 2.2mV) and increased Rin (n=4). However, hyperpolarizations (mean 3.1 ± 0.1 mV) with a decreased Rin were also seen (n=2).

Regardless of the effects on the membrane, NA shifted the cell's f-I plot up in all neurons tested, by a mean 22 ± 20% (p=0.008, n=6). This can be seen in **Figure 3.4**.

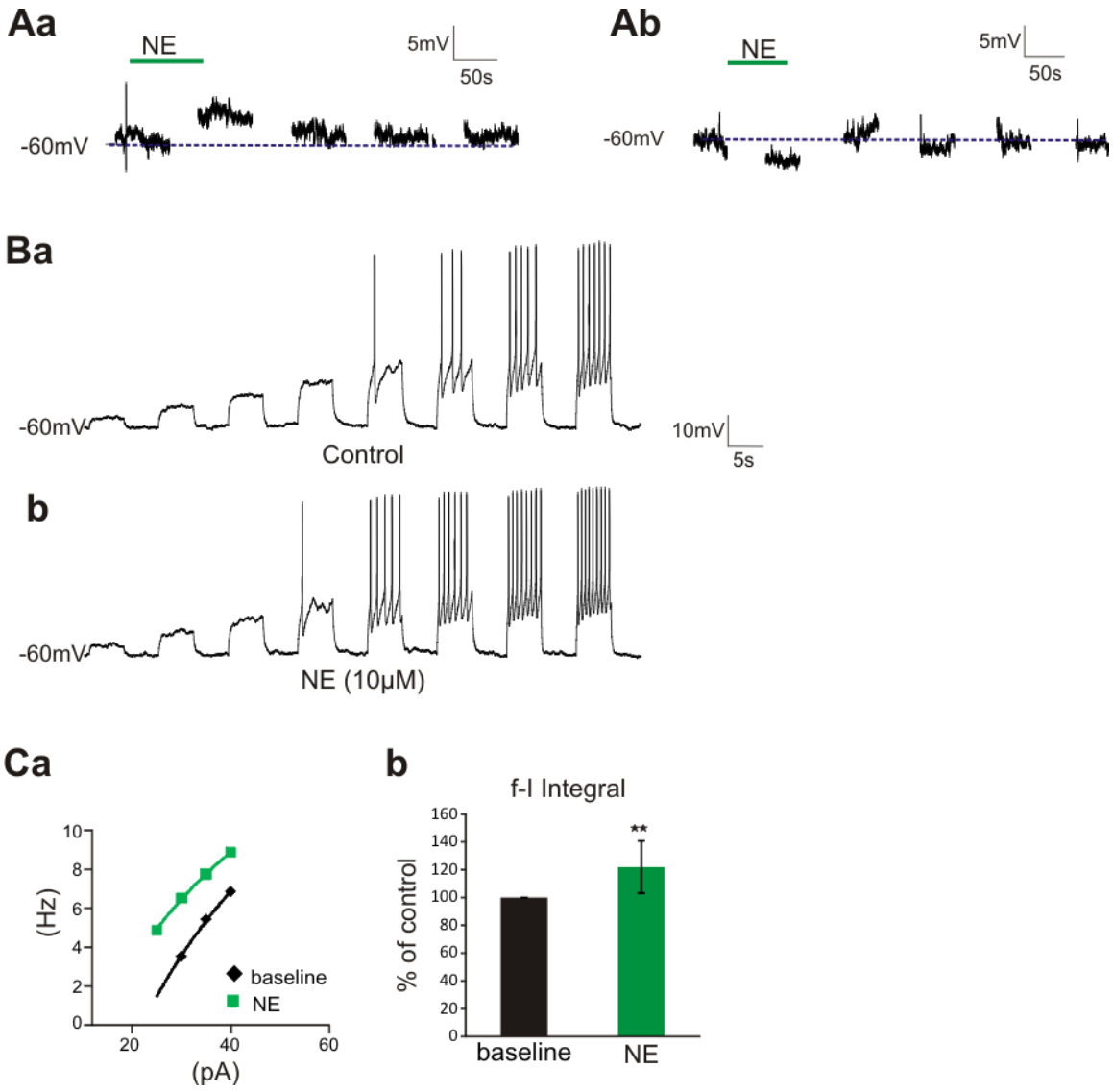

Figure 3.4 NE increases cellular excitability in a complex manner.

A. Sample of voltage traces recorded when NE (10µM, 1 min) was applied to the bath. **Aa**. NE primarily depolarized the membrane (mean 4.7 ± 2.2mV) and increased Rin (n=4). **Ab**. Hyperpolarizations (mean 3.1 ± 0.1 mV) with a decreased Rin were also seen (n=2). **B**. Voltage traces in response to series of current steps (5pA steps, 1s duration) in (**a**) control and (**b**) during peak of NE application. **C**. Regardless of the effects on the membrane, NE increased the cell's fI plot in all neurons tested (n=6). **a**. A sample frequency plot (fI) calculated from mean firing frequency at each current injection. **b**. The area under the fI plot for each cell was calculated and a paired t-test performed on control and NA values for all neurons tested (p=0.008, n=6). Average normalized values and standard deviation is shown.

3.4.1.3 Dopamine

DA bath application lead to both depolarizations (mean 6.0 ± 3.5 mV, n=7) and hyperpolarizations (mean 5.2 ± 0.9 mV, n=2) in SPNs, with unclear actions on input resistance. In contrast to 5HT and NE, while DA increased the cell's firing frequency in response to current injection in the majority of neurons (mean 11.5 ± 9.2%; p=0.004, n=8), decreased responses were also seen (mean -27.2 ± 3.4%; p= 0.05,n=3), as shown in **Figure 3.5**. Changes in excitability were not correlated to either changes in membrane potential or input resistance.

3.4.2 Monoamine-induced Net Changes in Excitability of Population Spinal Efferents

The monoamines have generally excitatory actions on motoneurons, similar to those reported above in SPNs [15, 97, 111] . In both the rodent and human thoracic spinal cord, their axon number in ventral roots likely exceeds those of somatic motoneurons [18, 50, 154]. Therefore in order to examine net modulatory actions on thoracic spinal efferents (where SPNs dominate), both ongoing changes in ventral root DC polarity and evoked VRP responses to visceral afferent stimulation were assessed with DC recordings.

3.4.2.1 Serotonin

Application of 5HT lead to a dose-dependent depression of the visceral afferent- evoked VRP. **Figure 3.6A** shows a sample for an individual day dose-response trial. When the evoked response was normalized to the initial VRP and compared across trials, a mean IC_{50} value of 0.98 μM was calculated (**Figure 3.6B**). In contrast, 5HT produced a dose-

dependent depolarization of the ventral root resting polarity (n=4/4; e.g **Figure 3.6C)** with a mean EC_{50} value of 0.54 μM (**Figure 3.6D**).

3.4.2.2 Norepinephrine

Similar to 5HT, application of NE led to a dose-dependent depression of the visceral afferent-evoked VRP. **Figure 3.7A** shows a sample for an individual dose-response trial, and **3.7B** shows the evoked VRP compared across trials (IC_{50}=0.49 μM). NE produced

either a slight depolarization (n=2/3) or a slight hyperpolarization (n=1/3) on the ventral root resting potential (**Figure 3.7C**). Variability in response precluded an estimation of EC_{50} values.

Interestingly, 5HT and NE greatly depressed ongoing spontaneous VRPs while concomitantly increasing ongoing activity in the ventral roots (n=4/4 and 3/3, respectively) (**Figure 3.8**). This increase in activity was often rhythmic. Coupled with the observed depressant actions on visceral-afferent evoked VRPs and increased responses to current injection in individual SPNs described earlier, these observations support the notion that 5HT and NE have excitatory actions on motor neurons (both somatic and autonomic), while depressing visceral afferent input.

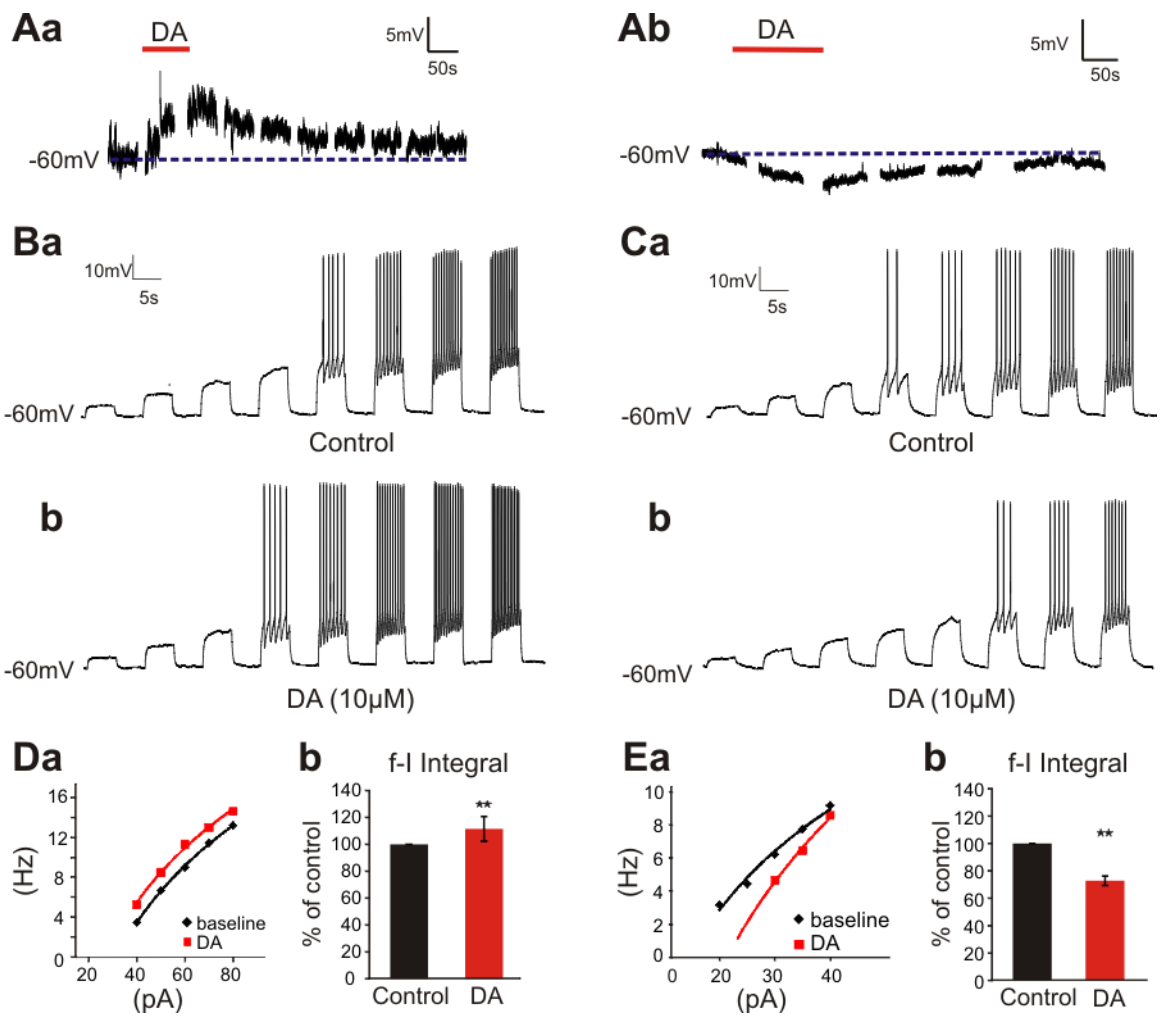

Figure 3.5 DA had mixed actions on SPN membrane properties.

A. Sample of voltage traces recorded when DA (10 μM, 60-90s) was applied to the bath. DA both (**a**) depolarized (mean 6.0 ± 3.5 mV, n=7) and (**b**) hyperpolarized (mean 5.2 ± 0.9 mV, n=2) the membrane, with unclear actions on input resistance. While DA (**B**) increased cellular excitability in the majority of neurons, (**C**) decreased excitability (n=3) was also seen. Voltage traces in response to series of current steps (5-15pA steps, 1s duration). **Da**. Sample frequency plot of increased excitability, based on the mean firing frequency at each current injection. **b**. The area under the fI plot was calculated and a paired t-test performed for all neurons showing increased excitability (p=0.004, n=8). Shown is the mean normalized values and standard deviation. **E**. Sample fI plot and mean normalized area under all fI plots showing decreased excitability (p= 0.05,n=3). Changes in excitability were not correlated to either changes in membrane potential or input resistance.

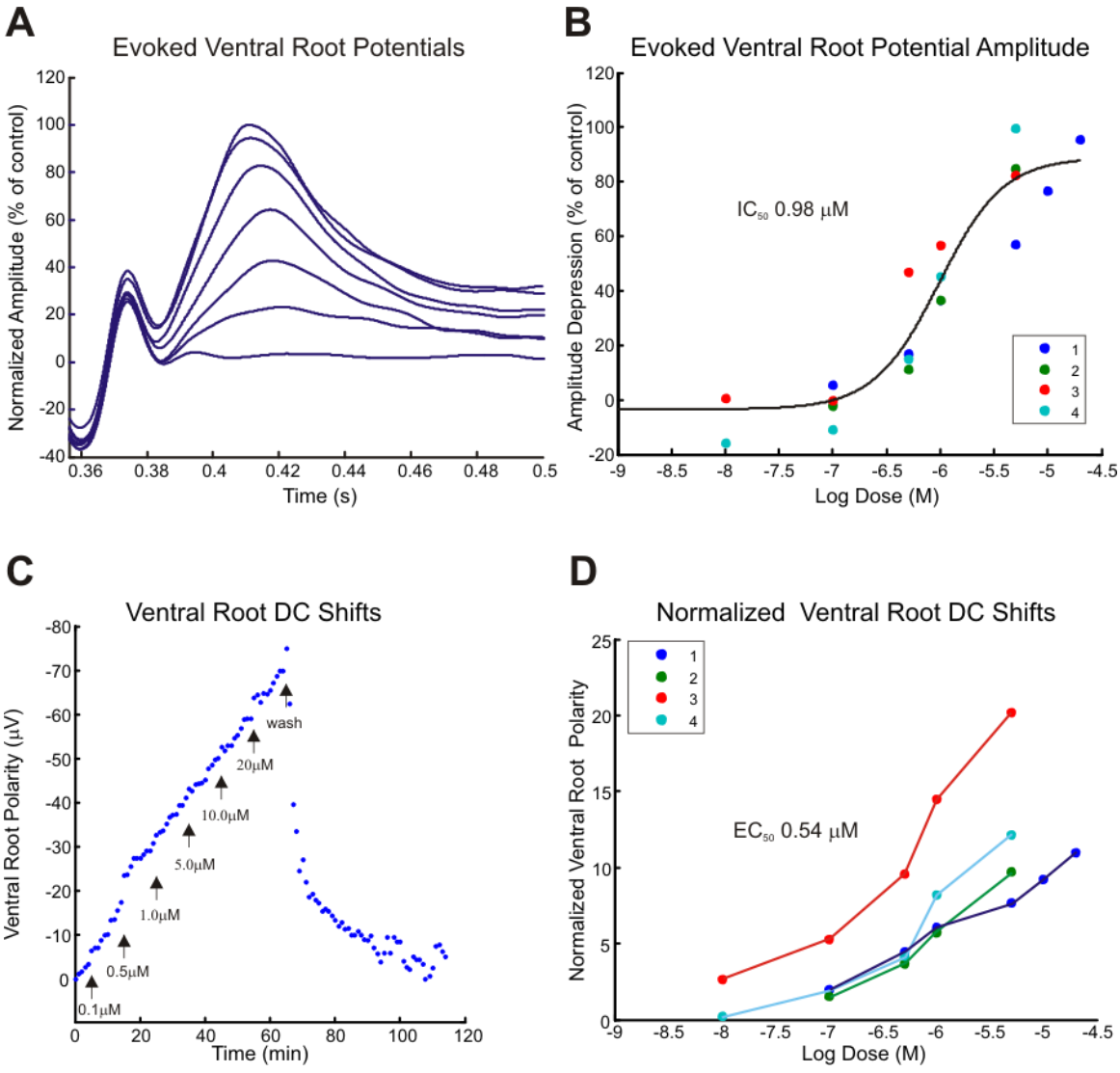

Figure 3.6. 5HT actions on evoked and resting ventral root properties.

A. Sample of ventral root potentials (VRPs) evoked by splanchnic nerve stimulation. Each trace is the mean, normalized trace of 5 sweeps for each dose increment. **B**. Dose response trials for 5HT, with each trial a separate color. Line is a best fit dose-response equation to all data points, IC_{50} value is the dose at which the evoked response is half the control value. **C**. Sample change in resting polarity during dose response. Each point is the mean value of the traces pre-stimulus, by convention negativity is upward. **D**. Normalized plots of resting ventral root polarity, average of 5 sweeps for each dose.

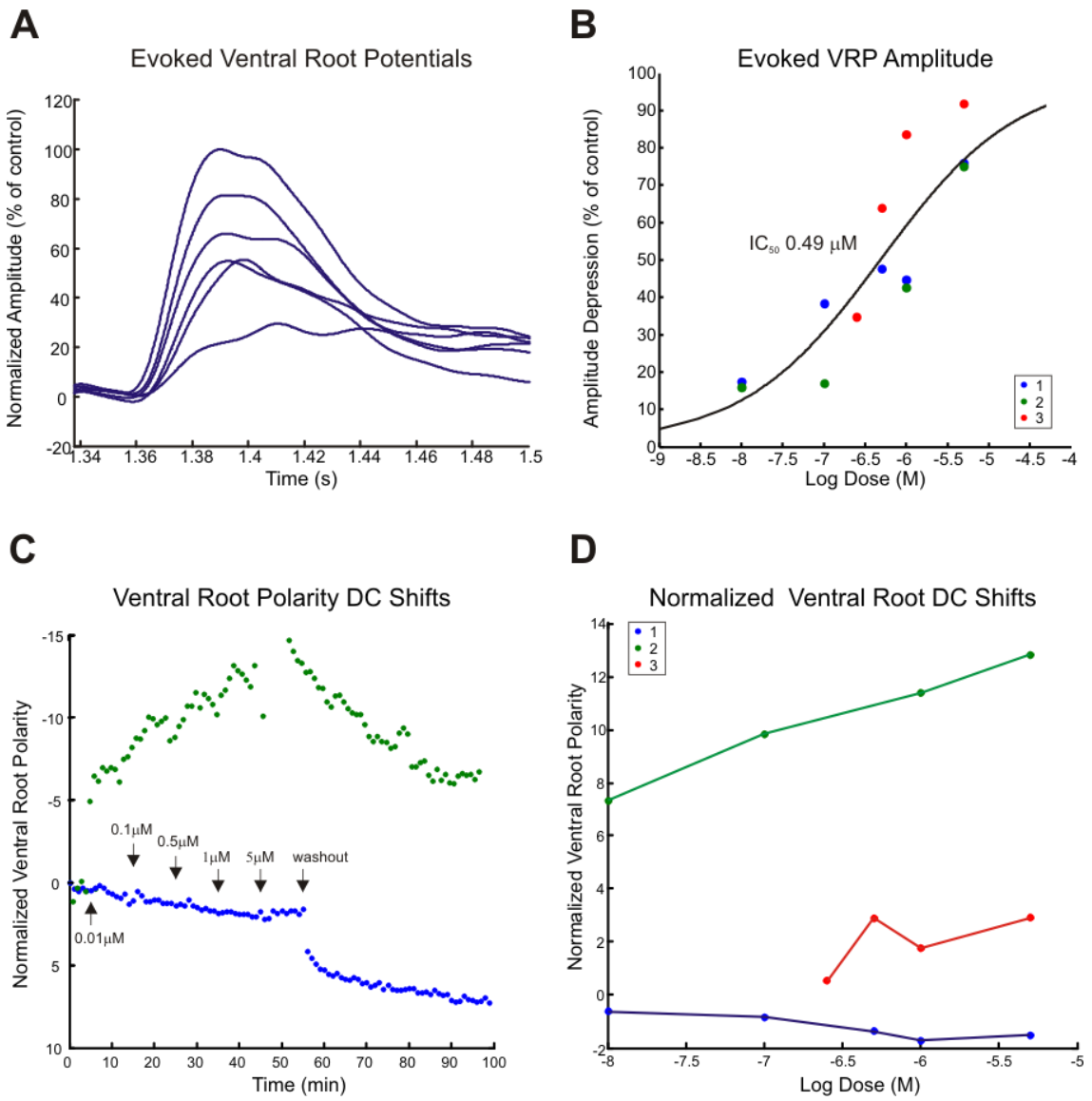

Figure 3.7 NE actions on evoked and resting ventral root properties.

A. Sample of ventral root potentials (VRPs) evoked by splanchnic nerve stimulation. Each trace is the mean, normalized trace of 5 sweeps for each dose increment. Dot denotes peak values. **B**. Dose response trials for 5HT, with each trial a separate color. Line is a best fit dose-response equation to all data points, IC_{50} value is the dose at which the evoked response is half the control value. **C**. Sample change in resting polarity during dose response. Each point is the mean value of the traces pre-stimulus, by convention negativity is upward. **D**. Normalized plots of resting ventral root polarity, average of 5 sweeps for each dose. Again, line is a best fit dose-response to maximal ventral root polarization for all trials.

3.4.2.3 Dopamine

Application of DA, like that of 5HT and NE, depressed visceral afferent evoked VRPs in a dose-dependent manner. Much higher concentrations of DA were needed to fully suppress the evoked response, with low concentrations having little effect. Of all the monoamines tested, DA was the least potent by about 10-fold with an IC_{50} value of 4.64 μM. **Figure 3.9A** shows a sample for an individual dose-response trial, while **Figure 3.9B** shows the evoked VRP compared across trials. Unlike the actions on evoked VRP responses, DC shifts in the ventral root were produced by DA at the lowest concentrations (less than 1μM) and always depolarized the ventral root (n=3/3; **Figure 3.9C**). Yet as the concentration increased past ~5μM, the ventral root potentials became hyperpolarizing in 2 of 3 cases (Figure 3.9D). To test whether this was a history- or dose- dependent shift, single doses of 10 μM DA were applied for 10 minutes and then washed out (Figure 3.9E). At this concentration, DA hyperpolarized the resting VR membrane potential in 3/3 trials, supporting membrane hyperpolarizations at higher DA doses.

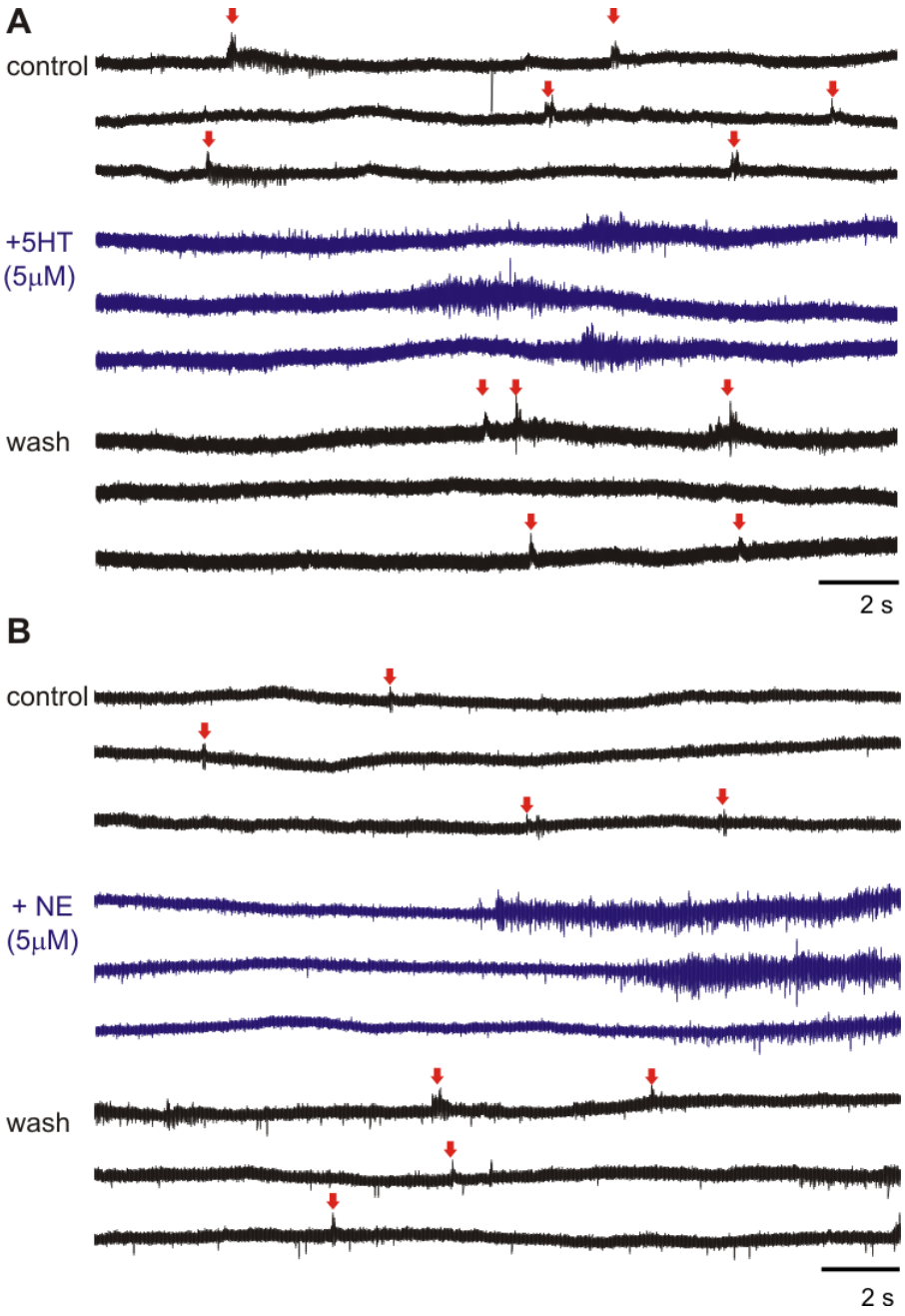

Figure 3.8 Changes in ongoing ventral root activity.

Figure shows changes in ongoing activity in control, drug, and washout. **A**. 3 out of 10 epochs covering 5 minutes for control, 5 minutes after 5HT (5 μM) was applied, and 15 minutes after washout. Note spontaneous bursting in the presence of 5HT. Arrows denote spontaneous ventral root potentials, some of which reach spike threshold. **B**. 3 out of 10 epochs covering 5 minutes, for control, 5 minutes after NE (5 μM) was applied, and 15 minutes after washout. Note both 5HT and NE increased background spiking and the emergence of bursting events, while eliminating spontaneous potentials. DA had limited effects on spontaneous activity and is not displayed.

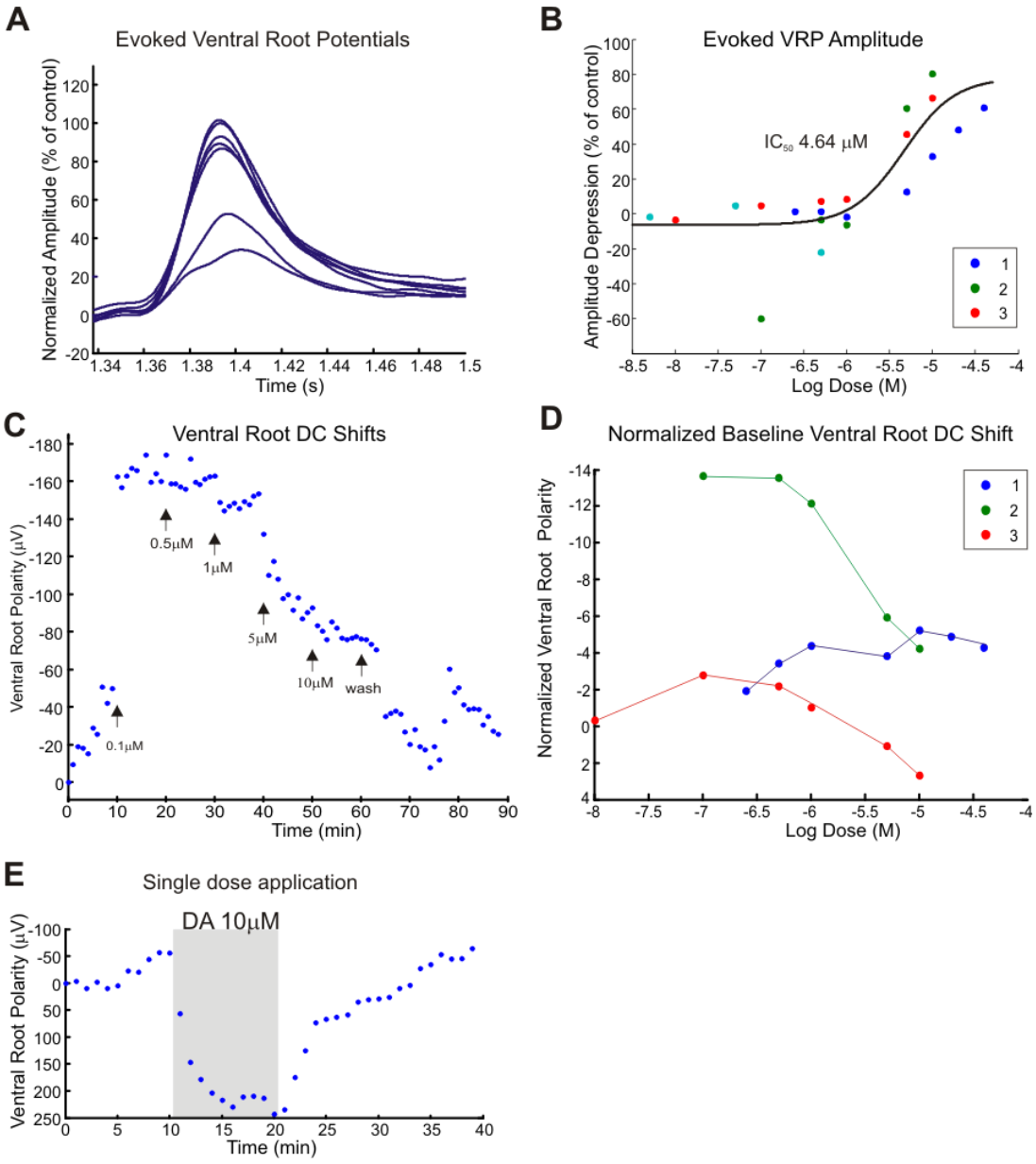

Figure 3.9 Figure 3.10 DA actions on evoked and resting ventral root properties.

A. Sample of ventral root potentials (VRPs) evoked by splanchnic nerve stimulation. Each trace is the mean, normalized trace of 5 sweeps for each dose increment.. **B.** Dose response trials for DA, with each trial a separate color. Line is a best fit dose-response equation to all data points, IC_{50} value is the dose at which the evoked response is half the control value. **C.** Sample change in resting polarity during dose response. Each point is the mean value of the traces pre-stimulus, by convention negativity is upward. **D**. Normalized plots of resting ventral root polarity, average of 5 sweeps for each dose. Note the bidirectional plot in 2/3 trials. **E**. Sample change in resting polarity during single dose (10 µM) DA application.

.

3.4.3 Distribution of Monoamine Receptors

3.4.3.1 Serotonin Receptors

As both $5HT_7$ and $5HT_2$ receptors are known to have excitatory actions on motoneurons [104, 189, 223] and implicated in 5HT actions on SPNs [145, 155, 159], we undertook immunolabeling studies to determine substrates of direct actions. Dual immunolabeling for both anti-GFP and various serotonergic receptors was assessed in the IML and intercalated nucleus (ICN). Immunohistochemistry revealed the presence of $5HT_{2A}$ and $5HT_7$ receptors on HB9+ neurons in these regions. **Figure 3.10** displays a comparison with HB9-GFP labeling with $5HT_{2A}$ receptor labeling, showing co-labeling both perisomatically and on processes. Staining in horizontal slices revealed HB9+ processes in the dorsal-ventral direction at the level of the IML, consistent with the projections of SPN axons. **Figure 3.11** displays a comparison between HB9-GFP labeling and $5H_7$ receptor labeling, and shows both perisomatic and process labeling in the IML. $5HT_{2c, 1d, 1f, and 5}$ receptors were also assessed, but the antibodies tested did not positively label any SPNs and are not shown.

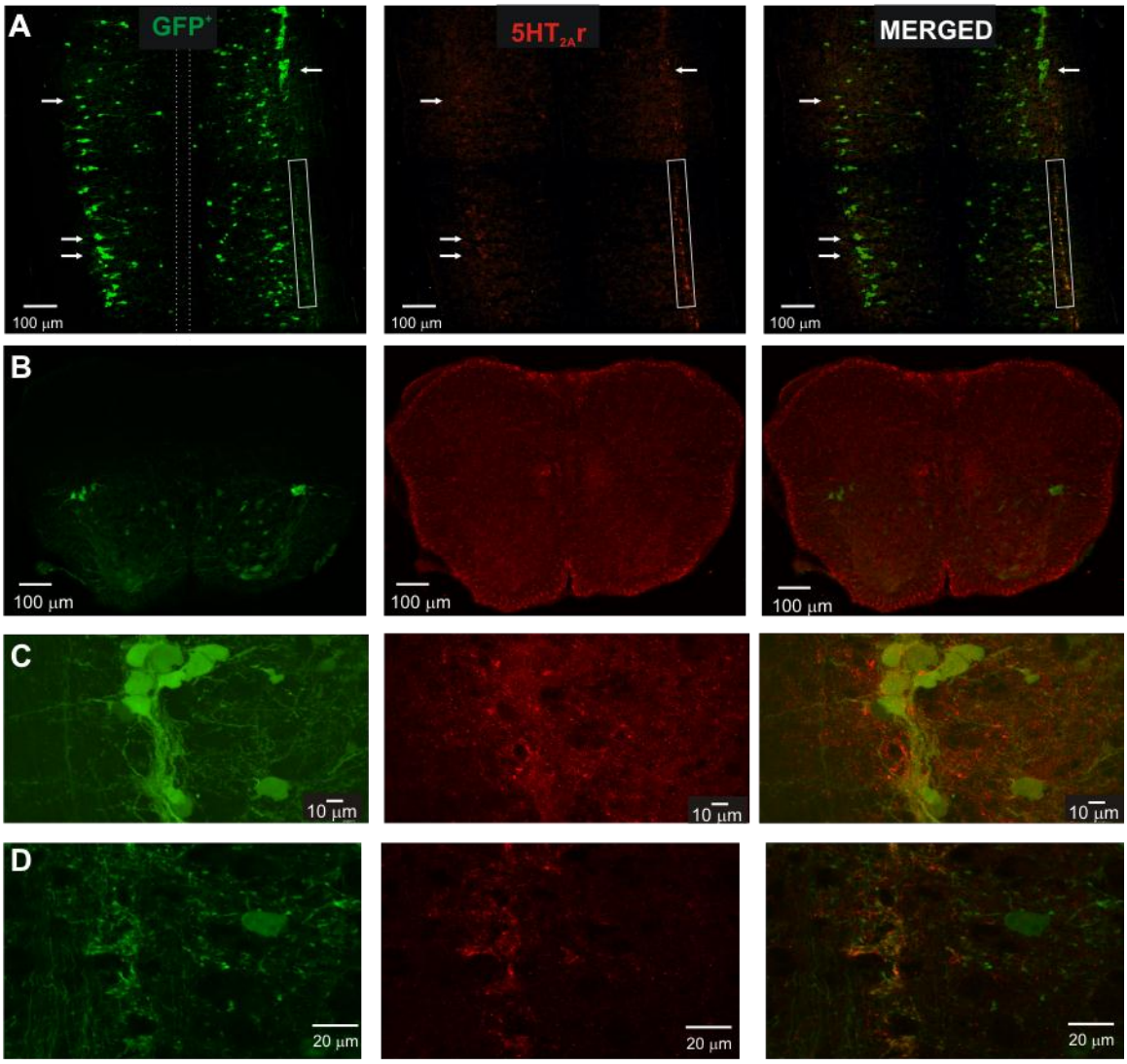

Figure 3.11 $5HT_{2A}$ receptors.

A. Horizontal spinal cord slice 10 μm thick, just dorsal to the central canal (at level for IML visualization); imaged with Nikon E800 Microscope and rendered in Neurolucida Virtual Scan software for composite shown. Dotted lines denote approximate location of central canal. Left column, GFP labeling; middle, $5HT_{2A}$ receptors; right, merged image. Note some co-labeled somas (arrows) and processes, including those in the dorsal-ventral plane (boxed region). **B**. Low magnification confocal image of a transverse spinal cord slice, 10 μm thick. Note widespread labeling, particularly in the ventral horn and some in the IML. **C**. Higher magnification confocal image of IML from a horizontal slice. Image represents composite of 10 consecutive images taken at 0.3 μm optical section thickness (3 μm total thickness). Note some punctate labeling on and nearby SPN somas, as well as GFP+ process co-labeling. **D**. Higher magnification of boxed region in A. Confocal image of horizontal slice, single image of 0.3 μm thickness. Note co-labeling of processes going into the page, in the dorsal-ventral plane.

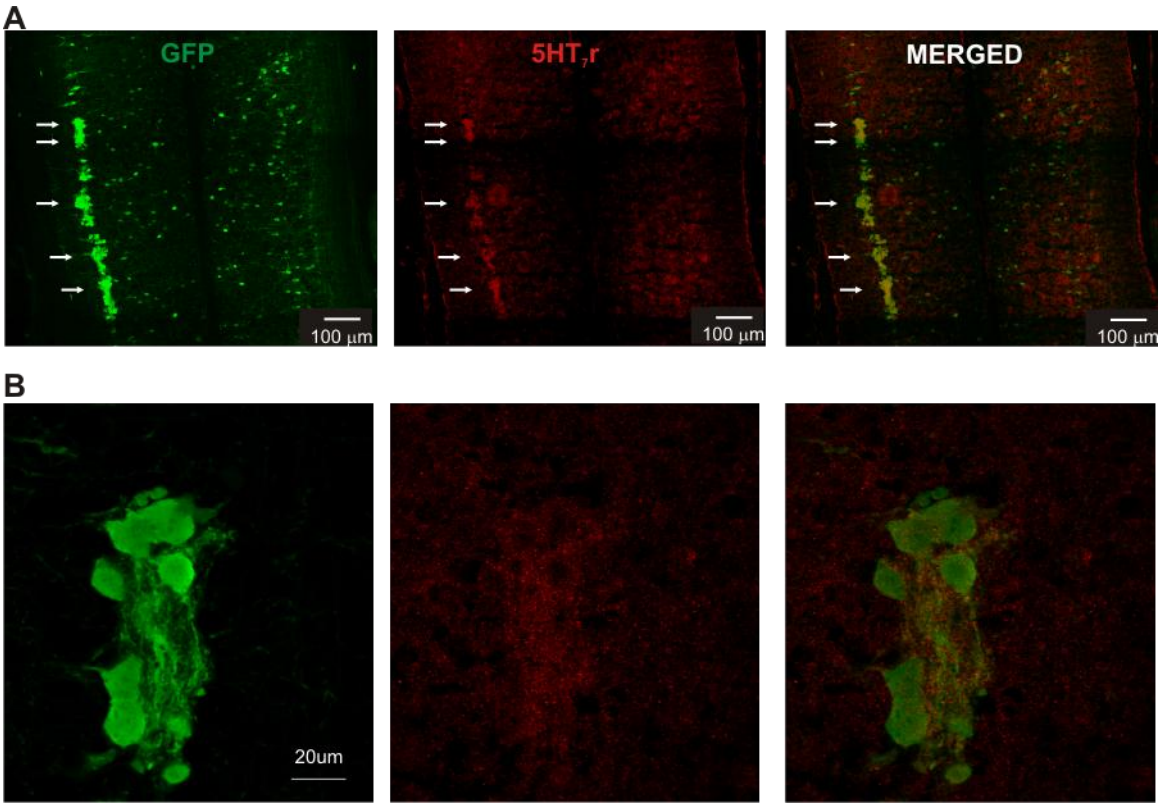

Figure 3.12 $5HT_7$ receptors.

A. Horizontal spinal cord slice 10 μm thick, just dorsal to the central canal (at level for IML visualization); imaged with Nikon E800 Microscope and rendered in Neurolucida Virtual Scan software for composite shown. Dotted lines denote approximate location of central canal. Left column, GFP labeling; middle, $5HT_7$ receptors; right, merged image. Note some co-labeled somas (arrows). **B**. Higher magnification confocal image of IML from a horizontal slice. Image represents single optical slice of 0.3 μm thickness. Note some punctate labeling perisomatically around SPNs as well as GFP+ processes between them.

3.4.3.2 Adrenergic Receptors

Dual immunolabeling for both anti-GFP and various adrenergic receptors was assessed in the IML and intercalated nucleus (ICN). Immunohistochemistry revealed the presence of both α_{1D} and α_{2A} receptors on HB9+ neurons in these regions. **Figure 3.12** displays a comparison with HB9-GFP labeling with α_{1D} receptor labeling, showing perisomatic co-labeling. Note weak labeling of α_{1D} in the IML compared to ventral horn and ICN. **Figure 3.13** displays a comparison between HB9-GFP labeling and α_{2A} receptor labeling. α_{2A} receptors strongly labeled the spinal white matter, suggesting a non-neural labeling and/or labeling of neural processes traveling within the white matter. In the grey matter, GFP^+ neurons in the IML were clearly co-labeled. β_1 receptors were also assessed, but the antibodies tested did not positively label any SPNs and are not shown.

3.4.3.3 Dopaminergic Receptors

Using immunohistochemistry, D_1, D_2, D_3, D_4, and D_5 receptors were tested. Of those tested, only D_2, D_3, and D_5 receptors co-labeled $HB9^+$ neurons in the IML and ICN (**Figures 3.14-3.16**). While $D_{2,3, \text{ and } 5}$ receptors were found on many non-GFP+ neurons as well. D_1 and D_4 receptors did not positively label any SPNs and are not shown.

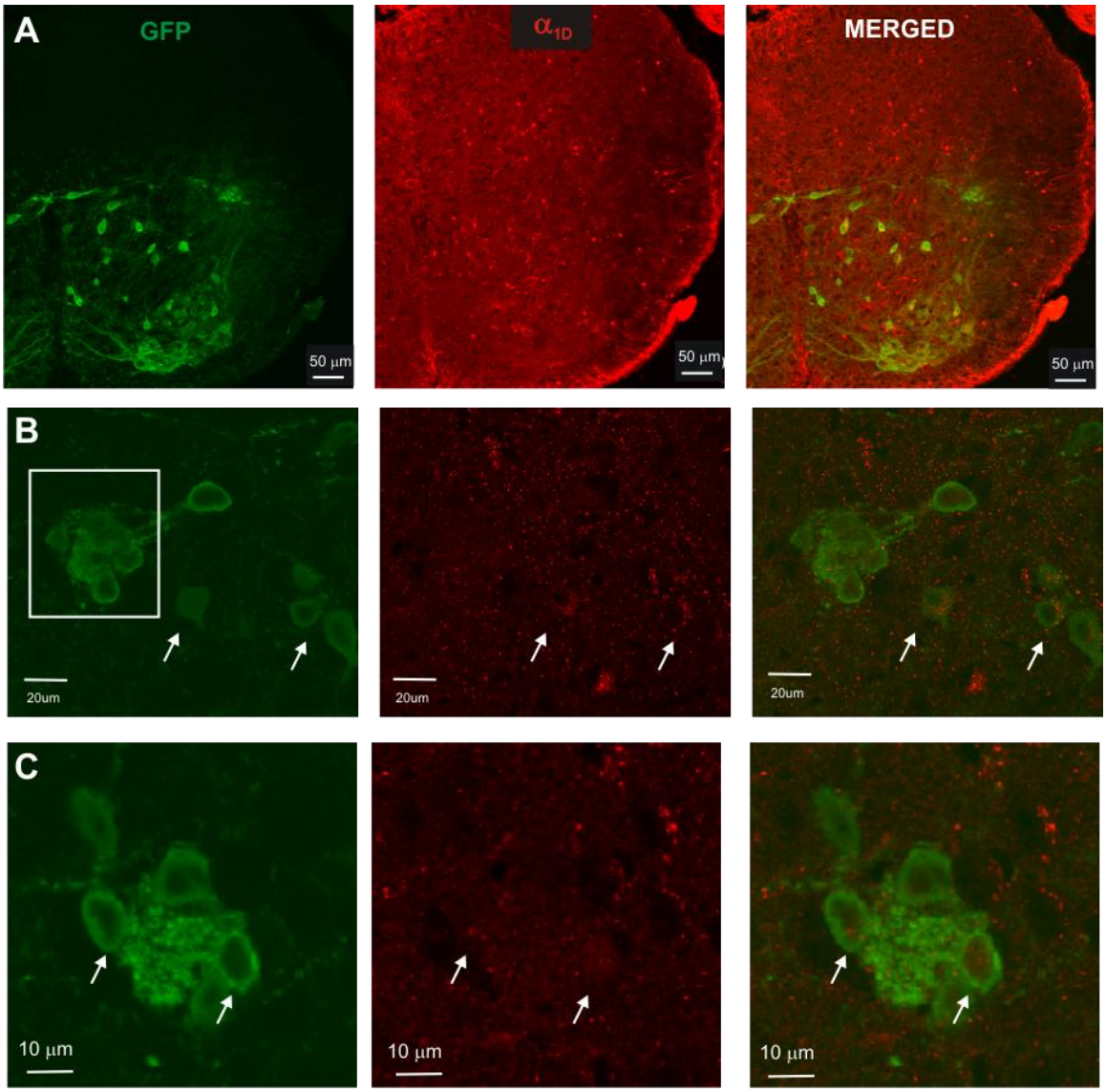

Figure 3.13 Adrenergic receptor α_{1D}.

A. Low power confocal image of lower thoracic spinal cord transverse slice, showing both Hb9 -GFP+ neurons and α_{1D} adrenergic receptor labeling. Notice sporadic labeling throughout the spinal cord, particularly in ventral horn. **B**. Higher magnification of IML in an adjacent slice. Image represents composite of 6 consecutive confocal images taken at 0.3 μm optical section thickness (1.8 μm total thickness). Note weak labeling of SPNs in the IML (boxed), but much stronger labeling of GFP+ neurons in other autonomic regions. **C**. Single section (0.3 μm optical thickness) deeper into the slice, showing weak labeling of IML neurons (arrows).

.

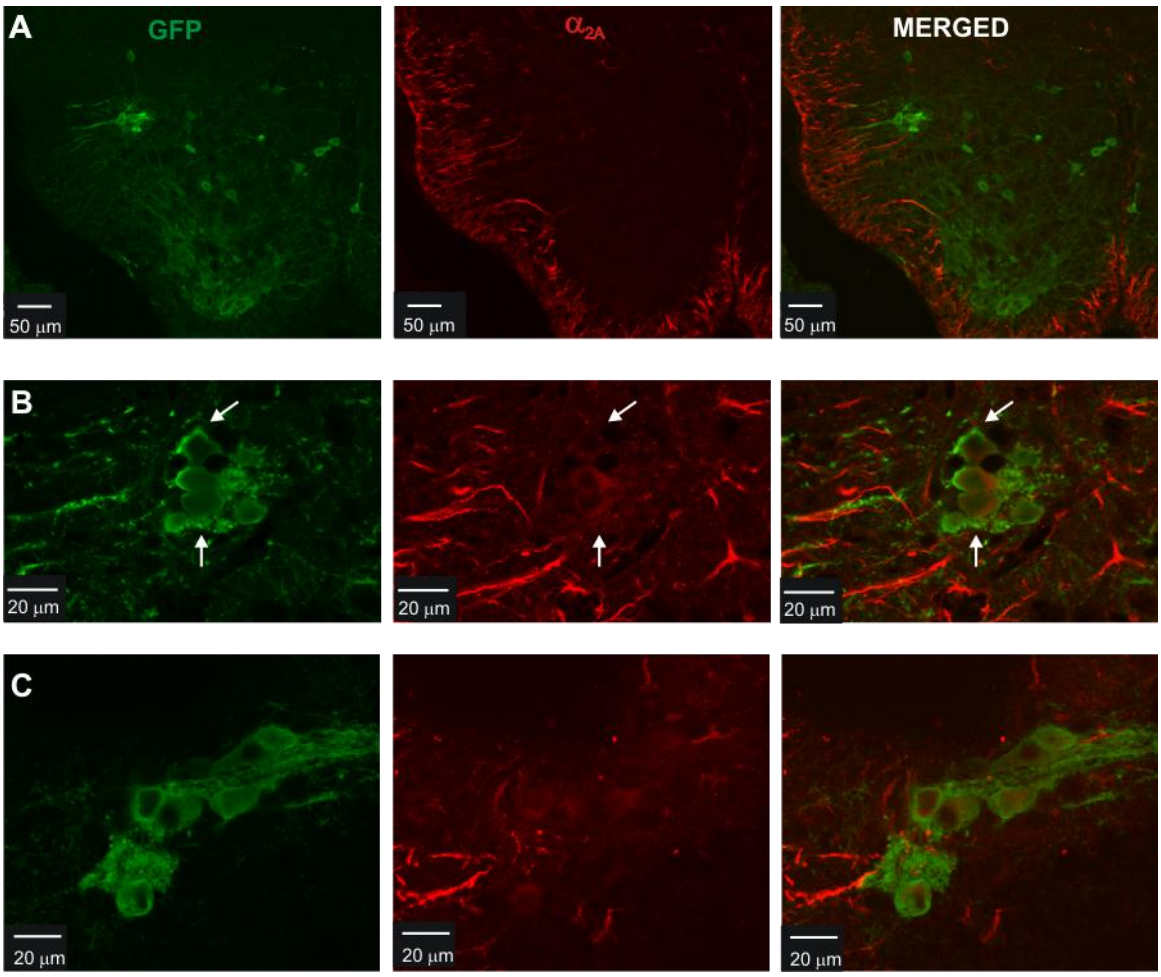

Figure 3.14 Adrenergic receptor α_{2A}.

A. Low power confocal image of lower thoracic spinal cord transverse slice, showing both Hb9 -GFP+ neurons and α_{2A} adrenergic receptor labeling. Notice relatively weak labeling of spinal grey matter, compared to strong white matter labeling. **B**. Higher magnification of IML in same slice. Image represents single optical slice of 0.3 μm thick. Note perisomatic labeling of SPNs (arrows) **C**. Composite of 7 consecutive confocal images from an adjacent slice, taken at 0.3 μm optical section thickness (2.1 μm total thickness). Again, note perisomatic labeling of SPNs.

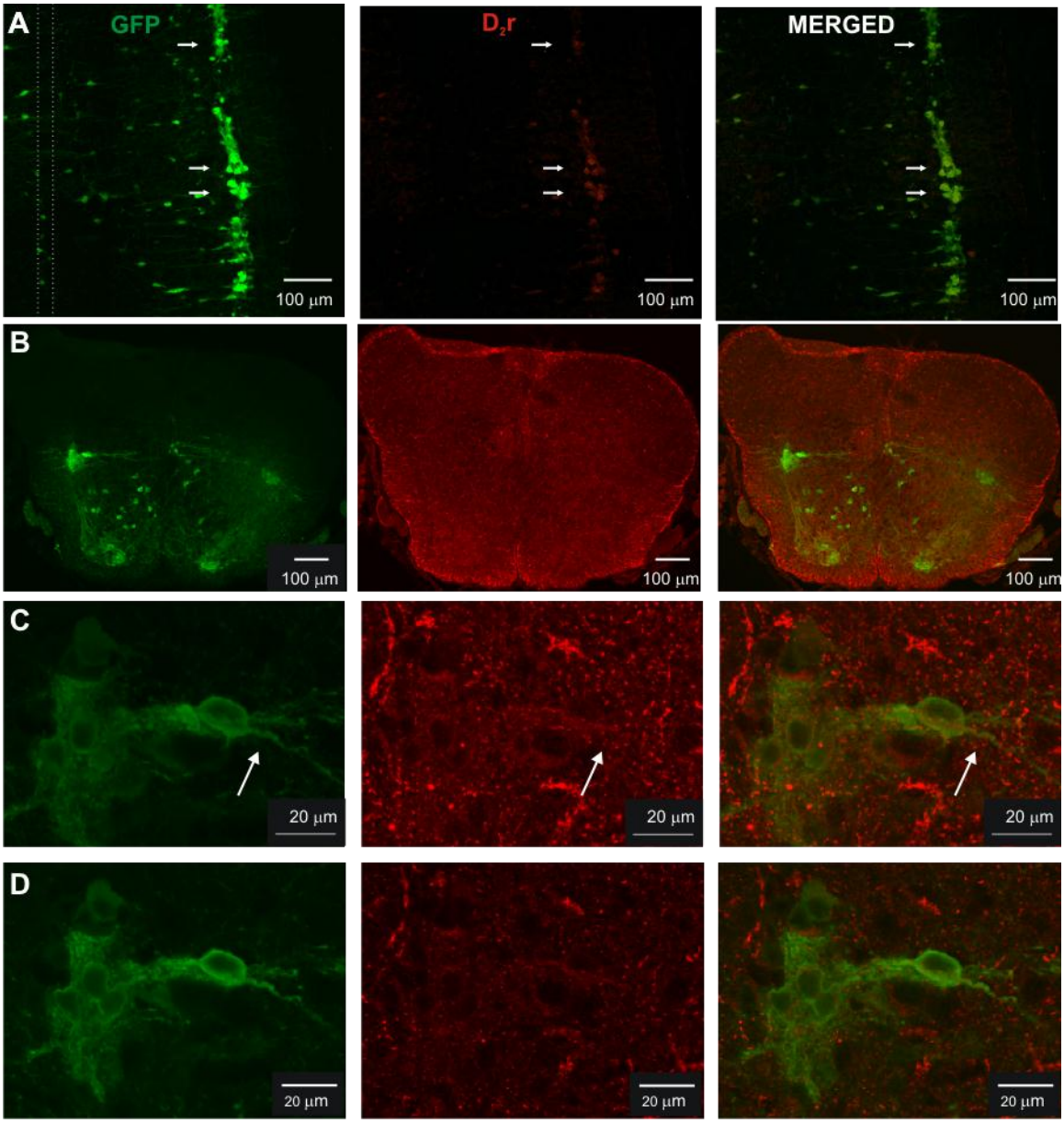

Figure 3.15 D_2 dopaminergic receptors.

A. Horizontal spinal cord slice 10 μm thick, just dorsal to the central canal; imaged with Nikon E800 Microscope and rendered in Neurolucida Virtual Scan software. Dotted lines denote approximate location of central canal. Left column, GFP labeling; middle, D_2 receptors; right, merged image. Note some co-labeled somas (arrows). **B**. Low magnification confocal image of a transverse spinal cord slice in a different animal, 10 μm thick. Note widespread labeling, particularly in the ventral horn and in the IML. **C**. Higher magnification confocal image of IML from a transverse slice. Image represents composite of 19 consecutive images taken at 0.3 μm optical section thickness (5.7 μm total thickness). Note punctate labeling throughout the IML and surrounding region, includes some SPN somas and processes. **D**. Single image of 0.3 μm thickness, same slice as in C. Note co-expression of D_2Rs and GFP.

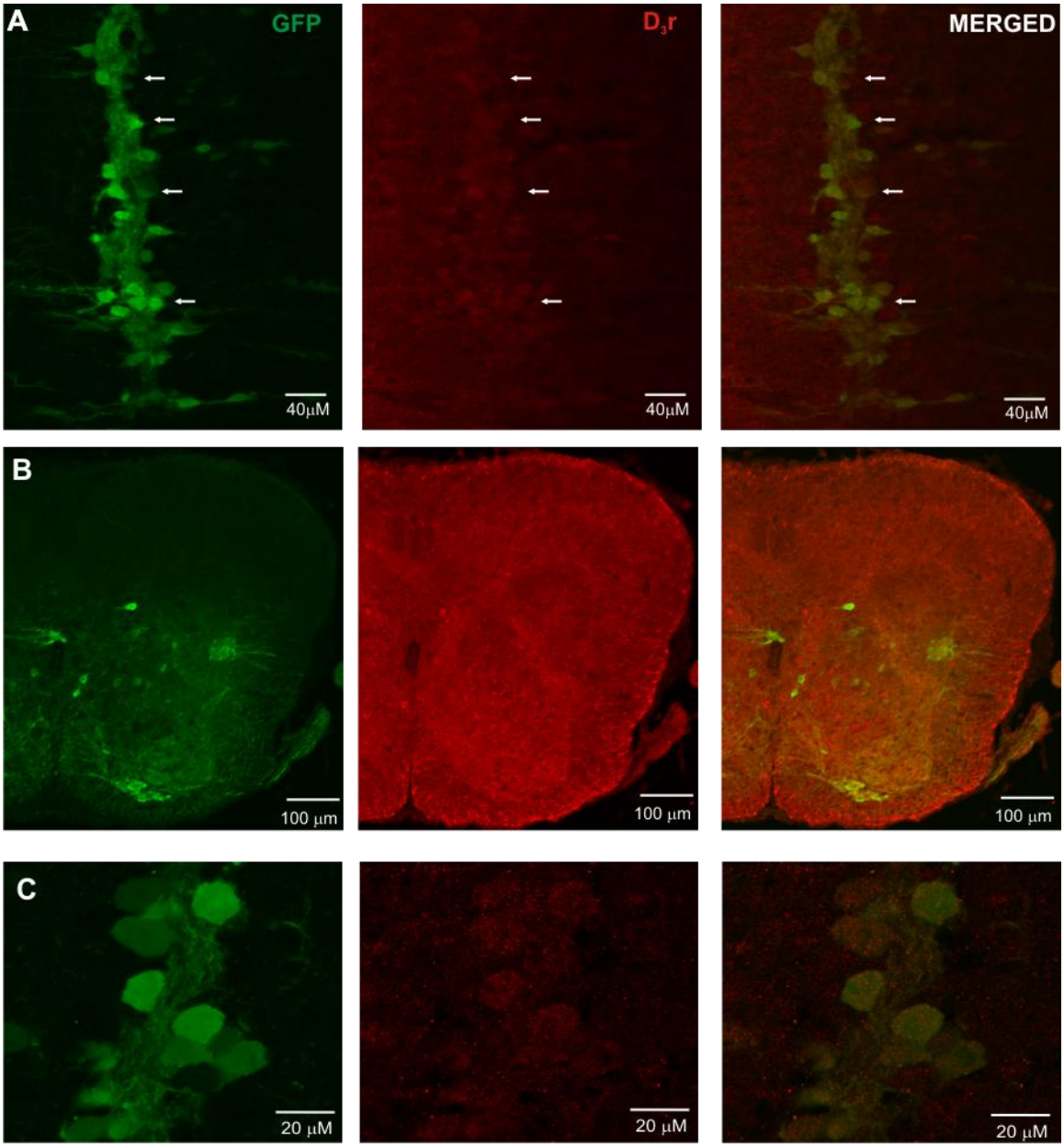

Figure 3.16 D_3 dopaminergic receptors.

A. Horizontal spinal cord slice 10 μm thick, just dorsal to the central canal; confocal image at low magnification. Left column, GFP labeling; middle, D_3 receptors; right, merged image. Note some co-labeled somas (arrows). **B**. Low magnification confocal image of a transverse spinal cord slice in a different animal, 10 μm thick. **C**. Higher magnification confocal image of IML from a transverse slice. Single image, 0.3 μm optical section thickness Note perisomatic labeling on SPNs.

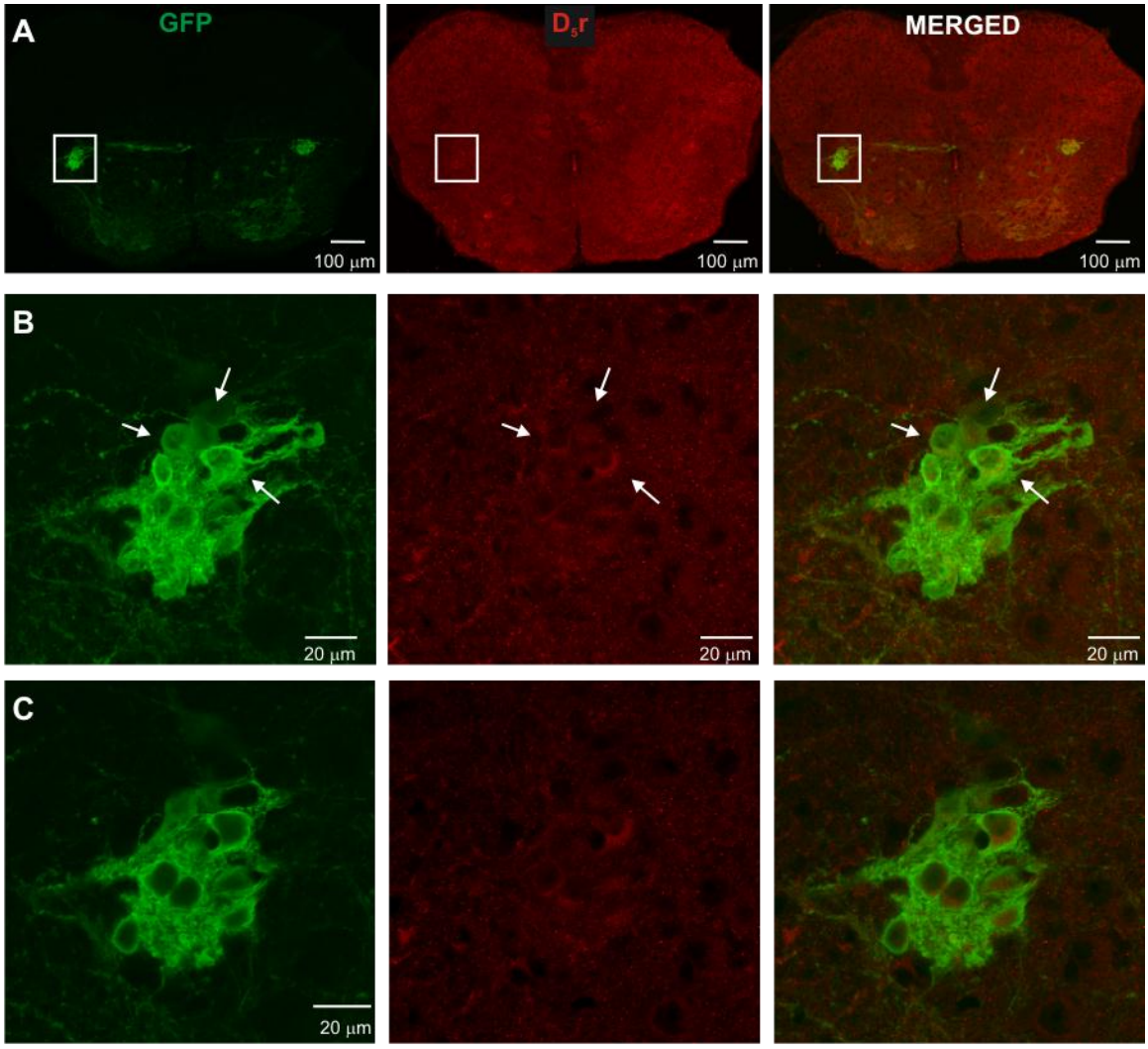

Figure 3.17 D_5 dopaminergic receptors.

A. Transverse spinal cord slice 10 μm thick, confocal image at low magnification. Left column, GFP labeling; middle, D_5 receptors; right, merged image. Note co-labeling in IML (boxed). **B**. Higher magnification confocal image of boxed region. Image represents composite of 20 consecutive images taken at 0.3 μm optical section thickness (6 μm total thickness). **C**. Single image of same region, 0.3 μm optical section thickness Note cytoplasmic labeling of SPNs.

3.5 DISCUSSION

While monoaminergic effects on SPNs have been partially explored in other species, I sought to compare the effects in the neonatal mouse to reported effects in the adult cat and neonatal rat. Additionally, I investigated what actions these descending systems usually have on overall SPN excitability, both by patch-clamp recordings of visually identified SPNs and population responses of SPNs and motoneurons in the ventral root. Lastly, I assessed how the monoamines modulate afferent evoked reflexes, given the conflicting reports.

3.5.1 Serotonin

5HT-induced membrane depolarizations and increases in input resistance are consistent with those reported in the neonatal rat in vitro [145, 155, 220]. 5HT also increased SPN responsiveness to current injections, which mimics incoming synaptic input. 5HT-induced depolarizations in the resting ventral root polarity and increased background activity in the ventral root reflect an overall excitatory action of 5HT on SPNs (see below for more detail). These overall increases in cellular excitability are also supported by reported increases in extracellular firing after iontophoretically applied 5HT in cats [89]. Interestingly, 5HT was also able to unmask rebound excitation in a proportion of SPNs, a trait crucial to the half-center oscillator models of central pattern generators [125]. In fact, intrathecal administration of 5HT has been shown to restore sympathetic rhythms in the rat tail after acute spinal cord transection [163].

The consistently positively coupled changes in SPN excitability are supported by our immunohistochemical results. Activation of both G_q and G_s coupled receptors increases

protein phosphorylation, including that of ion channels, increasing the general excitability of the neurons. Our immunohistochemistry identified 2 such serotonergic receptors on SPNs: $5HT_{2a}$ (G_q) and $5HT_7$ (G_s) receptors. Immunohistochemistry and electron microscopy in the rat previously showed the presence of $5HT_{2A}$ receptors in the IML, with mainly postsynaptic labeling on dendrites and somas, as well as some presynaptic labeling of axons in the ventral horn [240]. This axonal labeling is consistent with labeling of HB9 GFP^+ processes we found projecting dorso-ventrally from the IML. Additionally, the presence of $5HT_7$ receptors on SPNs is consistent with mild labeling reported in the cat and rat [189, 241]. The lack of G_i coupled 5HT receptors further reinforces the direct electrophysiologically shown enhanced excitability of SPNs.

3.5.2 Norepinephrine

In contrast to 5HT, NE elicited both depolarizations and hyperpolarizations of SPNs. These mixed membrane responses and accompanying changes in input resistance are consistent with activation of both α_1 and α_2 adrenergic receptors in the neonatal rat and adult cat [109, 179, 277, 278]. However, while previous electrophysiological evidence implied the presence of both G_i and G_s coupled adrenergic receptors, the relative density and location of the two receptor subtypes and the amount of NE released likely determines what functional consequences NE may have. The slight depolarizations and hyperpolarizations in the ventral root after NE application also imply mixed actions on the population of SPNs, and are consistent with this hypothesis. Populations of SPNs with differential recruitment and/or end targets may contribute to these mixed responses. In all my experiments, however, 10 μM NE increased SPN excitability and led to large increases in activity in the ventral root, suggesting a dominance of α_1 receptor activation.

Our immunohistochemical studies support these actions, showing the presence of both α_{1a} and α_{2a} receptors on SPN somas and processes. This is consistent with previous immunohistochemical and autoradiographic studies showing the existence of α_{1a} and α_{2a} receptors near the IML and in lamina X in the rat spinal cord [57, 230, 243]. The presence of both receptors, however, suggests the preferential activation of one based on dosage used, an hypothesis to be explored at a later date.

3.5.3 Dopamine

The actions of dopamine on SPNs seem to be the most complex of the monoamines studied. In the patch studies of SPNs, both depolarizations and hyperpolarizations were observed after applications of 10μM, but these were not consistently linked with changes in input resistance, suggesting indirect actions as well as direct actions of DA. When net potential changes were assessed in the ventral roots, polarity shifts were dose dependent, with low doses producing a depolarization and higher doses producing a hyperpolarization. These dose-dependent effects on efferent polarity are consistent with those reported in the pre-frontal cortex, where low doses of DA preferentially activated $D_{1\text{-like}}$ receptor pathways and higher doses of DA masked these effects by activation of $D_{2\text{-like}}$ effects [254, 280]. These results imply the presence and preferential activation of both $D_{1\text{-like}}$ (G_s-coupled) and $D_{2\text{-like}}$ (G_i-coupled) receptors on SPNs. Again, given the electrophysiological differences described in Chapter 2, these may reflect differential effects based on SPN subpopulation.

Our immunohistochemistry indicated the presence of both G_i-coupled (D_2 and D_3) and G_s-coupled (D_5) receptors on SPNs, both somas and processes. D_2 and D_3 labeling much

more specifically targeted SPNs and motoneurons, while D_5 labeling was diffuse throughout the spinal cord. The exact implications of this are yet unclear, but indicate a complex modulatory ability of dopamine based on dose- and location- dependent preferential binding of receptors.

3.5.4 Ventral Root Recordings and Visceral Afferent Mediated Reflexes

While the thoracic ventral roots T_{11}-T_{12} are predominantly SPN axons, there is a sizeable minority of somatic motoneurons as well [18, 50, 154]. Hence, in the absence of selective recordings from muscles (whose activity was blocked with pancuronium), I cannot exclude the possibility that evoked actions from visceral afferents or MA-induced changes in resting ventral root activity reflect changes exclusively in somatic or sympathetic efferents. In fact, stimulation of splanchnic afferents has been shown to evoke both autonomic and somatic motor spinal reflexes [4, 52, 64, 81, 136]. Yet even with mixed sympathetic and somatic motor output recorded in the ventral roots, the monoamines have been shown to have similar effects on both somato-sympathetic and somatic-somatic reflexes, with descending monoaminergic centers generally depressing the evoked reflexes (e.g. [47, 88, 156, 264]). Here we extend these findings to visceral afferent mediated spinal reflexes.

While the monoamines predominantly increased excitability of SPNs and motoneurons, visceral afferent mediated reflexes were depressed by 5HT, DA, and NA, in a dose-dependent fashion. Given the generally increased excitability of spinal efferents but decreased reflex response, the monoamines are likely acting on a site earlier in the reflex pathway than the motoneurons and SPNs. Moreover, this dichotomy of action

functionally implies that in the presence of the monoamines, there is a dose-dependent decoupling of output from visceral input, shifting the system to a central-drive only model.

Moreover, both 5HT and NE depressed spontaneous VRPs while concomitantly increasing background ventral root activity in a rhythmic manner. This likely reflects a decrease in synaptic transmission from intrinsic spinal circuits, yet an increase in the overall excitability and rhythmogenic capability of efferent neurons. However, an increase in the background activity may have secondary consequences on how easily the efferents are recruited. Inasmuch as the ventral root recordings reflect sympathetic output, decreased recruitment for both spontaneous and visceral afferent-evoked VRPs may be at least partially due to activity-dependent depression of recruitment. In SPNs, this decreased excitability after high intensity activity has been termed the "sympathetic silent period", and had been well documented by a number of investigators [171, 200, 224]. Indirect mechanisms of monoaminergic depression may therefore also contribute to the observed effects.

In conclusion, the present study shows that the monoamines can modulate sympathetic excitability in a complex fashion. By creating a novel metric for measuring changes in SPN excitability, this study also showed the flaws in assuming actions on resting membrane potential are always linked to changes in cellular excitability. 5HT consistently acts to increase SPN excitability, and potentially modifies the cellular properties to allow for rhythmogenesis. The actions of DA and NA are more complex, consistent with the dual presence of G_i and G_s coupled receptors for these modulators. The actions of all three monoamines depress visceral afferent mediated reflexes,

suggesting differential amplification of autonomic inflow and outflow from the spinal cord. This dichotomy will be further explored in Chapter 4.

CHAPTER 4

MODULATION OF VISCERAL AFFERENT MEDIATED REFLEXES AND PRESYNAPTIC INHIBITION

4.1 ABSTRACT

Stimulation of splanchnic afferents has been shown to evoke both autonomic and somatic spinal reflexes, and in the previous chapter I showed that the monoamines inhibit visceral-afferent evoked reflexes but directly excite SPNs. To date, no one has systematically investigated the site(s) of action of monoaminergic depression of visceral afferent mediated reflexes.

One of the most effective means of inhibiting afferent inflow is via presynaptic inhibition (PSI), yet there are conflicting reports whether visceral afferents exhibit PSI. The current study represents the first characterization of primary afferent depolarization-based PSI in mouse by visceral (splanchnic) afferents, and the first characterization in any species of the modulation of visceral primary afferent neurotransmission by the descending monoaminergic transmitters dopamine (DA), noradrenaline (NE), and serotonin (5-HT).

The major splanchnic nerve is a mixed nerve, comprised of SPNs, postganglionics, and $CGRP^{+}$ visceral afferents. Stimulation of this nerve leads to both dorsal and ventral root volleys, identified as afferent antidromic and SPN orthodromic compound action potentials, respectively. Subsequent Ca^{2+} -sensitive (synaptic transmission-dependent) dorsal root potentials (DRPs) and ventral root potentials (VRPs) were evoked, with the DRPs slower in onset than the VRPs. Simultaneous extracellular field potential (EFP)

recordings identified intraspinal sites of visceral afferent transmission, with prominent actions in the deep dorsal horn.

5HT reversibly and dose-dependently depolarized the resting dorsal root DC recordings and depressed the evoked DRP. Coupled with depression of the shortest latency EFP, 5HT depression of visceral afferent transmission and PSI are supported.

NE dose-dependently depressed the visceral afferent-evoked DRP at slightly higher efficacy than 5HT, but its actions were only partially reversible. Like 5HT, NE depressed the evoked EFP, suggesting actions on multiple sites of PSI circuitry.

DA also dose-dependently depressed the visceral afferent evoked DRP, but with much lower efficacy than 5HT or NE. This, and observed mixed actions on the dorsal root DC recordings and EFP suggest a more distinct control of the PSI circuitry by DA.

The monoamines also depressed the VRP. As this occurred with differing time- and dose-dependence, reflex depression at multiple sites for all transmitters are suggested. Overall, I conclude that the monoamines act to both depress afferent transmission (↓EFP) and facilitate selective afferent transmission (↓ DRP), resulting in a complex modulatory regulation of afferent input.

4.2 INTRODUCTION

Sensory information from viscera reaches the spinal cord largely through sympathetic nerves [13, 17, 229]. While visceral afferents only comprise a small percentage of DRG neurons in the thoracolumbar spinal regions [38, 134, 188], they project more diffusely than their somatic counterparts, often travelling multiple segments in the rostrocaudal

direction ([37, 65, 246]; see also Figure 4.1). Visceral afferents also have distinct spinal projection patterns from many of their somatic counterparts. Most spinal visceral afferents terminate in lamina I or in the deep dorsal horn (laminae IV-V), with a few collaterals reaching near lamina X [37, 188, 247]. Electrical stimulation of the greater splanchnic nerves has often been used to study visceral afferent inflow (e.g. [4, 64, 225, 251]), as they contains afferents of the gut, pancreas, spleen, kidneys, testis/ovaries, and pelvic organs [187]. Stimulation of splanchnic afferents has been shown to evoke both autonomic and somatic motor spinal reflexes [3, 4, 52, 64, 81, 136].

Monoaminergic systems descending from the brainstem have profound modulatory actions on both motor output and sensory input [15, 160, 193, 262]. However, given the relative scarcity of visceral to somatic afferent input, neuromodulation of visceral afferent input needs to be specifically addressed. Studies using visceromotor and pressor responses to colorectal distension in the awake rat have indicated antinociceptive actions of NE and 5HT [55, 56], and one study of spinal micturition reflexes has suggested inhibitory actions of DA [271]. Aside from our work detailed in Chapter 3, no one has systematically investigated the site of action and dose-dependent modulation of visceral afferent mediated reflexes.

Additionally, one of the most effective means of inhibiting afferent inflow is presynaptic inhibition (PSI), which can be seen as a summed, back propagated depolarization of primary afferent terminals (primary afferent depolarization, or PAD) [219]. Traditionally thought to be mediated by trisynaptic circuitry with last order GABAergic interneurons [102, 219], selective patterns of PAD are found in subsets of group I and II muscle and cutaneous afferents (e.g. [27, 28, 121, 213]). In spinal visceral afferents, PAD has been shown

in response to splanchnic nerve and sympathetic chain stimulation [228], while conditioning with splanchnic stimulation inhibited the intercostal-intercostal reflex in decerebrate and acute spinal cats [64]. While descending monoaminergic systems have been shown to play a strong role in sensory processing in spinal interneurons [84, 119] and modulating PAD in somatic afferents [24, 75], no one has studied whether these systems have actions on visceral afferent mediated PAD, nor whether these actions are consistent with those seen in somatic nerves.

In order to address these questions, we developed an in vitro spinal cord- sympathetic chain preparation in the neonatal mouse. This preparation allowed us to record both reflex responses and PAD to splanchnic nerve or sympathetic chain stimulation. Compared to *in vivo* models, this *in vitro* model allows for greater accessibility and pharmacological control of the environment as well as the avoidance of anesthetics, which can have a detrimental effect on the known mechanisms of PAD generation [80, 132]. The current study represents the first characterization of spinal visceral afferent-induced PAD in an *in vitro* model and the first in any model of visceral-evoked PAD modulation by the descending monoaminergic systems dopamine (DA), norepinephrine (NE), and serotonin (5HT).

4.3 MATERIALS AND METHODS

All procedures described here comply with the principles of The Care and Use of Animals outlined by the American Physiological Society and was approved by the Emory University Institutional Animal Care and Use Committee.

4.3.1 Dissection

All experiments were performed at postnatal day 5-8 litter of mice crossed from transgenic hemizygote HB9-eGFP females (JAX laboratories) and inbred C57/BL6 males. Mice were either HB9-eGFP$^{+/-}$ heterozygotes or wild type. Dissection followed the same protocols described in Chapter 3 for neonatal animals. Briefly, animals were decapitated and eviscerated, and a dorsal laminectomy and ventral vertebrectomy were performed in low-Ca^{2+}, high-Mg^{2-} ACSF to expose the dorsal and ventral sides of the spinal cord from the upper cervical region to the midsacral level. The splanchnic nerve was identified and cut midway between the sympathetic chain and the celiac ganglia. The perfusion solution was then switched to regular ACSF, and to limit movement of the preparation, 25 μM pancuronium bromide (Sigma-Aldrich) was added.

4.3.2 Recording Configuration

The recording configuration was also similar to that described in Chapter 3, and the recording configuration for most experiments can be seen in **Figure 4.1**. Briefly, slow potentials in spinal dorsal and ventral roots were recorded with bipolar glass suction electrodes (**Figure 4.2**). Visceral afferents were activated by stimulating the splanchnic nerve or sympathetic chain at a rate of .0167 Hz (once every 60s), as higher frequency stimuli were susceptible to depression [221]. This stimulation frequency was therefore used for subsequent experiments. Slow potentials were recorded from the T11-T13 dorsal and ventral roots with a custom built 4 channel DC amplifier.

Ventral root potentials (VRPs) in response to afferent stimulation were interpreted as compound excitatory postsynaptic potentials (EPSPs) of combined somatic and

sympathetic efferents. Dorsal root potentials (DRPs) are produced as a result of electrotonically back-propagating depolarizing potentials in primary afferent terminals. Primary afferent depolarization (PAD) at terminals leads to presynaptic inhibition by reducing transmitter release [219], so the slow DRPs were used as a measure of the magnitude on PAD-evoked presynaptic inhibition. DRPs were recorded with a suction electrode attached *en passant* to the root as close to the entry zone as possible to minimize electrotonic decay (**Figure 4.1 and 4.2**).

Electrical stimulation of the splanchnic nerve evoked short latency spiking components in the dorsal root recordings (**Figure 4.2**). These are orthodromically propagating population spikes in recruited afferent fibers and are discussed in more details in the Results section 4.4.2.

Neural activity was collected on a custom built 4 channel direct current amplifier, low pass filtered at 3 kHz, and digitized at 5 kHz (Digidata 1340, Molecular Devices) and recorded in Clampex (Molecular Devices) for

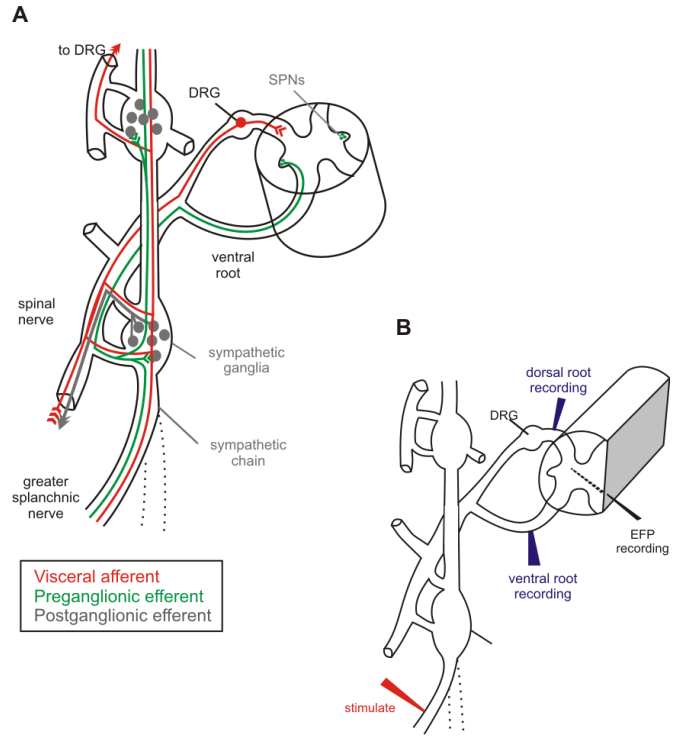

Figure 4.1 Sympathetic chain anatomy.

A. Schematic of the sympathetic chain and its connections to the spinal cord. **B**. Schematic of recording configuration, with stimulating electrode on greater splanchnic nerve and recording electrodes on dorsal and ventral roots. Field potential electrode penetrates into dorsal horn from cut surface of spinal cord.

off-line analysis.

4.3.3 Extracellular Field Potentials

When extracellular field potentials (**EFPs**) were recorded, a 2/3 sagittal section of the spinal cord was completed using fine insect pins. Micropipettes (tip diameter 1-2 μm, resistance 4-7 MΩ) were filled with 2 M KCl and penetrated the cut surface of the spinal cord at an approximately 35º angle until EFPs were seen. EFPs reflect population membrane voltage changes in the neurons around the tip of the electrode. Recording locations were approximated after the experiment using a transverse picture of the sectioned spinal cord, distance from the surface of the spinal cord marked during the experiment, and approximate angle of micropipette penetration (see **Figure 4.1B** for schematic and **Figure 4.6C** for estimated recording positions).

4.3.4 Drug Solutions and Applications

Stock solutions of drugs (10-100 mM) were made and stored at -20 ºC until needed. All drugs were dissolved in regular ACSF and perfused through the gravity perfusion line. For time response trials, 5-10μM of 5-hydroxytryptamine HCl (5HT), norepinephrine bitartrate (NE), or dopamine HCL (DA), all from SIGMA ALDRICH, was applied for 10 minutes, then washed out with regular ACSF + pancuronium for at least 30 minutes. For dose-response trials, increasing dosages of 5HT, NE, or DA were applied cumulatively, with 10 minutes in between each dose increment.

4.3.5 Data Analysis

The analysis methods described in Chapter 3 were again used for VRPs, DRPs, and when collected, EFPs. Changes were assessed in the spinal roots for both the evoked responses and changes in DC resting potential. A custom built MATLAB program was used to subtract the baseline values prior to the stimulus, low-pass filter the response at 100Hz, find the onset of the compound EPSP, peak of the response, and the integral under the filtered root response from onset to offset (defined as the time at which the slow potential decayed to 1/3 peak amplitude). Responses were averaged for the last 5 minutes of each drug dose increment for dose response curves. Changes in spinal root resting potentials were calculated using the mean baseline values for the last 5 minutes of each drug dose increment. In order to minimize effects of differences in suction in the recording electrodes, both evoked and resting ventral root potentials were normalized to baseline evoked values. Statistics were completed using a two-tailed paired t-test in Microsoft Excel. Timing of 1st afferent spikes was assessed visually in Clampfit (Molecular Devices).

4.3.6 Immunohistochemistry

For immunohistochemistry, the splanchnic nerve and sympathetic chain connecting the rostral three ganglia were isolated using the dissection described above. Sympathetic chains were fixed in 4% paraformaldehyde for 1 hour, then cyroprotected in 10% sucrose plus 0.1 M PO_3 (pH 7.4) and stored at 4^o C. Before staining, chains were washed overnight in 0.1M PO_3 buffered saline (PBS), then incubated with primary antibodies CGRP (goat, AbD Serotec, 1:200), TH (rabbit, Millipore, 1:1000), and anti-GFP (chicken, AbCam, 1:1000) for 48 hours at 4^o C, then washed three times in PBS-t for 30

minutes each at room temperature. Primary antibodies were stained with Alexa488 anti-chicken (diluted 1:100), cy3 anti-goat (diluted 1:250), and cy5 anti-rabbit (diluted 1:100) secondary antibodies, all from Jackson Immunoresearch.

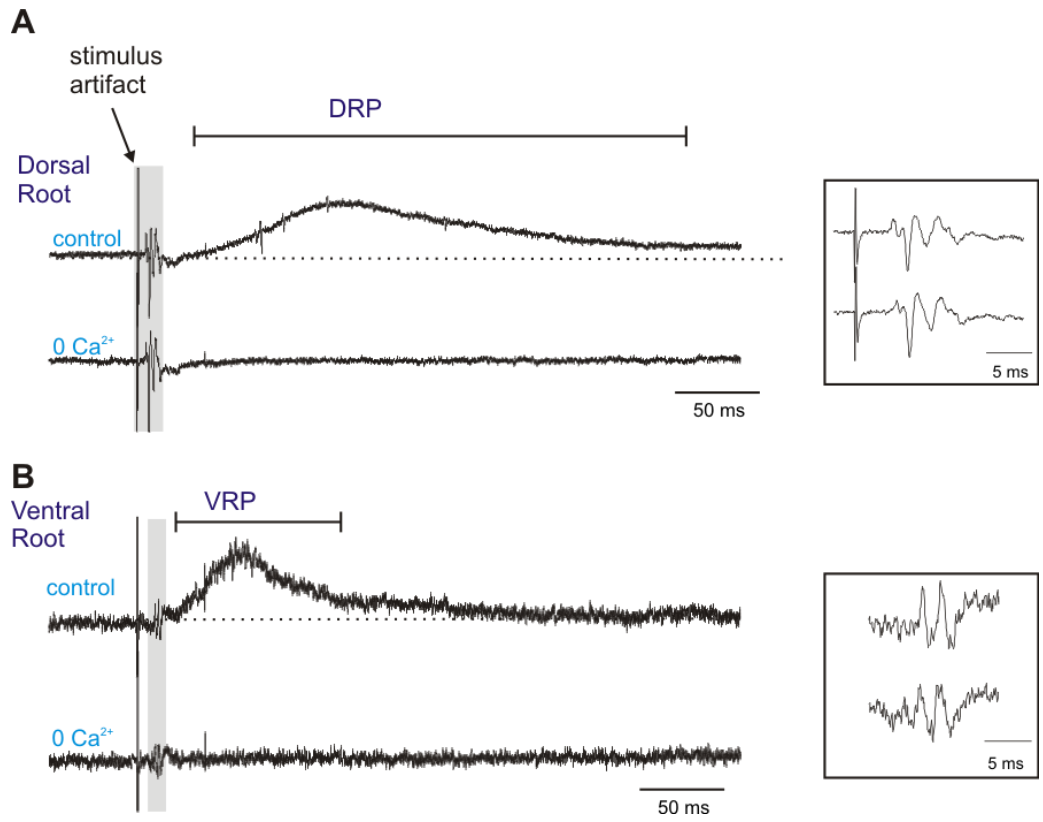

Figure 4.2 Example of events observed following splanchnic nerve stimulation.

Sample recorded dorsal root potential (DRP) recorded at dorsal root entry zone (**A**) and ventral root potential (VRP) recorded at ventral near exit from cord (**B**), both of which disappear with 0 Ca2+ aCSF (bottom traces). In A, DRP, with higher magnification of grey boxed orthodromic afferent spiking is shown at right. In B, VRP, with higher magnification of grey boxed antidromic spiking of SPNs is shown at right.

4.4 RESULTS

4.4.1 Composition of the Major Splanchnic Nerve and Sympathetic Chain

While many studies have shown that visceral afferents project to DRGs several segments away from their spinal nerves [37, 65, 246], few have suggested they reach the appropriate DRGs by traveling within the sympathetic chain [5, 13]. I therefore sought to confirm the presence of afferents in the sympathetic chain and major splanchnic nerve in the neonatal mouse model system. I used fixed tissue of dissected whole mounts of the major splanchnic nerve and sympathetic chain and immunohistochemistry coupled with cumulative stacks of confocal sections.

As calcitonin gene-related peptide (**CGRP**) is a peptide found in about 40-50% of dorsal root ganglia neurons, with a particularly strong preference for labeling visceral afferents [127, 149, 182], I identified $CGRP^+$ axons as afferents. I compared the pattern of $CGRP^+$ staining to tyrosine hydroxylase (**TH**), a marker for sympathetic postganglionic neurons [113]. TH is the first and rate-limiting enzyme involved in catecholamine synthesis [185]. Triple labeling for CGRP, TH, and HB9-GFP therefore assessed in the isolated sympathetic chain and greater splanchnic nerve the relative abundance of visceral afferent, postganglionic, and preganglionic axons, respectively.

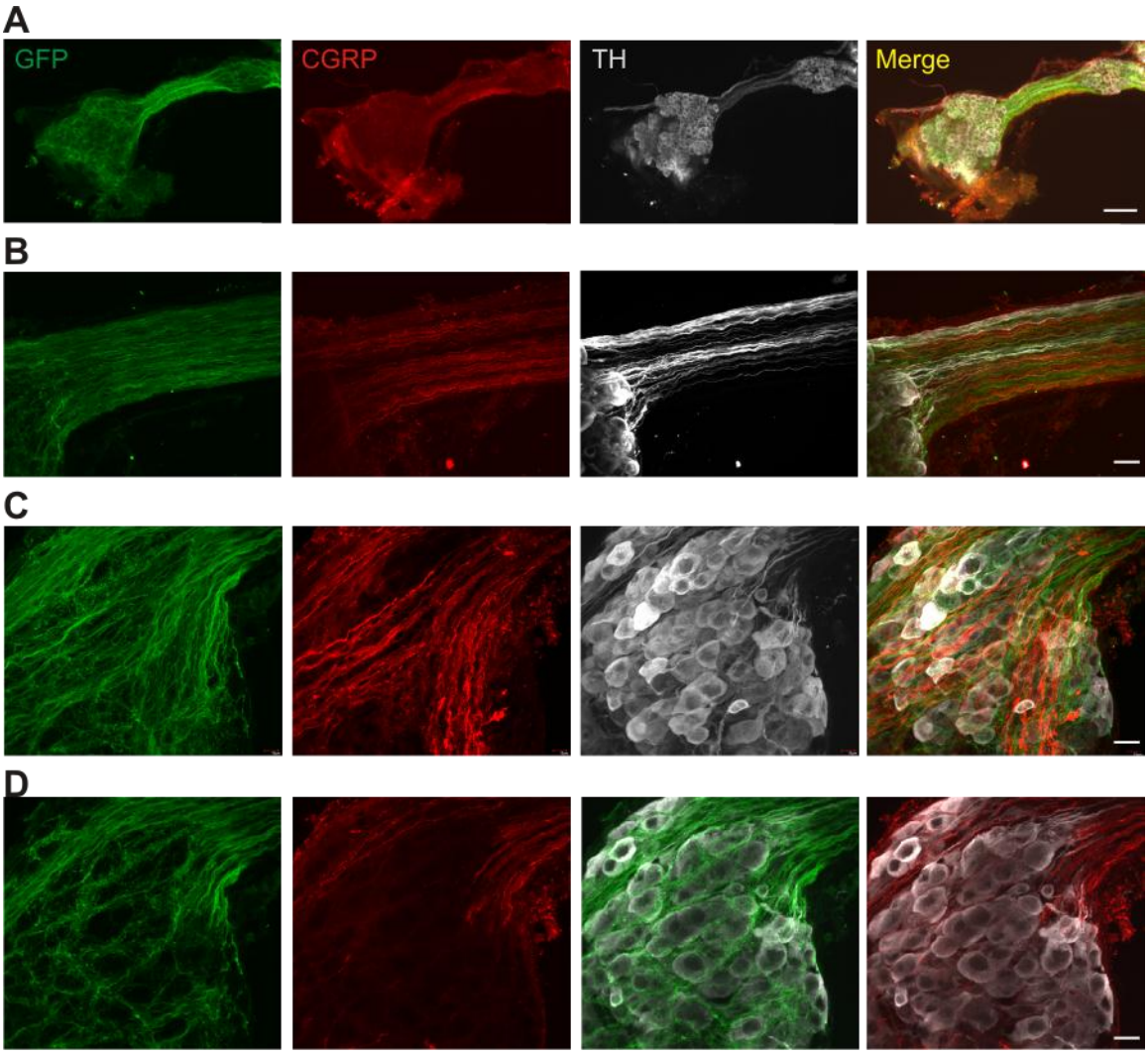

Figure 4.3 Axon fiber composition in paravertebral ganglia.

A. Lower power image of two sympathetic ganglia and connecting nerve bridge, showing nerve contains a mixture of at least 3 neurochemically distinct fiber populations: sympathetic preganglionics (SPNs), $CGRP^+$ visceral afferents, and TH^+ sympathetic postganglionics. **B**. SPNs (GFP^+), CGRP and TH immunolabeled axons in axon bundle between two sympathetic ganglia. Image represents composite of 73 consecutive confocal images taken at 0.38 μm optical section thickness (27.74 μm total thickness). **C**. SPNs (GFP^+), CGRP and TH immunolabeling in a sympathetic ganglion. Image is a collapsed stack of 35 consecutive confocal images taken at 0.38 μm optical section thickness (13.3 μm total thickness). **D**. Thinner section in central region of ganglia to show that while SPNs appear to form basket-like synapses around postganglionics, $CGRP^+$ afferents do not project through this region. Image is a collapsed stack of 11 consecutive confocal images (4.18 μm total). Scale bar is 100 μm in A and 20 μm in B-D.

I observed that axon bundles between ganglia contained considerable numbers of all three axon fiber types (**Figure 4.3B**). Within the ganglia, while many GFP^+ axons avoided the TH^+ somas entirely, many also appeared to synapse on TH^+ somas. In contrast, almost all $CGRP^+$ axons projected outside the region of TH^+ postganglionic somas, and there was no evidence of $CGRP^+$ afferents forming synapses on postganglionic cell somas (**Figure 4.3D**). Additionally no double labeling was seen for any of these makers, cleanly identifying these 3 axon fibers as distinct neurochemically-identifiable populations.

4.4.2 Splanchnic Nerve Stimulation Activates Spinal Reflexes and Primary Afferent Depolarization

Similar to peripheral muscle and cutaneous nerve stimulation, splanchnic nerve visceral afferent stimulation activated reflexes and slow VRPs in the ventral roots as well as slow dorsal root potentials (DRPs). Due to the mixed afferent/efferent composition of the splanchnic nerve, these slow potentials are preceded by orthodromic volleys in the dorsal roots and antidromic volleys in the ventral roots. Direct electrical recruitment of axons was verified by their persistence following block of chemical synaptic transmission after exchanging the bath to a nominally Ca^{2+} free ACSF (see **Figure 4.2B**). The presence of orthodromic afferent volleys was examined and found in roots as far rostral as T6, supporting projections to multiple spinal segments of afferents originating in the greater splanchnic nerve [13].

While afferent volleys and ventral root reflexes could be recruited at stimulus intensities as low as 8 μA, 50 μs, greater stimulus intensities were often required to elicit a DRP **Figure 4.4** provides an example of the relationship between stimulus intensity and the

recruitment of spike volleys, DRPs, and VRPs. Stimulus intensities above 100 μA/100 μs did not further increase DRP recruitment (**Figure 4.4A**), so this value was chosen for subsequent studies on neuromodulation. On average, the DRP was onset was 31.7 ± 6.1 ms after arrival of the first afferent volley, while the VRP onset was at 11.4 ± 8.0 ms (n=17). The onset of the VRP always preceded the DRP therefore, on average by 19.8 ± 8.4 ms. DRPs lasted on average 565.6 ± 11.8 ms, reaching its peak 50.1 ± 10.1 ms after onset. In 10/17 cases, the evoked DRP was accompanied by dorsal root reflexes (**Figure 4.2C**). Dorsal root reflexes represent a primary afferent depolarization of sufficient magnitude to be supra-threshold for action potential initiation in afferent terminals.

In addition to being quicker in onset than the DRP, the VRP had a lower threshold for recruitment in all stimulus intensity trials (n=4/4), suggesting that the circuitry responsible for evoking the VRP includes a distinct shorter latency pathway (**Figure 4.4B**). While the visceral afferent- evoked VRP could follow stimulation up to 5 Hz without depression, the DRP was unable to follow stimulus frequencies greater than .0167 Hz (see **Figure 4.4C**). Overall, these differences in onset, frequency sensitivity and threshold for recruitment all support the notion that evoked DRPs and VRPs are mediated by distinct circuits.

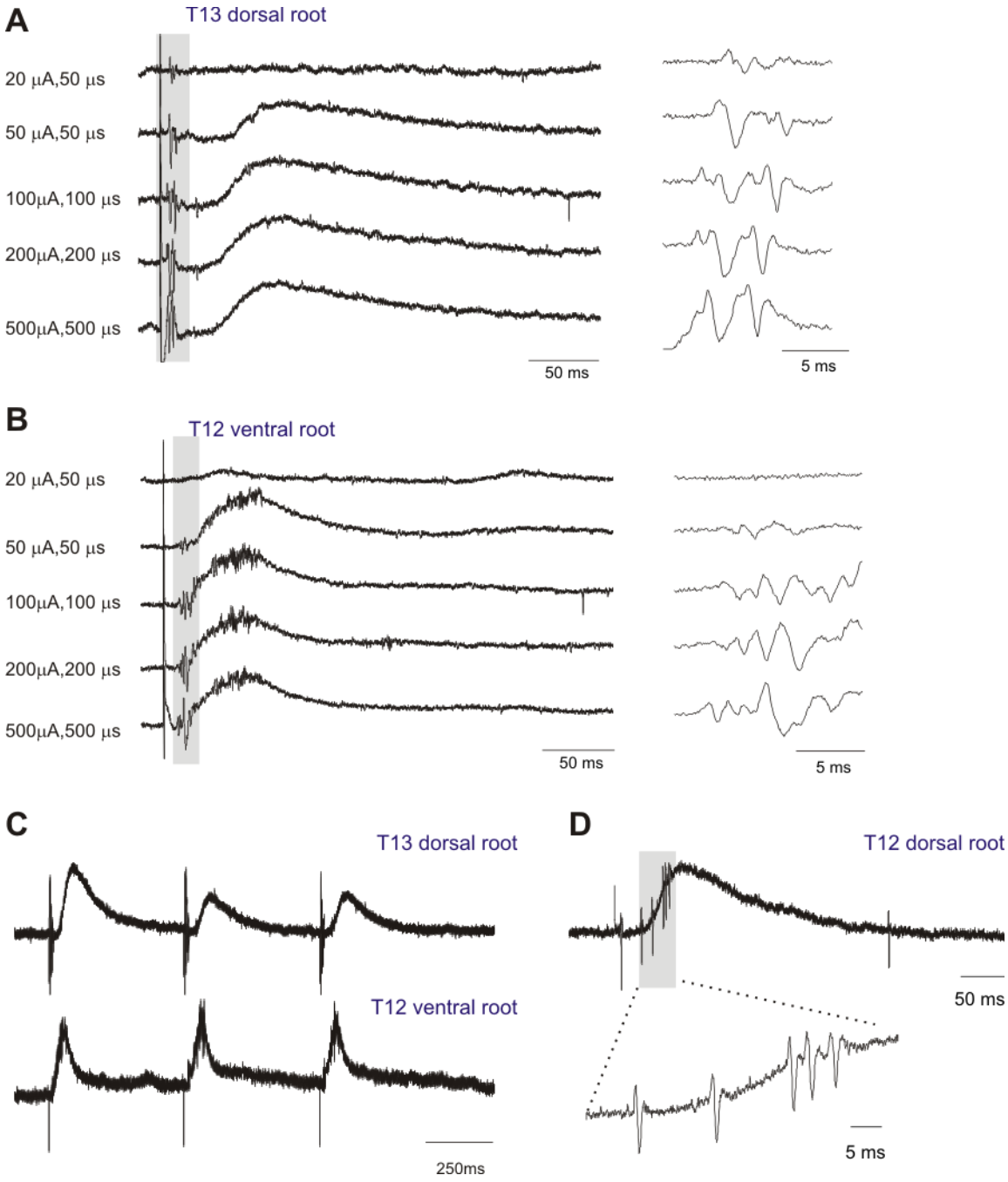

Figure 4.4 Differences in properties of DRPs and VRPs.

A. Increasing stimulus intensities lead to increased afferent volleys and subsequent DRPs. Each trace is an average of 5 sweeps. Note intensities greater than 100,100 increase afferent volleys (grey box), but not DRP. **B**. Increasing stimulus intensities and effects on VRP. Notice onset and duration difference between DRP and VRP. Grey box denotes orthodromic volleys, seen at higher magnification on the right. **C**. The DRP undergoes frequency dependent depression (here 2Hz). Note this is not the case for the VRP which can follow frequencies up to 5 Hz. **D**. Single trace of dorsal root from another experiment. Grey box and higher magnification below show an example of dorsal root reflexes evoked.

I further examined the relationships between afferent fiber recruitment and the generation of the DRP. The DRP did not appear to be recruited following activation of the lowest threshold afferents. While lower stimulus intensities recruited fast conducting afferent volley(s), the DRP was not recruited until a larger stimulus intensity was used (**Figure 4.4A**). This can be seen in even more detail by analyzing individual traces with a stimulus intensity that recruits DRPs only a fraction of the time (i.e. when stimuli are near the DRP threshold). Only when the stimulus successfully recruited additional, slower-conducting afferents was a DRP observed (**Figure 4.5A**). Additionally, DRP generation was widespread throughout the thoracic spinal cord, as DRPs were recorded at the spinal levels sampled (T_9-T_{13}) with similar shape and onset (**Figure 4.5B**). This suggests that visceral-afferent induced PAD is systemic throughout the thoracic spinal cord, and is consistent with the reported actions of somatosensory evoked PAD [146].

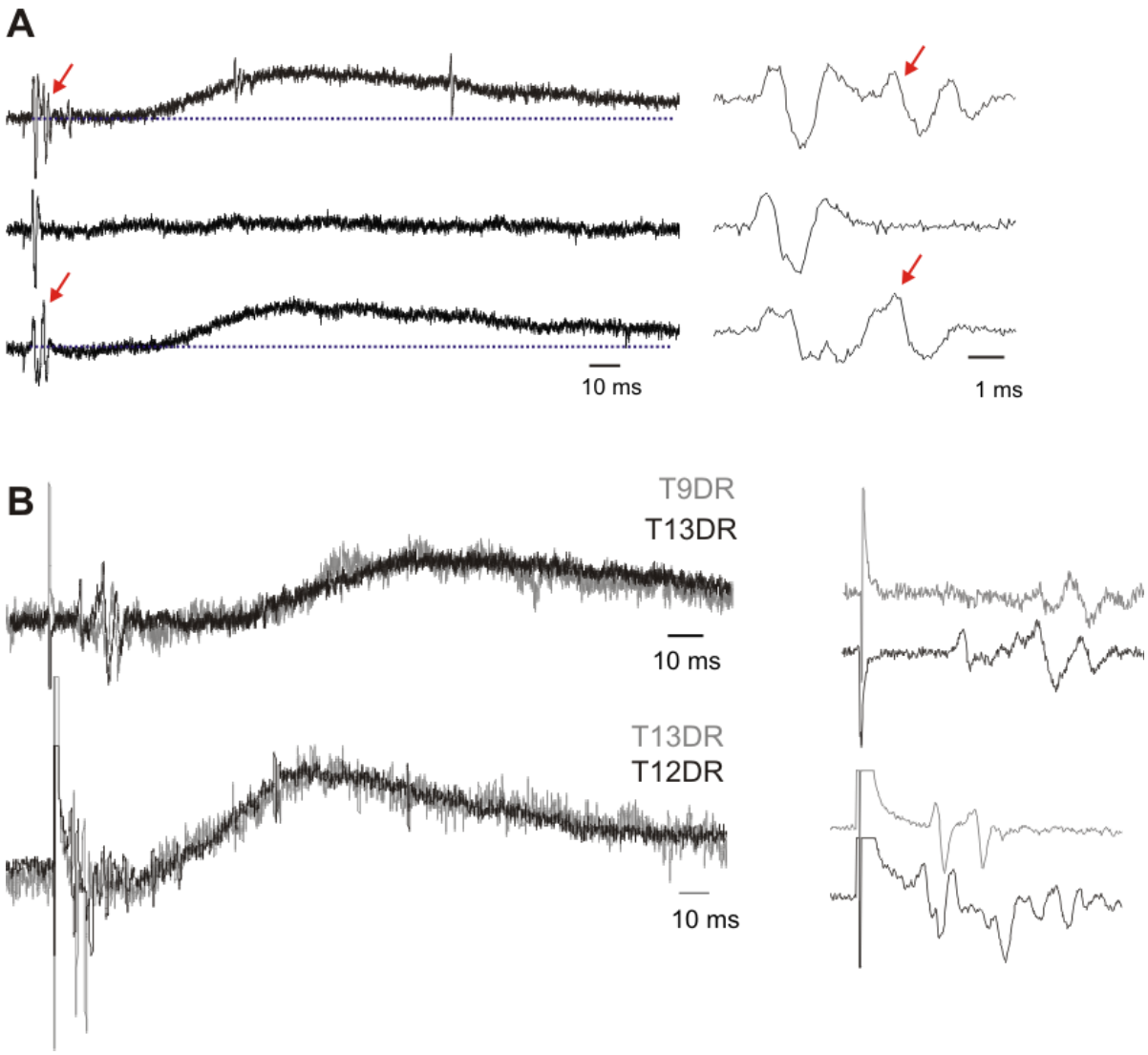

Figure 4.5 Relation between DRP, afferent fiber volley, and spinal segmental distribution.

A. Several single dorsal root traces are shown at a stimulus intensity that straddled threshold for DRP recruitment. Note that when the 2nd afferent spike is not present, no DRP is evoked (arrows). **B**. Comparison within the same animal of DRPs evoked in multiple roots. Top traces, T9 and T13 dorsal roots superimposed. Bottom traces, T12 and T13 dorsal roots superimposed in a different animal. Right panels show higher magnification of afferent volleys. Note that the later afferent volleys are similarly timed in roots as far as 4 spinal segments apart. Note also that DRPs are completely superimposable.

4.4.3 Extracellular Field Potentials

Intraspinal recordings were performed to examine monoamine transmitter modulation of population synaptic transmission. Extracellular field potentials (**EFPs**) reflect the postsynaptic transmembrane voltage changes evoked in the population of neurons around the tip of the electrode, here presumed to be population postsynaptic potentials. Short-latency EFPs have been used to report population monosynaptic afferent transmission [121, 206, 213]. The electro-anatomic location of splanchnic visceral afferent-evoked EFPs were estimated using systematic field potential tracking, with starting locations 100-400 μm below the ventral surface of the spinal cord and dorsally-angled penetrations up to 1100 μm. **Figure 4.6** shows approximate regions of the spinal cord where EFPs were recorded. EFPs were consistently estimated to be maximal in the deep dorsal horn, with evidence of an earlier arriving EFP in some tracks in the superficial dorsal horn. This is consistent with known afferent termination sites of visceral afferents [37, 188, 247].

The earliest onset of EFP in the deep dorsal horn was found to occur 4.5 ms after the first dorsal root afferent volley was seen, with a mean of 13.1 ± 6.9 ms across trials. Onset variability within an individual preparation reflects the ability to elicit an EFP in many regions in the dorsal horn. Interestingly, the largest amplitude EFP responses were not necessarily the earliest in onset, and had onsets 15.4 ± 5.8 ms after the first afferent spike was seen (occurring on average 20.6 ± 8.8 ms before onset of the DRP and often beginning before the VRP). Synaptic transmission at room temperature requires ~3ms [123], so the observed central latency is sufficiently long enough to be di- or tri-synaptic from the fastest arriving afferents volleys, or potentially monosynaptic from a later, slower conducting afferent fiber set (**see Figure 4.5**). Regardless of whether the EFP

reflects monosynaptic actions from slower conducting afferents or polysynaptic actions, modulation of the evoked EFP would indicate actions on afferent pathways located within the deep dorsal horn.

4.4.4 Monoaminergic Depression of Evoked Dorsal Root Potentials and Field Potentials

Visceral-afferent evoked DRPs were depressed with single dose applications of 5HT, NE, and DA, with differing efficacies. At 10μM, 5HT depressed the evoked DRP to a mean of 10.1 ± 10.5% of control (n=3, p=.004). At 5-10μM, NE also significantly depressed the evoked DRP to 6.4± 3.7% of control (n=3, $p=5e^{-4}$). At 10μM, DA depressed the DRP amplitude but to a lesser degree (to 39.8 ± 27.8% of control; n=6, p=.003). The largest amplitude evoked EFPs were used to assess monoaminergic modulation of afferent synaptic transmission. 5HT and NE depressed the EFP to a mean 27.7 ± 9.7 % and 12.1 ±5.4% of peak values, respectively (**Figure 4.7A and B**). DA had variable effects on the EFP: substantial depression in 2/4 preparations, partial depression in ¼ preparation, and facilitation in ¼ preparation, resulting in a mean depression of 61.5 ± 54.8% (n=4; **Figure 4.7C**). Interestingly, 5HT also induced a slight delay in afferent spike timing in the dorsal root (box, **Figure 4.7A**), indicating direct actions on the afferents themselves. The above depression in evoked EFP and DRP responses to 5HT, NE, and DA was not accompanied by a change in afferent volley amplitudes recorded in the dorsal root, indicating that the monoamines must be acting centrally.

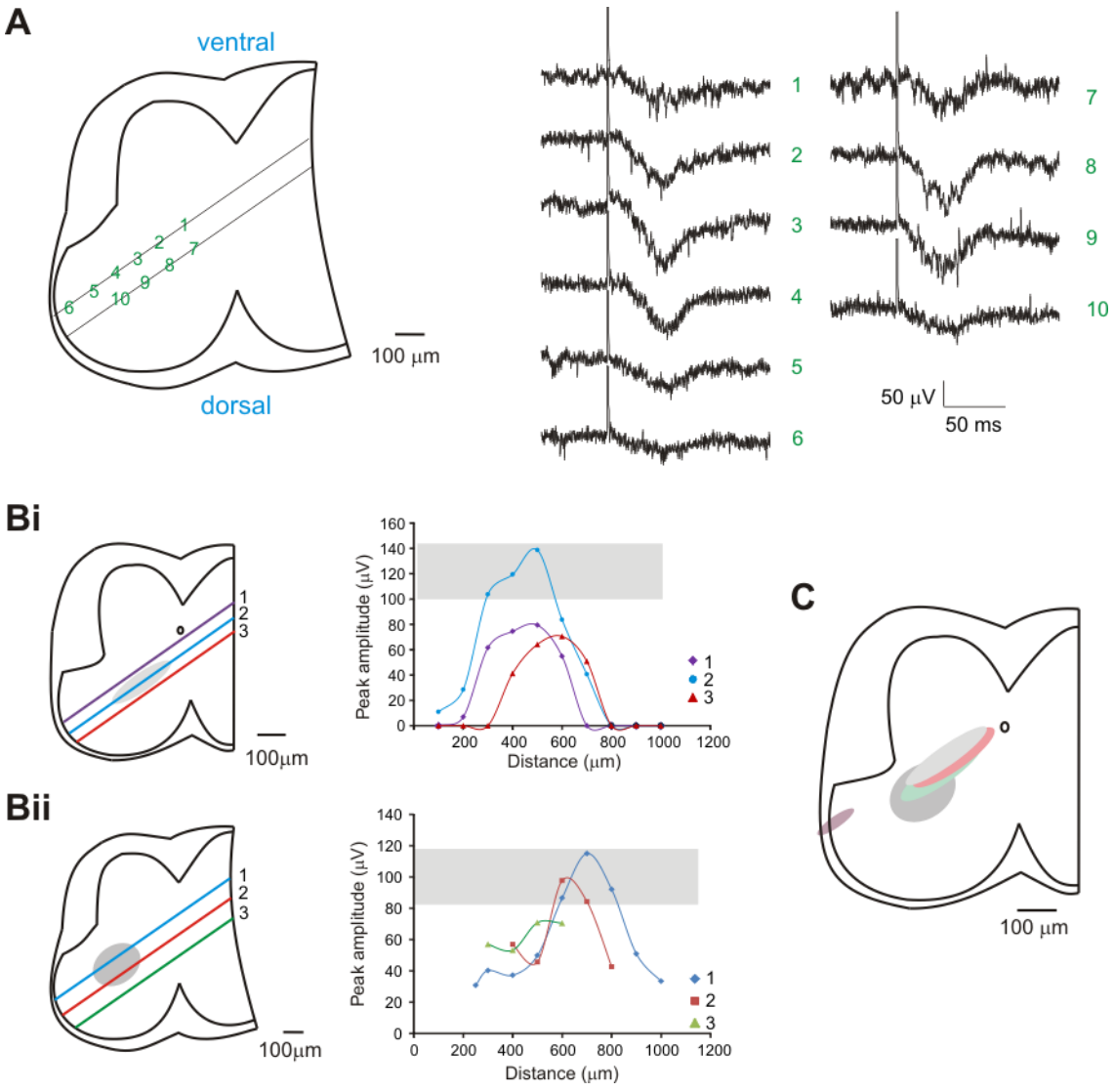

Figure 4.6 EFP recording locations.

A. Sample traces of EFPs evoked at various recording locations marked by numbers. Each trace is an average of 5 sweeps. **B**. Peak amplitude of evoked EFPs for 2 separate experimental days. Picture on left shows microelectrode path denoted by separate numbers. Plot on right displays peak amplitude of EFP versus distance into the cord the microelectrode traveled. Grey box and oval denote largest EFP amplitudes and their locations recorded. Bii corresponds to same experiment as traces in A. **C**. Composite sketch estimation of where maximal EFPs were recorded, compilation of 5 experiments.

Monoamine neuromodulatory actions depend on the receptor subtypes activated as well as their location within the spinal neuropil. Evidence supporting differing receptor subtypes and/or sites of action was suggested from the time course of depression and recovery. While the depression of DRP and EFP followed a similar trajectories for 5HT, the EFP recovered more rapidly after 5HT washout (**Figure 4.8A**). For NE, the DRP depression preceded the EFP depression yet recovered much more slowly (**Figure 4.8B**). For DA, the depression and recovery of the EFP and DRP had a similar time course (**Figure 4.8C**). Overall, as changes in the EFP should reflect those occurring at the first central synapse (see Discussion and Figure 4.13), an earlier and greater depression on the DRP compared to the EFP support modulatory actions at additional downstream sites for NE and DA. The slower and incomplete recovery of the DRP compared to the EFP also supports this interpretation for all monoamines.

Similar to actions reported for 5HT in lumbar spinal cord in the neonatal rat [152], both 5HT and NE depressed spontaneous DRPs in all cases where spontaneous DRPs were evident (n=3/3 for each; not shown). This suggests that 5HT and NE inhibit intrinsic spinal circuitry that generates these spontaneous potentials.

4.4.5 Dose Response

To determine relative efficacies of DRP and VRP depression, cumulative dose-response curves were generated for 5HT, NE, and DA.

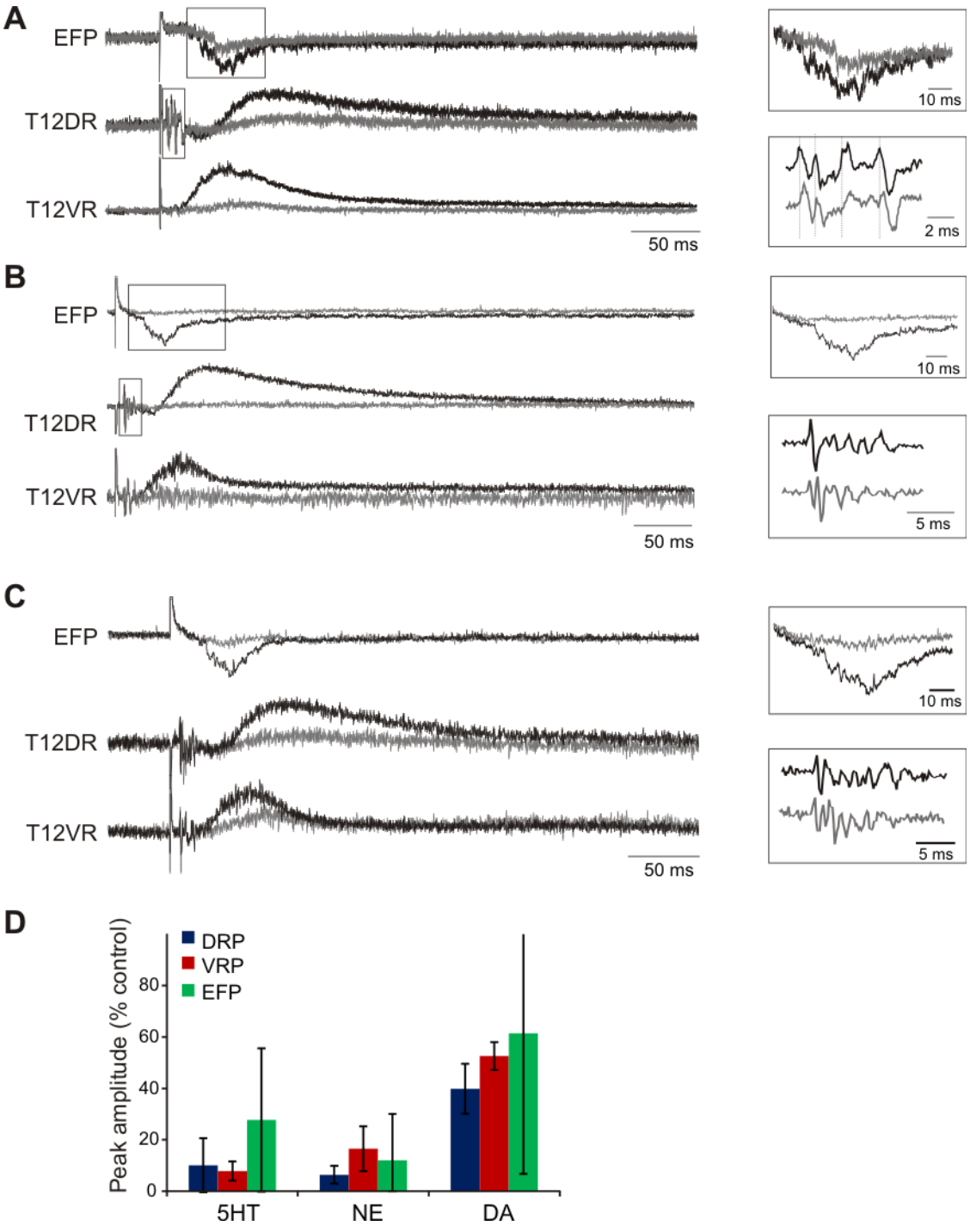

Figure 4.7 . Monoamine effects on splanchnic evoked responses.

A. Example of 5HT application. Control is in black, 5HT is in grey. Close up of the boxed areas are boxed on the right. Note slight delay in afferent volley timing in the presence of 5HT. **B.** Example of NE application. Control is in black, NE is in grey, with close up of boxed areas on the right. No change in afferent timing. **C**. Example of DA application (grey). No change in afferent spikes. **D**. Peak amplitude depression for each drug as a % of control values, with standard deviation standard deviation bars. Standard deviation bar clipped for DA EFP, large value due to the variability in response.

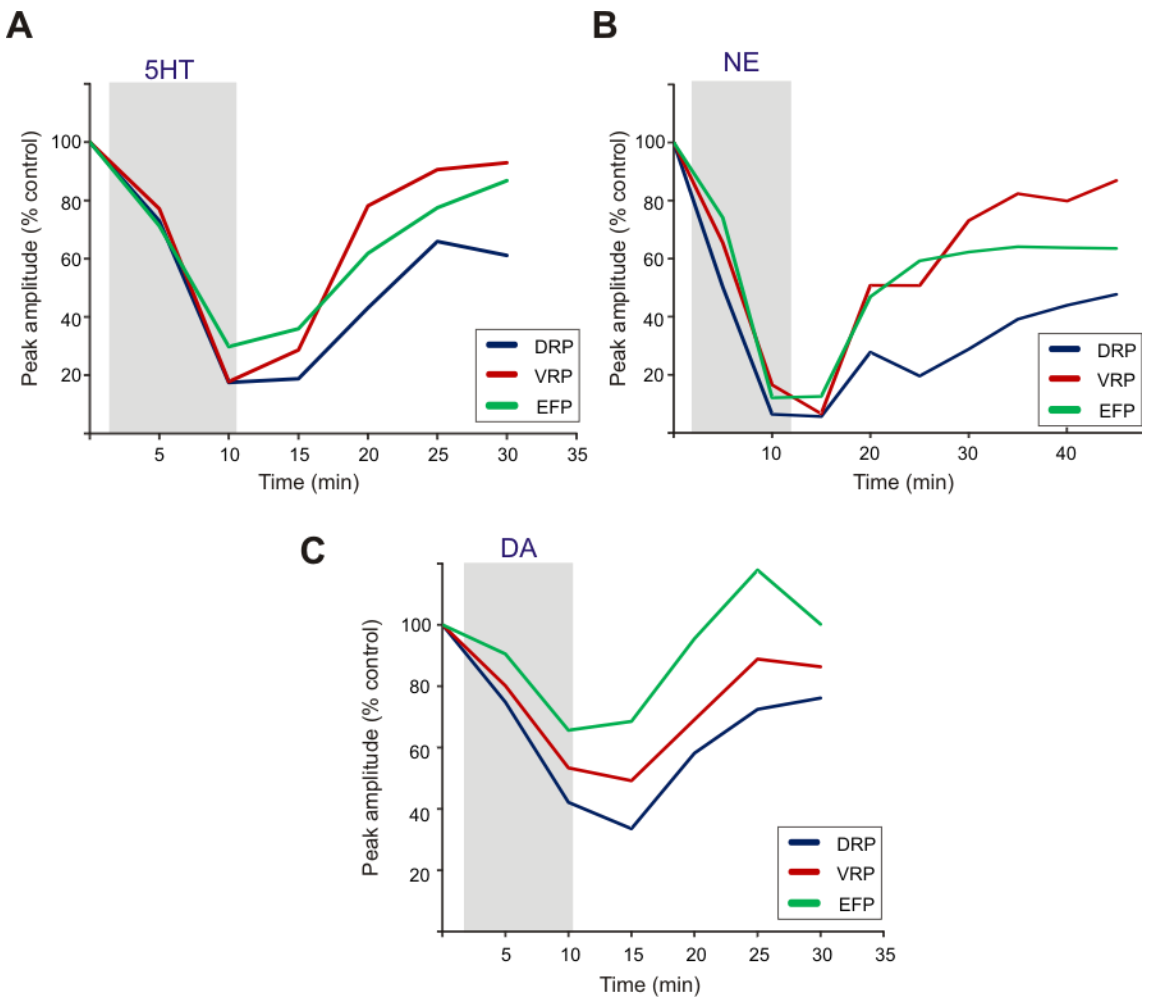

Figure 4.8 DRP, VRP, and EFP time-dependent comparison.

Time dependent comparison of DRP, VRP, and EFP depression. Time points before drug application and every five minutes afterward were computed by averaging 5 traces and normalizing their peak response to the pre-drug value. Lines connect the mean values across trials. **A.** 5HT: Note similar depression but delayed return to baseline of DRP compared to the VRP and EFP. **B**. NE: Note quicker depression and much slower return of DRP compared to other traces. **C**. DA; All three follow a similar shape but with different offsets.

4.4.5.1 Serotonin

Application of 5HT led to a dose-dependent depression of the visceral afferent- evoked DRP. **Figure 4.9A** shows a sample of a cumulative dose-response trial in a single preparation. When the evoked response was normalized to the initial DRP and compared across trials, a mean IC_{50} value of 0.42 μM was calculated (**Figure 4.9B**). Similar to that seen in the ventral root, 5HT produced a dose-dependent depolarization of the dorsal root resting polarity (n=4/4; **Figure 4.9C and D**).

4.4.5.2 Norepinephrine

Similar to 5HT, application of NE lead to a dose-dependent depression of the visceral afferent- evoked DRP, with an IC50 value of 0.18 μM (**Figures 4.10A and B**). The baseline of none of the dose-response trials for NE was stable enough to determine resting polarity shifts.

4.4.5.3 Dopamine

Application of DA had a biphasic action on the visceral afferent-evoked DRP. At low concentrations (i.e. < 5 μM) DA had little effect if any, and even facilitated the DRP in the majority of trials (n=3/4; see highlighted region in **Figure 4.11A**). On the other hand, at higher concentrations it dose-dependently depressed the DRP (**Figures 4.11 A and B**). The best-fit dose response curve calculated an IC_{50} value of 3.96 μM. Similarly to 5HT, DA produced a dose-dependent polarization of the dorsal root resting polarity (n=3/3; **Figure 4.11 C and D**)

4.4.5.4 Comparison of 5HT, NE, and DA Effects

Tables 4.1 and 4.2 show a summary of actions of 1 μM of 5HT, NE, and DA on the evoked DRPs and VRPs, respectively. Note that NE>5HT>>DA in efficacy of blocking both the DRP and VRP amplitude and integral. Since 1 μM DA had little effect, 5 μM values were also included for DA. Note also in the cases of 5HT and NE, 1 μM depresses much more of the DRP than the VRP.

Table 4.1: Dorsal root potential changes by drug.

Drug	Amplitude (% of control)	Integral to peak (% change)	Decay Integral (% change)	Total Integral (% change)
5HT (1μM)	34.83 ± 16.51*	-65.24 ± 35.19*	-73.37 ± 25.53*	-71.20 ± 27.97*
NE (1μM)	10.68 ± 11.62*	-89.66 ± 26.34	-91.91 ± 13.26‡	-91.41 ± 15.79‡
DA (1μM)	101.82 ± 9.93	-0.59 ± 19.96	12.41 ± 23.04	8.80 ± 22.28
DA (5μM)	49.46 ± 24.10*	-44.91 ± 31.83	-50.00 ± 24.78‡	-48.52 ± 26.33

* Denotes statistical significance, $p<0.05$. ‡ Denotes $0.05<p<0.1$. DA (5mM) is also shown since 1mM of DA had mixed (if any) effects.

Table 4.2: Ventral root potential changes by drug

Drug	Amplitude (% of control)	Integral to peak (% change)	Decay Integral (% change)	Total Integral (% change)
5HT (1μM)	56.75 ± 10.75*	-43.62 ± 36.07*	-50.56 ± 13.36*	-48.52 ± 21.39*
NE (1μM)	42.84 ± 22.94*	-52.37 ± 25.11	-58.34 ± 13.34	-57.30 ± 17.23
DA (1μM)	98.28 ± 9.64	25.49 ± 12.17	-37.91 ± 63.31	-27.44 ± 58.46
DA (5μM)	60.06 ± 24.53‡	-14.68 ± 26.31	-67.00 ± 52.16	-56.74 ± 52.72

* Denotes statistical significance, $p<0.05$. ‡ Denotes $0.05<p<0.1$. DA (5μM) is also shown since 1μM of DA had mixed (if any) effects.

4.4.6 Comparison of Monoaminergic Depression on Visceral Afferent- evoked Responses in the Dorsal Root and Ventral Root

4.4.6.1 Serotonin

As described in Chapter 3, 5HT also depressed the visceral-afferent evoked VRP in a dose-dependent manner. However, the depression of the DRP was not the same as that of the VRP. This could be seen by comparing the depression of the VRP versus that of the DRP in **Figure 4.12A.** For each dose-response trial, the relationship can be split into three time periods: 1) at low doses, where the DRP is slightly inhibited and the VRP is practically unchanged or even facilitated, 2) in midrange dosages, where both are depressed but to different degrees, and 3) at higher doses were both are nearly completely depressed. This can be seen also by comparing the dose-response curves of both (**Figure 4.12B**). Note that both the slope and IC_{50} values differ, suggesting greater efficacy and likely an additional site of action of 5HT in depressing the DRP.

4.4.6.2 Norepinephrine

NE also depressed the visceral-afferent evoked VRP in a dose dependent manner. In contrast to 5HT, the relationship of VRP to DRP depression was almost linear (**Figure 4.12C**), with a slope of less than 1, indicating greater DRP depression than VRP depression at each point. This can also be seen by comparing the dose response curves, as the dose-response of the DRP mirrored that of the VRP with a leftward shift (**Figure 4.12D**).

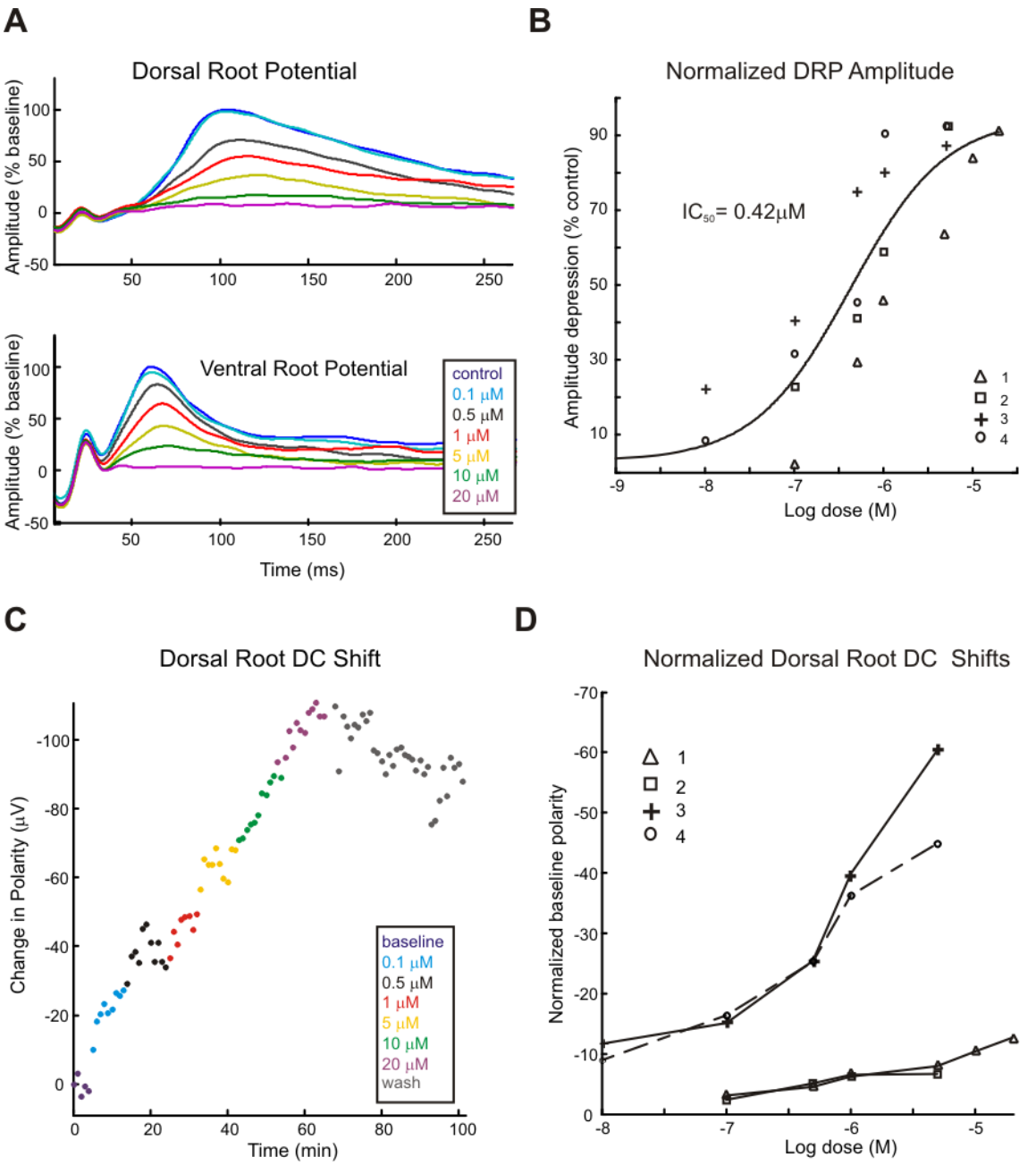

Figure 4.9. 5HT actions on evoked and resting dorsal root properties.

A. Sample of dorsal and ventral root potentials (VRPs) evoked by splanchnic nerve stimulation. Each trace is the mean, normalized trace of 5 sweeps for each dose increment. Each trace is color coded with corresponding dosage. **B**. Dose response trials for 5HT, with each trial a separate color. Line is a best fit dose-response equation to all data points, IC_{50} value is the dose at which the evoked response is half the control value. **C**. Sample change in resting polarity during dose response. Each point is the mean value of the traces pre-stimulus, by convention negativity is upward. **D**. Normalized plots of resting ventral root polarity, average of 5 sweeps for each dose.

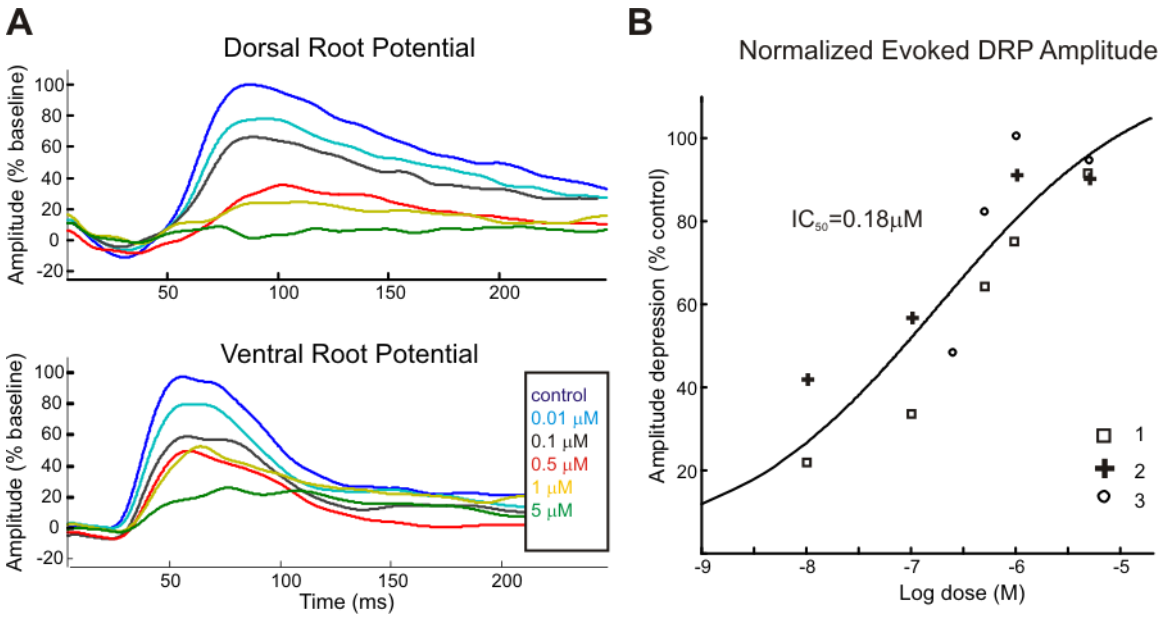

Figure 4.10 NE actions on evoked and resting dorsal root properties.

A. Sample of dorsal and ventral root potentials (VRPs) evoked by splanchnic nerve stimulation. Each trace is the mean, normalized trace of 5 sweeps for each dose increment. Each trace is color coded with corresponding dosage. **B**. Dose response trials for 5HT, with each trial a separate color. Line is a best fit dose-response equation to all data points, IC_{50} value is the dose at which the evoked response is half the control value. No analysis of resting dc polarity shifts was done for NE due to unstable baselines.

4.4.6.3 Dopamine

As mentioned above, at low doses, DA facilitated the evoked DRP and had little effect on the evoked VRP, represented by the negative values in **Figure 4.12E**. However, at higher doses the depression of the DRP and VRP followed a similar course, displaying a near linear relationship, similar to NE. Thus, the dose-response curves for the VRP and DRP nearly overlapped at lower doses but followed a different slope for higher doses (**Figure 4.12F**).

Had 5HT, NE, or DA depressed both the DRP and VRP in the same manner, one could hypothesize that the depression was occurring at a shared site. Yet the above mentioned differences in dose-response curves and time-course of depression between the DRPs and VRPs implicate additional, separate, sites of action in the visceral-afferent evoked PSI and reflex circuitry.

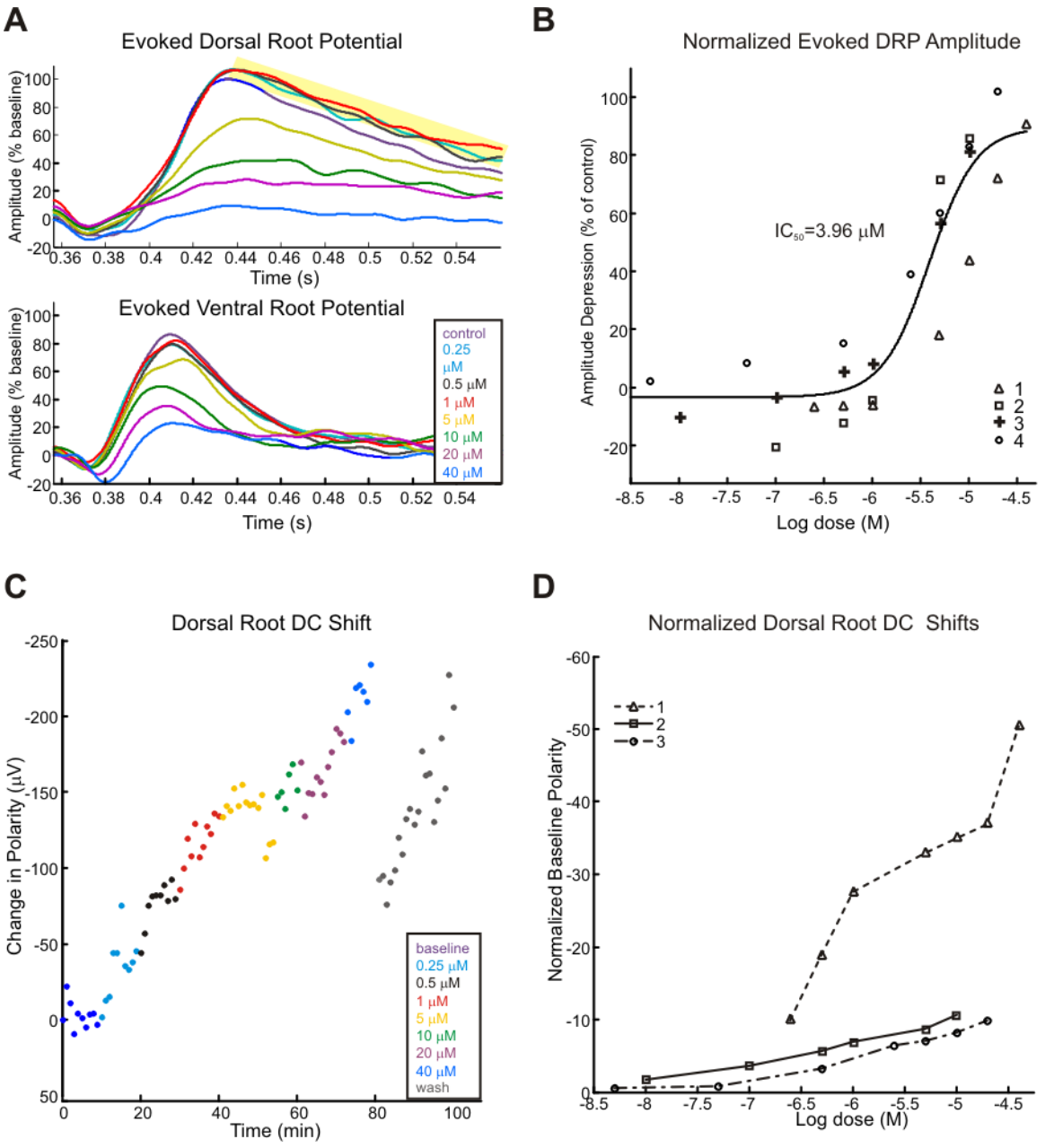

Figure 4.11. DA actions on evoked and resting dorsal root properties.

A. Sample of dorsal and ventral root potentials (VRPs) evoked by splanchnic nerve stimulation. Each trace is the mean, normalized trace of 5 sweeps for each dose increment. Each trace is color coded with corresponding dosage. Highlighted region notes concentrations less than 5uM which facilitated the evoked DRP but depressed the VRP. **B**. Dose response trials for DA, with each trial a separate color. Line is a best fit dose-response equation to all data points, IC_{50} value is the dose at which the evoked response is half the control value. **C**. Sample change in resting polarity during dose response. Each point is the mean value of the traces pre-stimulus, by convention negativity is upward. **D**. Normalized plots of resting dorsal root polarity, average of 5 sweeps for each dose.

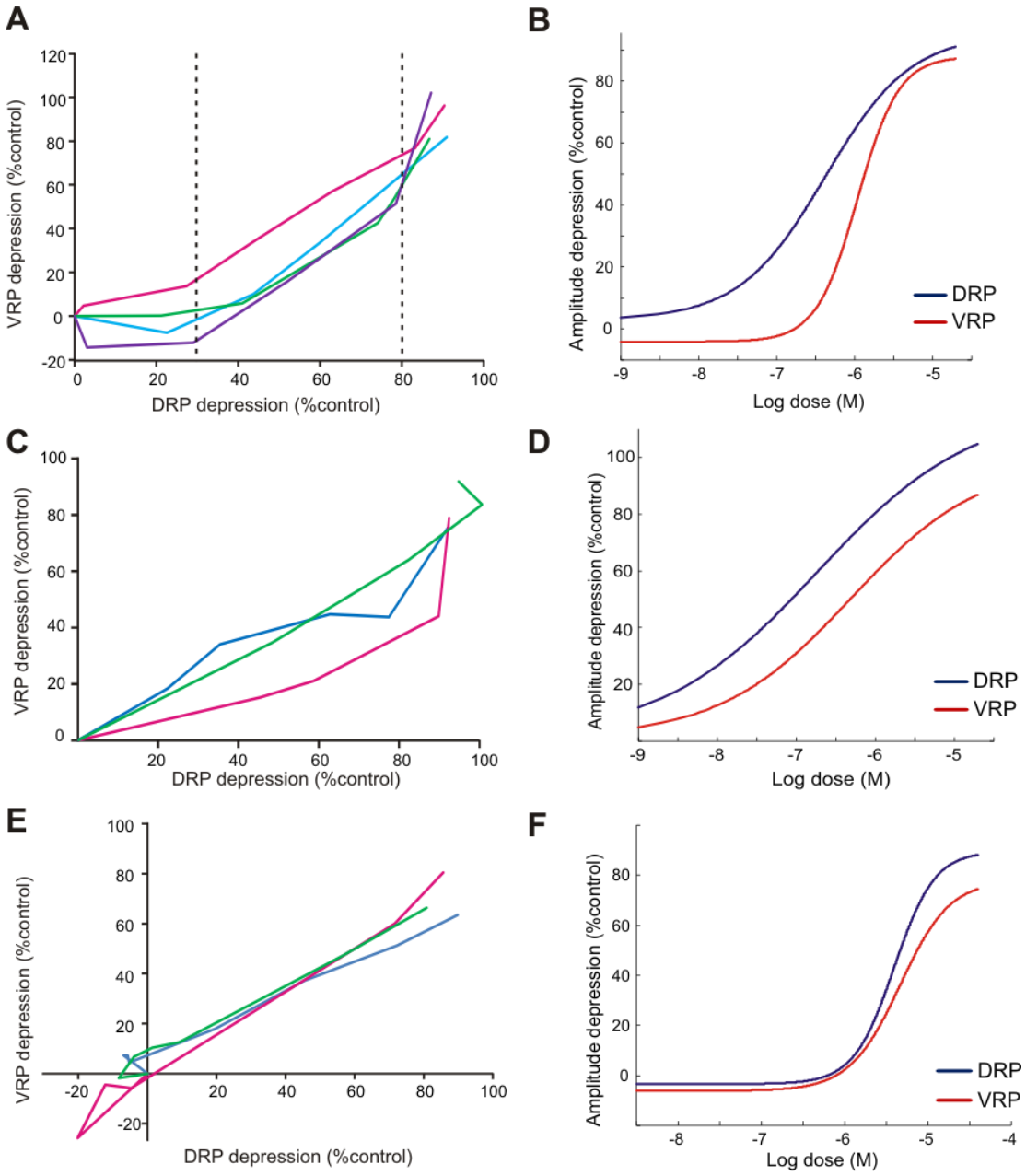

Figure 4.12 Comparison of dorsal and ventral root effects.

A. 5HT induced depression of the ventral root potential (VRP) versus the dorsal root potential (DRP). Lines are individual experiments, the depression of the VRP plotted as a function of the DRP, all normalized to % depression of control peak amplitude. Vertical dashed lines denote general regions of differing slope. **B**. 5HT-induced dose response comparison of DRP and VRP. Lines are the fitted dose-response curves for the DRP and VRPs computed earlier. **C**. NE induced depression of the VRP versus the DRP. **D**. Dose response curves for NE-induced depression. **E**. DA induced depression of the VRP versus the DRP. **F**. Dose response curves for DA-induced depression.

4.5 DISCUSSION

While the spinal cord receives a multitude of sensory information, only a small percentage of that information is visceral (e.g. [38, 188]). Yet, this comparatively minor sensory contribution is able to inhibit other types of afferent inflow [64, 71, 228]. This study introduced a novel *in vitro* preparation to characterize spinal visceral afferent stimulation-evoked primary afferent depolarization (PAD)-mediated presynaptic inhibition (PSI), and builds on the first investigation of this phenomenon over 40 years ago [228]. Splanchnic and sympathetic chain stimulation produced a DRP, a measure of PAD, in dorsal roots of multiple thoracic spinal segments, similar in duration to that reported after the stimulation of muscle and cutaneous afferents (e.g. [67, 68, 102, 213]). This DRP was strongly depressed by the monoamines serotonin (5HT), norepinephrine (NE), and dopamine (DA), with IC_{50} values of 0.42, 0.18, and 3.4 μM, respectively. Assuming that the DRP is an expression of PAD-evoked PSI, this implies that the activation of the descending monoamine systems serves to limit visceral afferent activity-dependent inhibition, thereby enhancing the role that certain types of sensory information can have on spinal circuitry. Yet the extracellular field potential (EFP), indicative of the visceral afferents' first site of communication with the spinal cord, was also diminished. This implies that the monoamines have the ability to depress both specific visceral afferent transmission to the spinal cord, as well as the PAD of visceral and other afferents evoked by visceral activity. The implications of these opposing actions will be discussed in more detail below.

4.5.1 Composition of the Sympathetic Chain and Greater Splanchnic Nerve

Triple labeling for CGRP, TH, and HB9-GFP indicated the presence of 3 distinct fiber populations that travel between the paravertebral sympathetic ganglia. $CGRP^+$ visceral afferents did not appear to synapse on TH^+ sympathetic postganglionic neurons, often avoiding postganglionic cell bodies entirely, unlike direct synapses reported between afferents and postganglionic neurons in pre-vertebral ganglia [130, 208]. That visceral afferents are known to show both spontaneous activity [12, 131] and responses to neuromodulators [101] should caution against interpreting recordings from the sympathetic chain or splanchnic nerve as solely efferent and predominantly preganglionic (e.g.[222, 245]).

4.5.2 Visceral-afferent Evoked Dorsal Root Potentials

Overall I observed that electrical stimulation of the splanchnic nerve or sympathetic chain strongly activated motor reflexes and presynaptically inhibited afferent inflow via a PAD-mediated DRP at multiple spinal segments. Splanchnic or sympathetic chain stimulation produced a DRP in every preparation tested.

The DRP duration measured was similar to that reported in response to activation of muscle and cutaneous afferents, but the average DRP onset and peak amplitude occurred much later [67, 102, 146, 206] . Given that visceral afferents in the splanchnic nerve often travel multiple segments in the sympathetic chain before entering the spinal cord [5, 13] and project to multiple rostral-caudal levels upon entering it [37, 65, 246], it difficult to speculate how many interneurons in the spinal cord integrate this multi-segmental (and likely differentially timed) afferent inflow. Additionally, while a previous study

indicated that visceral afferent activation could lead to PAD-mediated DRP in both visceral and cutaneous afferents [228], further investigation is required to discern which types of afferents were responsible for generating the DRP (and thus were inhibited by visceral afferent stimulation).

Interestingly, the DRPs evoked in multiple segments followed a similar time course. This similar patterning at multiple spinal levels is supported by previous work from Lidierth in 2006, who showed that nonspecific afferent stimulation lead to two types of DRP: one short latency to onset in dorsal roots close to the stimulation site, and one longer latency recorded from more distant segments [146]. While the short-latency DRP onset increased with each spinal segment distal to the stimulation site, the longer latency DRP had similar onset latency across multiple segments. In the splanchnic-spinal cord preparation, only the latter, diffuse activation of DRPs was present. It is likely that this diffuse activation allows visceral afferents to presynaptically inhibit visceral and somatic afferent inflow throughout the spinal cord [71, 227, 228].

Yet, even compared to the diffuse longer-latency DRPs described by Lidierth, visceral afferent-evoked DRPs had a much later onset than previously reported for somatic DRPs [67, 146, 206]. Observed DRP latencies were, however, comparable to those reported in the one other study analyzing visceral afferent evoked DRPs [228]. Differences in latency observed between somatic vs. visceral afferent-evoked DRPs are likely due at least in part to the composition of splanchnic afferents, which are predominantly thinly myelinated and unmyelinated Aδ and C fibers, respectively [2, 3, 78, 134, 188]. These fibers are more slowly conducting than somatic cutaneous and muscle afferents, which also contain much faster conducting Aβ and group I and II afferents respectively. Differences

in latency may also have been observed because the latencies I reported were measured from the arrival of the first afferent volley identified. If the DRP was induced by higher-threshold, slower-conducting axons (Figure 4.5A), or axons innervating a different spinal segment, this measure of central delay may be artificially inflated. On the other hand, I observed that ventral root reflexes recruited by the stimulation of the same afferent fiber population occurred on average 20ms earlier, demonstrating that long central latencies are not primarily caused by afferent conduction delays. One additional explanation would be if visceral afferents also constitute the majority of fibers underlying the evoked DRP, where differences in conduction speed may also slow back propagation of afferent depolarization to the recording site. Lastly, the intrinsic spinal circuitry responsible for generating visceral afferent evoked PAD may differ in mechanism and/or number of synaptic connections than that evoked by muscle and cutaneous afferents. The validity of these hypotheses needs to be explored more fully in future studies.

Interestingly, dorsal root reflexes (DRRs) were often elicited by visceral afferent activation. DRRs in fine afferents have been linked to inflammation in joint and cutaneous afferents (e.g [116, 153], see [268] for review), as dorsal root activity can propagate antidromically to peripheral nerve endings, due at least in part to the release of neuropeptides (such as substance P and CGRP) from sensory nerve terminals (e.g. [8, 23]). In the case of visceral afferents, whose peptidergic phenotypes are well established [127, 147, 182, 258], DRRs may lead to visceral hypersensitivity and potentially recruitment of additional nociceptors [86]. As visceral afferents are also thought to regulate local organ function and blood flow from back-propagating afferent activity [112], DRRs may also contribute to the regulation of basic organ function. Additionally, as recently proposed by

Rudomin [219], neuropeptides co-released by visceral afferents in the dorsal horn could serve to modulate glutamate release [126] or otherwise alter visceral afferent CNS transmission. The PAD-induced DRP accompanied by DRRs, can therefore have a dual nature, exerting presynaptic inhibitory actions on central synaptic transmission while concomitantly modulating visceral organ function [268].

4.5.3 Visceral Afferent-evoked Field Potentials

Extracellular field potentials (EFP) were recorded to investigate the modulation of visceral afferent transmission at the first synapse in the spinal cord. Our EFP tracking experiments identified maximal responses in the deep dorsal horn (with responses recorded in select regions in the deep and superficial dorsal horn). This is consistent with extracellular recordings of spinal neurons in the cat and rat [2, 3, 41, 98, 201, 251] as well as anatomical labeling studies of visceral afferent projections in the spinal cord [37, 188]. Yet, EFPs recorded were of a surprisingly long latency from the first afferent spike timing recorded. These long-latency, afferent-evoked DRPs (figure 4.5A) may thus be mechanistically associated with EFPs arising from afferents with slow central conduction times. Supporting this assertion, earlier researchers indicated that while visceral nerves contain some larger myelinated axons [134], only stimulus intensities large enough to activate at least Aδ fibers were required for activation of spinal neurons or cord dorsum recordings [3, 98]. Further exploration is thus warranted to determine the makeup and timing of afferent spikes causal to the DRP. Only then can time-dependent analysis of the number of synapses be completed in analyzing the evoked EFPs.

4.5.4 Monoaminergic Modulation of Dorsal Root Potentials and Field Potentials

In addition to the depression of visceral afferent evoked spinal reflexes noted in Chapter three, the monoamines (MAs) also depressed visceral afferent evoked DRPs in a dose-dependent manner (for exceptions see DA effects in 4.5.4). Yet DRP generation depends on visceral afferent transmission to the spinal cord (**Figure 4.13**), and any actions directly inhibiting this transmission would diminish the DRP. EFPs, an indication of synaptic transmission of visceral afferents at the first synapse, were also potently depressed by 5HT, NE, and sometimes DA. This suggests that much of the observed actions on DRPs are not associated with a depression of the spinal circuits that generate PAD, but rather simply due to a block of all incoming afferent transmission to the spinal cord. In essence, by depressing synaptic transmission of visceral afferents, the MAs act to generally impede the amount of visceral information reaching the central nervous system, and do so with much greater efficacy than do low threshold muscle and cutaneous afferents [206]. This interpretation is consistent with previous work showing that the monoamines generally depress afferent-evoked monosynaptic transmission to individual neurons in the deep dorsal horn [84].

However, time-dependent differences and efficacies of MA depression of DRPs, EFPs, and VRPs suggest that this is not the only site of action. While our low frequency of stimulation made it difficult to ascertain temporal differences in the onset of depression, EFPs and VRPs often recovered from MA-induced depression sooner than DRPs (Figure 4.8). Coupled with the observed nonlinear MA-induced depression between evoked dorsal root and ventral root responses (Figures 4.12) and the simultaneous inhibition of spontaneous DRPs, it is unlikely that the depression of the DRP is simply a depression of

synaptic transmission at the first-order afferents. Overall, it appears that the monoamines modify spinal processing of afferent input in at least two ways: 1) decreasing visceral afferent transmission to the spinal cord (↓EFP) and 2) increasing afferent transmission by limiting PAD-mediated presynaptic inhibition circuitry (↓ DRP). These differential actions on afferent transmission have been shown in response to low threshold muscle and cutaneous afferent stimulation [206], and are consistent with actions on subsets of low threshold afferents (depression of group II afferent transmission but facilitation of group I afferents) [24, 25, 119, 233].

The functional consequences of this dichotomy likely depend on the selectivity of the evoked PAD. If PAD-mediated PSI in visceral afferents serves primarily to facilitate specific organ function (e.g. inhibiting pudendal afferent evoked responses during micturition [9]), descending monoamines may act to decrease the effectiveness of these functions by acting on PAD circuits. With visceral-related PAD depressed, visceral and related afferents would have greater accessibility to the CNS (thus allowing more information flow). If, on the contrary, PAD is evoked in non-function specific visceral and somatic afferents, blocking afferent-evoked PAD would have more widespread actions. The powerful depression of spontaneous DRPs supports a depression of PSI in multimodal afferents, thus increasing the accessibility of all afferents to the spinal cord. Taken in combination with reportedly selective actions on subsets of muscle and cutaneous afferents, where monoamines have been shown to inhibit synaptic transmission of nociceptive cutaneous and group II muscle afferents but have little or facilitative action on transmission from low-threshold cutaneous and group I muscle afferents [24, 25,

[120], this would effectively shift the responsiveness of the CNS in favor of low threshold mechanosensory and cutaneous afferent information.

Conversely, if the MAs instead acted directly on primary afferents to block synaptic transmission via metabotropic receptor-mediated presynaptic inhibition, all afferents would be diminished in their ability to alter ongoing spinal circuit actions. Clearly, the site and pattern of MA release within the spinal cord is crucial to understanding their functional role.

If descending tracts were activated in a more physiological manner, would synaptic transmission at the first synapse and later sites of action in the spinal cord be differentially affected? Within the dorsal horn, descending monoaminergic tracts appear not to synapse directly on individual neurons but rather act via volume transmission [175]. This implies that primary afferent terminals and nearby interneurons may receive similar monoaminergic input, and is consistent with laminar and functional selectivity in modulation reported for field potentials evoked by muscle afferents [120]. The combination of direct function-specific inhibition of visceral afferent transmission and location- and function-specific depression of PAD, offer the spinal cord nuanced control over selecting afferent input.

Even with nonspecific release of monoamines throughout dorsal horn, there may be functionally important, time-dependent differences for each site of action. When both 5HT and NE were applied, the DRP recovered much more slowly than the EFP, suggesting that short exposure to these monoamines would lead to a lengthy depression of PAD, and thus subsequently increased access of visceral afferents to the CNS. This

prolonged DRP depression (especially in the case of NE) may in turn produce a state of enhanced responsiveness to visceral afferent information and, as referenced above, likely a disruption of normal organ regulation. Similarly, EFP and DRP depression may have different dose sensitivity, shifting the balance in favor of exaggerated or depressed accessibility of visceral afferent information to the CNS, depending on activity levels of the descending MA systems.

MA release patterns and activation selectivity are vital next steps to understanding the role and extent of these seemingly opposing actions, but are beyond the scope of the current study.

4.5.5 Dopamine's Dose-dependent Actions

Interestingly, actions of DA on ventral root and dorsal root responses were different depending on the dose used. Low doses of DA increased the evoked DRP (increasing PAD-mediated PSI of afferent inflow) while having little effect on the VRP, thus more effectively preventing afferent input from reaching the central nervous system. Differences may relate to a segregation of receptor subtypes of differing receptor affinities for DA, with receptors that facilitate the DRP activated at lower concentrations. As mentioned in Chapter 3, this is consistent with dose-dependent actions in the pre-frontal cortex, where low doses of DA preferentially activated $D_{1\text{-like}}$ receptor pathways and higher doses of DA masked these effects by activation of $D_{2\text{-like}}$ effects [254, 280]. This has particularly strong implications for circadian and disease related decreases in DA release [48, 49], as it is likely that visceral afferent information would be preferentially dysregulated.

4.5.6 Putative Mechanisms

The descending monoaminergic systems may influence both monosynaptic transmission of visceral afferents and visceral-afferent induced PAD differently based on differing receptor expression patterns. Monoamines can affect neuronal excitability by activating metabotropic receptors that both modulate ion channels directly (e.g. [35, 137]) and modulate common signal transduction pathways (see [176, 178] for review, Figure 1.4 for more detail). Many monoaminergic receptors are present in spinal neurons and primary afferents (see [175] for review). Therefore, the site of modulation may be (1) on primary afferents themselves, (2) their first site of synaptic transmission to the spinal cord, (3) interneurons involved in generating PAD, or (4) on afferent fibers receiving PAD. Figure 4.13 shows a schematic of the potential sites of action.

4.5.6.1 Direct Actions on Primary Afferents

Given that 5HT and DA produced depolarizations of the resting dorsal root polarity, and 5HT delayed the arrival of afferent volleys in the dorsal roots, the monoamines may have direct actions on visceral afferents themselves. Potential sites of action are ionotropic $5HT_3$ receptors shown to be present on afferent axons, a subset of which are $CGRP^+$ [51, 167]; and metabotropic G_i-coupled inhibitory autoreceptors, such as $5HT_1$ serotonergic, $D_{2\text{-like}}$ dopaminergic, and α_2 adrenergic receptors, which may inhibit transmitter release by inhibiting Ca^{2+} channels and facilitating K^+ channels (e.g. [70, 79], see [175, 178] for review).

4.5.6.2 Postsynaptic Actions on the First Synapse or Interneurons Involved in PAD Generation

EFPs were also predominantly depressed by the monoamines. Inasmuch as they are a reflection of first synaptic activation by visceral afferents, EFP depression reflects an

inhibition of primary afferent synaptic transmission within the dorsal horn. This could be caused by post-synaptic $5HT_1$, α_2 adrenergic, and $D_{2\text{-like}}$ G_i -coupled receptors, which have been shown to reduce phosphorylation of non-NMDA glutamatergic receptors (e.g. [184]) and modulate the release of CGRP (e.g. [249]) in the spinal cord. Additionally, G_i coupled receptors could act post-synaptically to inhibit Ca^{2+} channels and enhance K^+ channel function, generally inhibiting neuronal function. This has been shown to occur in the dorsal horn for $5HT_{1A/1B/7}$ serotonergic [85, 279] , α_2 adrenergic [83, 215, 265], and $D_{2\text{-like}}$ dopaminergic receptors [250].

4.5.6.3 Actions on Synaptic Relay to Primary Afferents Producing PAD

Lastly, the monoamines could be acting on higher-order interneurons, including the last-order interneurons necessary to produce PAD. The present series of experiments did not assess the composition of afferents that were depolarized to produce the DRP. However, given the known interactions with visceral inhibition of somatic circuits (e.g. [228]) and interactions between multiple afferent types (e.g. [219]), the DRP may reflect a heterogeneous mix of both visceral and somatic afferents. The direct actions on primary afferents discussed above (i.e. general depolarizations of the resting dorsal root polarity) may also act to inhibit DRP generation by preventing further depolarization of the primary afferents (i.e. depolarization block). Lastly, if the visceral-afferent evoked DRP is indeed generated by last order GABAergic interneurons, G_i coupled receptor activation could additionally inhibit GABAergic transmission (e.g. [76, 238]).

Overall, the contribution of various monoamine receptors at specific sites in the PAD generating pathway in unclear. The speculations above describe many of the potential sites of action, but further investigation is required to fully assess these.

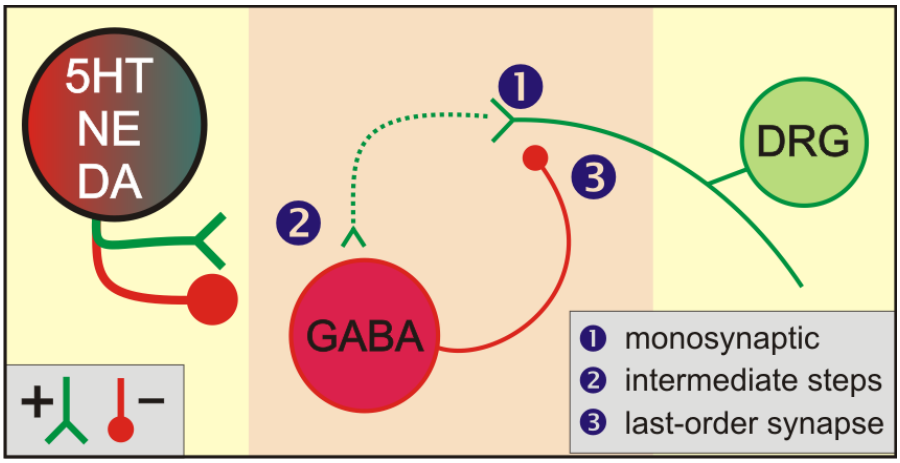

Figure 4.13 PAD-mediated presynaptic inhibition circuitry.

The intraspinal circuit responsible for PAD may involve one or more interposed interneurons. 5-HT, NE and DA may exert actions on one or multiple of the following locations: 1) presynaptically directly inhibiting afferent transmission, 2) inhibiting synaptic transmission to putative interneurons or altering their excitability so that fewer are recruited to produce PAD, or 3) inhibiting last order GABAergic transmission to the afferents producing PAD. Dashed line represents connections that may be directly or oligosynaptic.

4.6 CONCLUSIONS

In this chapter, I developed an *in vitro* mouse model to assess how the spinal cord processes visceral afferent information. This model, and its ability for direct manipulation of the extracellular environment, will be a useful tool in exploring visceral-evoked PAD-mediated presynaptic inhibition. The monoamines 5HT, NE, and DA all acted to suppress visceral afferent evoked DRPs and EFPs, suggesting complex regulation of afferent input to the CNS. 5HT, NE, and DA all had a unique signature of effects. It is likely these differences in signatures reflect multiple sites of action for each drug tested.

CHAPTER 5

CHAPTER 5: CONCLUSIONS

Most of the motor output to the visceral organs is not under our voluntary control, nor does sensation from them often reach consciousness. The spinal cord therefore plays an integral role in processing visceral sensory information and generating visceral motor output. Understanding how the spinal cord does this, and how descending systems modulate this activity, is crucial to understanding the subconscious regulation of this significant and unfortunately understudied part of the nervous system.

5.1 Summary and Discussion of Key Findings

The primary objective of this work was to understand spinal processing of sympathetic output and visceral sensory input, and what role the descending monoamines play in modulating this.

Aim 1 characterized the electrophysiological properties in the final central output neurons of the sympathetic nervous system, sympathetic preganglionic neurons (SPNs). I used the HB9-GFP transgenic mouse as a model system, both due to the ease of identifying SPNs as well as the ability to lay the foundation for future transgenic approaches to characterize autonomic function. Using whole-cell patch clamp recordings from visually identified SPNs in the intermediolateral column (IML) of neonatal and juvenile mice, I demonstrate a diversity of SPN electrophysiological properties. Mouse SPNs showed similar passive and active membrane electrical properties when compared to other animal models, although individual properties varied significantly across the neurons tested. Given that SPNs with varying end-targets are known to co-localize

within the same IML clusters, and that the SPNs recorded from in this study were likely functionally diverse, this suggested that SPNs may be differentiable based on electrophysiological characteristics. Indeed, while linear regression analysis identified strong relationships between many cellular properties in all neurons tested, cluster analysis was able to identify four subpopulations of SPNs. This demonstrated that the IML contains populations of SPNs that are differentiable by their membrane properties, and that sympathetic efferent populations may have a differential recruitment order similar to that of somatic efferents (motor neurons). Motor neurons also express the HB9 transcription factor that defines these two efferent neuronal classes as originating from a common 'efferent' progenitor population [11, 252].

Given that there are differentiable populations of SPNs, one question is whether descending systems treat subpopulations of SPNs differently. The descending monoaminergic systems are state-dependently active, yet what role they play in modulating spinal sympathetic output and visceral input is poorly understood. In **Aim 2**, I sought to reconcile sometimes contradictory evidence on the effects of the monoamines serotonin (5HT), norepinephrine (NE), and dopamine (DA) on SPNs. To do so I took a three pronged approach. First, I directly assessed the influence of 5HT, NE, and DA on intrinsic properties of individual SPNs, using patch-clamp recordings in the neonatal slice preparation. Next, I developed a novel *in vitro* spinal cord and sympathetic chain preparation, which allowed me to assess the neuromodulation of population responses of SPNs (and motor neurons) to visceral afferent stimulation. Lastly, I complemented physiological experiments on monoamine transmitter neuromodulation with immunohistochemical detection of putative receptors underlying these effects.

I observed that each monoamine had a unique signature of effects on sympathetic motor output. 5HT consistently depolarized all intracellularly recorded SPNs, increased their response to injected current, and often led to increased spontaneous activity recorded in the ventral root. NE actions were more mixed, leading to both depolarizations and hyperpolarizations in intracellularly recorded SPNs. Yet regardless of action on resting membrane potential, in all cases NE increased SPN firing responses to injected current, and increased spontaneous activity in the ventral root. Using immunohistochemistry, I identified $5HT_{2A/7}$ serotonergic, and $\alpha_{1a/2a}$ adrenergic receptors on some SPN somas and processes. $5HT_{2A}$, $5HT_7$, and α_{1a} receptors are G_Q or G_s coupled, and likely activate signal transduction pathways that ultimately underlie increases in SPN excitability. In comparison, α_{2a} adrenergic receptors are G_i-coupled, and likely inhibit signal transduction pathways that are ultimately responsible for inhibitory actions of NE [62, 176].

Dopamine exerted the most complicated actions. Like NE, DA depolarized some while hyperpolarizing other intracellulary recorded SPNs. However, unlike 5HT and NE, DA also had mixed responses on SPN firing to injected currents. These mixed actions on SPN excitability were supported by differential dose-dependent effects identified in the ventral root recordings, where DA was depolarizing at lower doses and hyperpolarizing at higher doses. Immunohistochemical evidence was provided for SPN expression of D_2, D_3, and D_5 receptor subtypes. The presence of both G_s-coupled receptors (D_5) and G_i-coupled receptors ($D_{2,3}$) identified likely underlie this dichotomy, given their opposing actions common signal transduction pathways [178].

In contrast, however, all three monoamines consistently depressed visceral-afferent evoked responses. Taken together, my results indicate that as a whole, the descending monoaminergic systems both facilitate autonomic motor output and inhibit visceral sensory input. This is consistent with a general hypothesis about 5HT forwarded by Jacobs and Fornal [111] almost 20 years ago on the somatic sensory and motor systems, that 5HT acts to suppress afferent information but enhance motor output. Given that multiple autonomic reflexes are driven by visceral afferents [115], this would result in a decoupling of autonomic output from visceral input, instead favoring descending input or intrinsic spinal circuitry mediated- output.

These seemingly contradictory effects of exciting sympathetic output yet inhibiting reflex responses to visceral input were explored further in **Aim 3**. One of the most effective means of inhibiting afferent inflow is presynaptic inhibition (PSI), yet there are conflicting reports whether visceral afferents exhibit PSI. Using the preparation developed in Aim 2, I showed that visceral afferents in the splanchnic nerve and sympathetic chain do indeed evoke a widespread dorsal root potential (DRP), indicative of primary afferent depolarization (PAD), an ionotropic form of PSI. Both 5HT and NE dose-dependently depressed the DRP. Yet, measurements of the earliest evoked extracellular field potential (EFP) in the deep dorsal horn, reflecting initial synaptic transmission from primary afferents, were also depressed by 5HT and NE. Temporal differences in depression and recovery implicate at least two distinct sites of action: (i) direct inhibition of afferent transmission to the spinal cord, and (ii) inhibition of the interneuronal circuitry that leads to PAD. Interestingly, at low doses DA facilitated the DRP, thus increasing PAD (and limiting afferent accessibility to the spinal cord), while at

higher doses acting like 5HT and NE and inhibiting the DRP and visceral afferent transmission to the spinal cord. My results demonstrate that minus low doses of DA, the monoamines can depress both visceral afferent transmission to the spinal cord and PAD evoked by visceral afferents. The functional implications of this will be discussed further in section 5.3.

5.2 Function of Visceral Afferent-evoked Presynaptic Inhibition

Spinal visceral afferents encode physical changes (e.g. distension, contraction) or chemical events in the viscera and transmit this to the CNS, leading to organ regulation and reflexes (and occasionally conscious sensation) [112]. Yet, except for sacral afferents, most spinal visceral afferents lack functional specificity, responding to mechanical, chemical, and sometimes thermal stimuli (e.g. [143], see [113] for review). Additionally, spinal visceral afferents are the predominant conduit for visceral pain information, yet the majority of them are also active under resting conditions [12, 113]. With this multimodal barrage of visceral sensory inflow, how do central neurons differentiate between organ regulation, non-painful sensation, and visceral pain?

Further complicating matters, spinal visceral afferents activate both sympathetic and parasympathetic reflexes, which often have opposing actions on the target tissue. How does the CNS decode complex visceral information and determine the appropriate response?

One of the most influential and afferent-specific forms of limiting synaptic transmission is to inhibit afferents presynaptically. Yet, studies of visceral-afferent mediated PSI are quite limited. After findings suggesting that some vagal afferents are devoid of PSI [218]

(but see [217]), the prevailing opinion has been that visceral afferents lacking PSI allow for automatic regulation of organ function, without filtering out vital visceral afferent information [219]. Yet vagal afferents have much greater functional specificity, often selectively relaying a single type of visceral sensory information, and most are not involved with relaying visceral pain [112]. On the other hand, spinal visceral afferents convey multiple modalities of visceral sensory information and are the predominant pathway to the central nervous system for visceral pain conduction. It seems imperative that spinal visceral afferents (even more so than their vagal counterparts) have the PSI toolkit with which to selectively filter afferent inflow.

Indeed, organ specific presynaptic inhibition has been implicated in control of micturition [9, 30]. Additionally, often overlooked earlier work of Selzer and Spencer showed that visceral afferents can inhibit both visceral and cutaneous afferents, with presumed presynaptic mechanisms [228]. This dissertation explored this further, specifically addressing afferents in the greater splanchnic nerve that innervate the majority of abdominal viscera. Splanchnic afferent stimulation induced a DRP in multiple spinal segments, suggesting that visceral afferent activation can presynaptically inhibit afferent input throughout the spinal grey. Given the relative scarcity of visceral input to the spinal cord compared to their somatic counterparts, the extent of the visceral afferent-mediated reflex responses and DRP generation are particularly noteworthy.

Interestingly, evoked DRPs were commonly associated with depolarizations of sufficient magnitude to recruit backward propagating dorsal root reflexes. An implication of this is that spinal circuits can use afferents to function as efferents [268]. This would lead to back-propagating afferent synaptic transmission into the periphery, releasing

neuromodulators (e.g. CGRP) and/or other signaling molecules that regulate organ function and blood flow [10, 106, 112, 161]. If true, DRPs may not serve to primarily provide PSI to central afferents, but instead serve as a vehicle to centrally induce peripheral sensitization.

The present study does not identify the afferent modalities responsible for initiating DRPs or whether these are the same afferents that generate DRPs. However, it is generally true that PSI is strongest on the same fiber types [219]. Clearly, knowledge of which visceral afferents are inhibited is crucial to understanding the physiological role of the generated PSI. For example, is the primary function of abdominal visceral afferent mediated PAD the local coordination of organ regulation, such as the effects of inhibiting perineal afferents involved in micturition [30]? Or does visceral-afferent mediated PAD spread to unrelated afferents? Visceral stimulation (colorectal distension) has been shown to have inhibitory actions of on renal afferent related dorsal horn interneurons [41], suggesting that functionally unrelated visceral afferents may interact with one another and/or have actions on shared spinal circuitry. Additionally, given that spinal visceral afferents are known conduits of visceral pain information, was our intensity of stimulation used to elicit DRPs sufficient to generate pain? Future studies are warranted to address these and other questions vital to understanding central regulation of visceral afferents.

5.3 Monoaminergic Modulation of Spinal Autonomic Circuits

Both 5HT and NE simultaneously inhibited visceral afferent transmission to the spinal cord as well as spinal circuitry generating PAD in dorsal root afferents. Below, I'll outline the implications of this in terms of (i) afferents inhibited at or before the first

synapse to the spinal cord, (ii) afferents disinhibited by depression of the DRP, and (iii) autonomic reflexes and organ regulation.

Regulation of afferent input at the first synapse depends on the type of sensory fiber activated. It appears that while monoamines strongly depress initial transmission from group II muscle afferents [24, 25, 119], cutaneous nociceptors [75], and from this dissertation, visceral afferents, they can have little effect or even facilitatory actions on non-pain encoding low threshold muscle and cutaneous afferents [24, 206]. If spinal visceral afferent transmission is in fact predominantly nociceptive [112], this is consistent with known anti-nociceptive actions of 5HT, NE, and DA in the spinal cord [175]. In effect, by depressing synaptic transmission of these subsets, 5HT and NE act to prune the sensory information received by the spinal cord, making it easier to focus on other types of presumably behaviorally relevant sensory input.

Not only do 5HT and NE appear to directly inhibit visceral afferent transmission to the spinal cord, but as evidenced by differential dose and time-dependent effects on evoked DRPs, VRPs, and EFPs, they also act on downstream sites in the PAD-mediated PSI circuitry (Figure 4.13). Yet what are the functional consequences of inhibiting visceral-afferent evoked PAD and visceral afferent transmission? First, if PAD acts as an activity-dependent filter of sensory information, by removing this filter the monoamines alter the state of spinal visceral sensory processing. In the presence of descending monoamines, the central nervous system would thus receive a wider array of sensory information at a lower gain. This may serve to dampen low-intensity afferent inflow but still allow for processing of high-intensity or systemic afferent signaling.

Additionally, afferent-evoked PAD often functions as a local spinal phenomenon, even having the potential to occur only in certain branches of the same afferents [69]. Combined with the potential efferent functions activated via dorsal root reflexes that can accompany the DRP, the same selectivity mechanisms may be transferable peripherally to locally influence organ function and blood flow. Therefore, it is conceivable that monoaminergic depression of the DRP could alter peripheral visceral function and disrupt organ regulation.

However, by analyzing the effects of bath applied MAs, this study assessed the combined effects of nonspecific neuromodulation of the spinal cord. Differential, location specific regulation would therefore not be visible with the current configuration. Yet, if descending 5HT and NE tracts indeed do not synapse directly on dorsal horn neurons but rather act via volume transmission [175], actions on primary afferents terminals as well as nearby dorsal horn neurons should be affected similarly. In fact, laminar selectivity in modulatory action has been reported for muscle-afferent evoked field potentials [120], with each monoamine having more potent actions at distinct spinal sites. Additionally, descending nuclei may be differentially activated [207], allowing for more targeted modulation of sensory input. Taken together, monoaminergic depression at the first spinal synapse may be differential based on afferent modality, while later actions within the spinal cord PSI circuitry differ based on anatomical location.

On the output side, 5HT and NE inhibited both spontaneous and visceral afferent-evoked motor reflexes in the ventral root, yet increased overall excitability of SPNs. If activated simultaneously, this pairing of increased excitability to sympathetic efferents and decreased responsiveness to autonomic afferents would argue for a decoupling of

sympathetic output from visceral input, perhaps preferentially shifting autonomic nervous system to a feed-forward system, where descending command pathways or intrinsic spinal circuits dictate motor output.

However, as opposed to their diffuse projections in the dorsal horn, 5HT and NE directly provide conventional chemical synapses onto SPNs [175], often through distinct pathways [22, 82, 150]. This suggests the descending MA systems have much more selective control over sympathetic output than for primary afferents. The brain could, in effect, increase sympathetic responses to visceral input by releasing monoamines only in the IML and allowing synaptic transmission to continue as usual in the dorsal horn. On the other hand, by releasing the monoamines in the dorsal horn alone, the balance would be shifted to ignore visceral input and its associated sympathetic output. This selective activation and its functional application should be explored further in future studies.

Excluded from the above analyses were the actions of DA. Of all the monoamines tested, DA had the lowest potency for depressing both the DRP and VRP. Additionally, the effects on both sympathetic efferents and visceral afferents were highly dose-sensitive. Low doses of DA appeared to excite SPNs and motor neurons in the ventral root, while higher doses had inhibitory actions. Similarly, low doses of DA facilitated the DRP, thus exaggerating the PAD (and therefore likely presynaptic inhibition) induced by visceral afferents. This suggests that with only small amounts of DA, there would be a facilitation of sympathetic efferent activity while even greater visceral-afferent mediated inhibition of afferents, potentially increasing coordination of afferents and efferents necessary for organ regulation. Evidence in the pre-frontal cortex suggests this may be due to differences in receptor affinity [254, 280]. These dose-dependent bimodal actions may have

particularly strong ramifications where spinal dopamine levels are thought to be low, such as in restless leg syndrome [48] and Parkinson's disease [259]. The differences in potency of both DRP and VRP depression of DA versus 5HT and NE also argues for distinct mechanisms, a notion suggested by previous work in the lab studying its actions on locomotion [93].

Overall, the complex actions of the monoamines and the diversity of receptor subtypes identified on SPNs with immunohistochemistry equip the descending monoaminergic systems with a variety of tools with which to modulate spinal autonomic circuits.

5.4 FUTURE STUDIES

This dissertation has laid the groundwork for understanding spinal processing of visceral input and sympathetic output. The *in vitro* spinal cord and sympathetic chain preparation is well suited for the study of visceral afferent processing, by allowing direct access to the CNS in the absence of the blood brain barrier, where ionic concentrations and neurotransmitters may be easily manipulated. What follows are what I believe to be the most important next steps.

(i) To more fully understand the function of PSI in the autonomic nervous system, and what the implications are of its removal, it is imperative to know the identity of the giving and receiving afferents involved in visceral afferent induced PAD. This can be investigated with modality- selective stimulation of end organs while recording from single identified afferents, such as has been done in muscle afferents [122].

(ii) Whether visceral-afferent induced PAD is generated using the traditionally touted tri-synaptic circuit with last order GABAergic interneurons or an alternative pathway may shed light onto the causes of slower DRP onset in visceral afferents. This can be addressed by assessing the GABAergic sensitivity of PAD generation and examining histological basis for axo-axonic synapses of visceral afferents [219].

(iii) The functional implications of descending monoamines would be better understood with detailed study of physiological release patterns of the monoamines into the spinal cord. As a starting point, the brainstem could be left intact in this in vitro prep and various monoaminergic nuclei targeted for selective stimulation.

(iv) If the descending monoamines do have actions on both synaptic transmission and DRP-generating circuitry in the spinal cord, there should be anatomical evidence of (at least) two separate sites of action. To investigate potential anatomical substrates, immunohistochemistry could be used to analyze monoamine receptors co-localized with $CGRP^{+}$ afferent terminals as well as monoaminergic nerve terminals nearby.

(v) The transgenic mouse model can be utilized in future studies of both sympathetic output and visceral afferent processing. Conditional neuronal knockout/silencing of molecularly distinct cell populations [92], optogenetics [61, 96], and selective retrograde tracing of monosynaptically connected

neurons [242] can be utilized to define functional spinal organization of the autonomic nervous system, as well as alterations by disease or injury.

(vi) As the monoamines appear to influence the overall state of visceral sensory and sympathetic output processing in the spinal cord, this work lays the groundwork for modulating spinal autonomic circuitry after spinal cord injury. Potential therapies for restoring visceral afferent-dependent and ongoing sympathetic activity after injury could include intrathecal monoaminergic agonist delivery to specific spinal locations. Investigations into receptor laminar specificity and monoaminergic release patterns, as well as spinal plasticity after injury would aid immensely to developing such treatments.

In conclusion, my dissertation has begun to elucidate the mechanisms by which the spinal cord processes sympathetic motor output and visceral afferent input. By establishing a mouse model and *in vitro* sympathetic chain and spinal cord preparation I have laid the groundwork for delving more into understanding this vital autonomic integration and modulation center.

REFERENCES

1. Aars, H and Akre, S, *Reflex Changes in Sympathetic Activity and Arterial Blood Pressure Evoked by Afferent Stimulation of the Renal Nerve.* Acta Physiologica Scandinavica, 1970. **78**(2): p. 184-188.
2. Akeyson, EW, Knuepfer, MM, and Schramm, LP, *Splanchnic input to thoracic spinal neurons and its supraspinal modulation in the rat.* Brain Research, 1990. **536**(1-2): p. 30-40.
3. Akeyson, EW and Schramm, LP, *Processing of splanchnic and somatic input in thoracic spinal cord of the rat.* American Journal of Physiology - Regulatory, Integrative and Comparative Physiology, 1994. **266**(1): p. R257-R267.
4. Albano, JP and Garnier, L, *Bulbo-spinal respiratory effects originating from the splanchnic afferents.* Respiration Physiology, 1983. **51**(2): p. 229-239.
5. Ammons, WS, Blair, RW, and Foreman, RD, *Greater splanchnic excitation of primate T1-T5 spinothalamic neurons.* Journal of Neurophysiology, 1984. **51**(3): p. 592-603.
6. Anderson, C, Mclachlan, EM, and Srb-Christie, O, *Distribution of sympathetic preganglionic neurons and monoaminergic nerve terminals in the spinal cord of the rat.* The Journal of Comparative Neurology, 1989. **283**(2): p. 269-284.
7. Anderson, CR, Mclachlan, EM, and Srb-Christie, O, *Distribution of sympathetic preganglionic neurons and monoaminergic nerve terminals in the spinal cord of the rat.* The Journal of Comparative Neurology, 1989. **283**(2): p. 269-284.
8. Andrews, PV and Helme, RD, *Tachykinin-induced vasodilatation in rat skin measured with a laser-Doppler flowmeter: evidence for receptor-mediated effects.* Regulatory Peptides. **25**(3): p. 267-275.
9. Angel, MJ, et al., *Primary afferent depolarization of cat pudendal afferents during micturition and segmental afferent stimulation.* The Journal of Physiology, 1994. **479**(Pt 3): p. 451-461.
10. Apodaca, G, *The Uroepithelium: Not Just a Passive Barrier.* Traffic, 2004. **5**(3): p. 117-128.
11. Arber, S, et al., *Requirement for the Homeobox Gene Hb9 in the Consolidation of Motor Neuron Identity.* Neuron, 1999. **23**(4): p. 659-674.
12. Bahns, E, et al., *Functional characteristics of lumbar visceral afferent fibres from the urinary bladder and the urethra in the cat.* Pflügers Archiv European Journal of Physiology, 1986. **407**(5): p. 510-518.
13. Bain, WA, Irving, JT, and Mcswiney, BA, *The afferent fibres from the abdomen in the splanchnic nerves.* The Journal of Physiology, 1935. **84**(3): p. 323-333.
14. Barraud, Q, et al., *Neuroanatomical Study of the A11 Diencephalospinal Pathway in the Non-Human Primate.* PLoS ONE, 2010. **5**(10): p. e13306.
15. Bell, JA and Matsumiya, T, *Inhibitory effects of dorsal horn and excitant effects of ventral horn intraspinal microinjections of norepinephrine and serotonin in the cat.* Life Sciences, 1981. **29**(15): p. 1507-1514.
16. Benarroch, EE, *Descending monoaminergic pain modulation.* Neurology, 2008. **71**(3): p. 217-221.
17. Berthoud, H-R and Neuhuber, WL, *Functional and chemical anatomy of the afferent vagal system.* Autonomic Neuroscience, 2000. **85**(1-3): p. 1-17.

18. Biscoe, TJ, Nickels, SM, and Stirling, CA, *NUMBERS AND SIZES OF NERVE FIBRES IN MOUSE SPINAL ROOTS.* Experimental Physiology, 1982. **67**(3): p. 473-494.
19. Björklund, A and Skagerberg, G, *Evidence for a major spinal cord projection from the diencephalic A11 dopamine cell group in the rat using transmitter-specific fluorescent retrograde tracing.* Brain Research, 1979. **177**(1): p. 170-175.
20. Black, IB, *Regulation of Autonomic Development.* Annual Review of Neuroscience, 1978. **1**(1): p. 183-214.
21. Black, IB, Hendry, IA, and Iversen, LL, *Trans-synaptic regulation of growth and development of adrenergic neurones in a mouse sympathetic ganglion.* Brain Research, 1971. **34**(2): p. 229-240.
22. Bowker, RM and Abbott, LC, *Quantitative re-evaluation of descending serotonergic and non-serotonergic projections from the medulla of the rodent: evidence for extensive co-existence of serotonin and peptides in the same spinally projecting neurons, but not from the nucleus raphe magnus.* Brain Research, 1990. **512**(1): p. 15-25.
23. Brain, SD, et al., *Calcitonin gene-related peptide is a potent vasodilator.* Nature, 1985. **313**(5997): p. 54-56.
24. Bras, H, et al., *Comparison of effects of monoamines on transmission in spinal pathways from group I and II muscle afferents in the cat.* Experimental Brain Research, 1989. **76**(1): p. 27-37.
25. Bras, H, et al., *Comparison of Effects of Various Types of NA and 5-HT Agonists on Transmission from Group II Muscle Afferents in the Cat.* European Journal of Neuroscience, 1990. **2**(12): p. 1029-1039.
26. Bregman, BS, *Development of serotonin immunoreactivity in the rat spinal cord and its plasticity after neonatal spinal cord lesions.* Developmental Brain Research, 1987. **34**(2): p. 245-263.
27. Brink, E, Jankowska, E, and Skoog, B, *Convergence onto interneurons subserving primary afferent depolarization of group I afferents.* Journal of Neurophysiology, 1984. **51**(3): p. 432-449.
28. Brown, AG and Hayden, RE, *Presynaptic depolarization produced by and in identified cutaneous afferent fibres in the rabbit.* Brain Research, 1972. **38**(1): p. 187-192.
29. Brownstone, RM, *Beginning at the end: Repetitive firing properties in the final common pathway.* Progress in Neurobiology, 2006. **78**(3-5): p. 156-172.
30. Buss, RR and Shefchyk, SJ, *Excitability changes in sacral afferents innervating the urethra, perineum and hindlimb skin of the cat during micturition.* The Journal of Physiology, 1999. **514**(2): p. 593-607.
31. C. R. Anderson, EMMOS-C, *Distribution of sympathetic preganglionic neurons and monoaminergic nerve terminals in the spinal cord of the rat.* The Journal of Comparative Neurology, 1989. **283**(2): p. 269-284.
32. Cabot, JB, et al., *Spinal cord lamina V and lamina VII interneuronal projections to sympathetic preganglionic neurons.* The Journal of Comparative Neurology, 1994. **347**(4): p. 515-530.

33. Calaresu, FR, Stella, A, and Zanchetti, A, *Haemodynamic responses and renin release during stimulation of afferent renal nerves in the cat.* The Journal of Physiology, 1976. **255**(3): p. 687-700.
34. Calinski, T and Harabasz, J, *A Dendrite Method for Cluster Analysis.* Communications in Statistics, 1974. **3**(1): p. 1-27.
35. Castelletti, L, et al., *Potassium channels involved in the transduction mechanism of dopamine D2 receptors in rat lactotrophs.* The Journal of Physiology, 1989. **410**(1): p. 251-265.
36. Cervero, F, *Visceral Nociception: Peripheral and Central Aspects of Visceral Nociceptive Systems.* Philosophical Transactions of the Royal Society of London. B, Biological Sciences, 1985. **308**(1136): p. 325-337.
37. Cervero, F and Connell, LA, *Distribution of somatic and visceral primary afferent fibres within the thoracic spinal cord of the cat.* The Journal of Comparative Neurology, 1984. **230**(1): p. 88-98.
38. Cervero, F, Connell, LA, and Lawson, SN, *Somatic and visceral primary afferents in the lower thoracic dorsal root ganglia of the cat.* The Journal of Comparative Neurology, 1984. **228**(3): p. 422-431.
39. Cervero, F and Laird, JMA, *Understanding the signaling and transmission of visceral nociceptive events.* Journal of Neurobiology, 2004. **61**(1): p. 45-54.
40. Chaouloff, F, Berton, O, and Mormède, P, *Serotonin and Stress.* Neuropsychopharmacology, 1999. **21**(2, Supplement 1): p. 28S-32S.
41. Chau, D, Johns, DG, and Schramm, LP, *Ongoing and Stimulus-Evoked Activity of Sympathetically Correlated Neurons in the Intermediate Zone and Dorsal Horn of Acutely Spinalized Rats.* J Neurophysiol, 2000. **83**(5): p. 2699-2707.
42. Chesnoy-Marchais, D and Barthe, J, *Voltage-dependent block of NMDA responses by 5-HT agonists in ventral spinal cord neurones.* British Journal of Pharmacology, 1996. **117.1** p. 133-141.
43. Christopher J. Madden, SFM, *Serotonin potentiates sympathetic responses evoked by spinal NMDA.* The Journal of Physiology, 2006. **577**(2): p. 525-537.
44. Clark, FM and Proudfit, HK, *The projection of locus coeruleus neurons to the spinal cord in the rat determined by anterograde tracing combined with immunocytochemistry.* Brain Research, 1991. **538**(2): p. 231-245.
45. Clark, FM and Proudfit, HK, *The projection of noradrenergic neurons in the A7 catecholamine cell group to the spinal cord in the rat demonstrated by anterograde tracing combined with immunocytochemistry.* Brain Research, 1991. **547**(2): p. 279-288.
46. Clark, FM and Proudfit, HK, *The projections of noradrenergic neurons in the A5 catecholamine cell group to the spinal cord in the rat: anatomical evidence that A5 neurons modulate nociception.* Brain Research, 1993. **616**(1-2): p. 200-210.
47. Clemens, S and Hochman, S, *Conversion of the Modulatory Actions of Dopamine on Spinal Reflexes from Depression to Facilitation in D3 Receptor Knock-Out Mice.* The Journal of Neuroscience, 2004. **24**(50): p. 11337-11345.
48. Clemens, S, Rye, D, and Hochman, S, *Restless legs syndrome: Revisiting the dopamine hypothesis from the spinal cord perspective.* Neurology, 2006. **67**(1): p. 125-130.

49. Clemens, S, Sawchuk, MA, and Hochman, S, *Reversal of the circadian expression of tyrosine-hydroxylase but not nitric oxide synthase levels in the spinal cord of dopamine D3 receptor knockout mice.* Neuroscience, 2005. **133**(2): p. 353-357.
50. Coggeshall, RE, et al., *Unmyelinated and small myelinated axons in rat ventral roots.* The Journal of Comparative Neurology, 1977. **173**(1): p. 175-184.
51. Conte, D, et al., *Transmitter content, origins and connections of axons in the spinal cord that possess the serotonin (5-hydroxytryptamine) 3 receptor.* Neuroscience, 2005. **134**(1): p. 165-173.
52. Coote, JH, Downman, CBB, and Weber, WV, *Reflex discharges into thoracic white rami elicited by somatic and visceral afferent excitation.* The Journal of Physiology, 1969. **202**(1): p. 147-159.
53. Coote, JH, et al., *The response of individual sympathetic preganglionic neurones to microelectrophoretically applied endogenous monoamines.* Brain Research, 1981. **215**(1-2): p. 135-145.
54. Cramer, NaH-W, Rm, *Properties of Hb9 interneurons in the adult mouse spinal cord.* Society for Neuroscience Abstracts, 2008. **34**.
55. Danzebrink, RM and Gebhart, GF, *Antinociceptive effects of intrathecal adrenoceptor agonists in a rat model of visceral nociception.* Journal of Pharmacology and Experimental Therapeutics, 1990. **253**(2): p. 698-705.
56. Danzebrink, RM and Gebhart, GF, *Evidence that spinal 5-HT1, 5-HT2 and 5-HT3 receptor subtypes modulate responses to noxious colorectal distension in the rat.* Brain Research, 1991. **538**(1): p. 64-75.
57. Day, HEW, et al., *Distribution of [alpha]1a-, [alpha]1b- and [alpha]1d-adrenergic receptor mRNA in the rat brain and spinal cord.* Journal of Chemical Neuroanatomy, 1997. **13**(2): p. 115-139.
58. De Groat, WC, *Chapter 11 Spinal cord projections and neuropeptides in visceral afferent neurons*, in *Progress in Brain Research*, F. Cervero and J.F.B. Morrison, Editors. 1986, Elsevier. p. 165-187.
59. Dembowsky, K, Czachurski, J, and Seller, H, *An intracellular study of the synaptic input to sympathetic preganglionic neurones of the third thoracic segment of the cat.* Journal of the Autonomic Nervous System, 1985. **13**(3): p. 201-244.
60. Dembowsky, K, Czachurski, J, and Seller, H, *Three types of sympathetic preganglionic neurones with different electrophysiological properties are identified by intracellular recordings in cat.* Pflügers Archiv : European journal of physiology, 1986. **406**: p. 112-120.
61. Depuy, SD, et al., *Control of breathing by raphe obscurus serotonergic neurons in mice.* The Journal of neuroscience : the official journal of the Society for Neuroscience, 2011. **31**(6): p. 1981-90.
62. Docherty, JR, *Subtypes of functional [alpha]1- and [alpha]2-adrenoceptors.* European Journal of Pharmacology, 1998. **361**(1): p. 1-15.
63. Doly, S, et al., *5-HT5A receptor localization in the rat spinal cord suggests a role in nociception and control of pelvic floor musculature.* The Journal of Comparative Neurology, 2004. **476**(4): p. 316-329.

64. Downman, CBB, *SKELETAL MUSCLE REFLEXES OF SPLANCHNIC AND INTERCOSTAL NERVE ORIGIN IN ACUTE SPINAL AND DECEREBRATE CATS.* Journal of Neurophysiology, 1955. **18**(3): p. 217-235.
65. Downman, CBB and Evans, MH, *The distribution of splanchnic afferents in the spinal cord of cat.* The Journal of Physiology, 1957. **137**(1): p. 66-79.
66. Ebbesson, SOE, *Quantitative studies of superior cervical sympathetic ganglia in a variety of primates including man. I. The ratio of preganglionic fibers to ganglionic neurons.* Journal of Morphology, 1968. **124**(1): p. 117-131.
67. Eccles, JC, *Presynaptic Inhibition in the Spinal Cord*, in *Progress in Brain Research*, J.C. Eccles and J.P. Schadé, Editors. 1964, Elsevier. p. 65-91.
68. Eccles, JC, Schmidt, RF, and Willis, WD, *Presynaptic inhibition of the spinal monosynaptic reflex pathway.* The Journal of Physiology, 1962. **161**(2): p. 282-297.
69. Eguibar, JR, Quevedo, J, and Rudomin, P, *Selective cortical and segmental control of primary afferent depolarization of single muscle afferents in the cat spinal cord.* Experimental Brain Research, 1997. **113**(3): p. 411-430.
70. Eisenach, JC, Zhang, Y, and Duflo, F, *[alpha]2-adrenoceptors inhibit the intracellular Ca2+ response to electrical stimulation in normal and injured sensory neurons, with increased inhibition of calcitonin gene-related peptide expressing neurons after injury.* Neuroscience, 2005. **131**(1): p. 189-197.
71. Evans, MH and Mcpherson, A, *The effects of stimulation of visceral afferent nerve fibres on somatic reflexes.* The Journal of Physiology, 1958. **140**(2): p. 201-212.
72. Ezerman, EB and Forehand, CJ, *Development and segmental organization of rostrocaudal dendrites of rat sympathetic preganglionic neurons.* Journal of the Autonomic Nervous System, 1996. **57**(1-2): p. 29-35.
73. Fleetwood-Walker, SM and Coote, JH, *Contribution of noradrenaline-, dopamine- and adrenaline-containing axons to the innervation of different regions of the spinal cord of the cat.* Brain Research, 1981. **206**(1): p. 95-106.
74. Fleetwood-Walker, SM, Hope, PJ, and Mitchell, R, *Antinociceptive actions of descending dopaminergic tracts on cat and rat dorsal horn somatosensory neurones.* The Journal of Physiology, 1988. **399**(1): p. 335-348.
75. Fleetwood-Walker, SM, et al., *An [alpha]2 receptor mediates the selective inhibition by noradrenaline of nociceptive responses of identified dorsal horn neurones.* Brain Research, 1985. **334**(2): p. 243-254.
76. Flores-Hernandez, J, et al., *D1 Dopamine Receptor Activation Reduces GABAA Receptor Currents in Neostriatal Neurons Through a PKA/DARPP-32/PP1 Signaling Cascade.* Journal of Neurophysiology, 2000. **83**(5): p. 2996-3004.
77. Forehand, CJ, et al., *Segmental patterning of rat and chicken sympathetic preganglionic neurons: correlation between soma position and axon projection pathway.* J. Neurosci., 1994. **14**(1): p. 231-241.
78. Foreman, RD, Hancock, MB, and Willis, WD, *Responses of spinothalamic tract cells in the thoracic spinal cord of the monkey to cutaneous and visceral inputs.* Pain, 1981. **11**(2): p. 149-162.

79. Formenti, A, et al., *Multiple modulatory effects of dopamine on calcium channel kinetics in adult rat sensory neurons.* The Journal of Physiology, 1998. **509**(2): p. 395-409.
80. Franks, NP and Lieb, WR, *Molecular and cellular mechanisms of general anaesthesia.* Nature, 1994. **367**(6464): p. 607-614.
81. Franz, D, Evans, M, and Perl, E, *Characteristics of viscerosympathetic reflexes in the spinal cat.* American Journal of Physiology -- Legacy Content, 1966. **211**(6): p. 1292-1298.
82. Fritschy, J-M and Grzanna, R, *Demonstration of two separate descending noradrenergic pathways to the rat spinal cord: Evidence for an intragriseal trajectory of locus coeruleus axons in the superficial layers of the dorsal horn.* The Journal of Comparative Neurology, 1990. **291**(4): p. 553-582.
83. Galeotti, N, et al., *Role of potassium channels in the antinociception induced by agonists of α2-adrenoceptors.* British Journal of Pharmacology, 1999. **126**(5): p. 1214-1220.
84. Garraway, SM and Hochman, S, *Modulatory Actions of Serotonin, Norepinephrine, Dopamine, and Acetylcholine in Spinal Cord Deep Dorsal Horn Neurons.* J Neurophysiol, 2001. **86**(5): p. 2183-2194.
85. Garraway, SM and Hochman, S, *Pharmacological characterization of serotonin receptor subtypes modulating primary afferent input to deep dorsal horn neurons in the neonatal rat.* British Journal of Pharmacology, 2001. **132**(8): p. 1789-1798.
86. Gebhart, GF, *Visceral pain—peripheral sensitisation.* Gut, 2000. **47**(suppl 4): p. iv54-iv55.
87. Gerin, C, Becquet, D, and Privat, A, *Direct evidence for the link between monoaminergic descending pathways and motor activity. I. A study with microdialysis probes implanted in the ventral funiculus of the spinal cord.* Brain Research, 1995. **704**(2): p. 191-201.
88. Gilbey, MP, et al., *Inhibition of sympathetic activity by stimulating in the raphe nuclei and the role of 5-hydroxytryptamine in this effect.* Brain Research, 1981. **226**(1-2): p. 131-142.
89. Gilbey, MP and Stein, RD, *Characteristics of sympathetic preganglionic neurones in the lumbar spinal cord of the cat.* J Physiol, 1991. **432**(1): p. 427-443.
90. Gladwell, SJ and Coote, JH, *Inhibitory and indirect excitatory effects of dopamine on sympathetic preganglionic neurones in the neonatal rat spinal cord in vitro.* Brain Research, 1999. **818**(2): p. 397-407.
91. Gladwell, SJ, et al., *D1-like dopamine receptors on retrogradely labelled sympathoadrenal neurones in the thoracic spinal cord of the rat.* Experimental Brain Research, 1999. **128**(3): p. 377-382.
92. Gosgnach, S, et al., *V1 spinal neurons regulate the speed of vertebrate locomotor outputs.* Nature, 2006. **440**(7081): p. 215-219.
93. Gozal, L, *Trace amines as novel modulators of spinal motor function*, in *Department of Biomedical Engineering*. 2010, Georgia Institute of Technology and Emory University: Atlanta, GA.
94. Green, T and Dockray, GJ, *Characterization of the peptidergic afferent innervation of the stomach in the rat, mouse and guinea-pig.* Neuroscience, 1988. **25**(1): p. 181-193.

95. Guyenet, PG and Cabot, JB, *Inhibition of sympathetic preganglionic neurons by catecholamines and clonidine: mediation by an alpha-adrenergic receptor.* J. Neurosci., 1981. **1**(8): p. 908-917.
96. Hagglund, M, et al., *Activation of groups of excitatory neurons in the mammalian spinal cord or hindbrain evokes locomotion.* Nature neuroscience, 2010. **13**(2): p. 246-52.
97. Han, P, et al., *Dopaminergic Modulation of Spinal Neuronal Excitability.* The Journal of Neuroscience, 2007. **27**(48): p. 13192-13204.
98. Hancock, MB, Rigamonti, DD, and Bryan, RN, *Convergence in the lumbar spinal cord of pathways activated by splanchnic nerve and hind limb cutaneous nerve stimulation.* Experimental Neurology, 1973. **38**(2): p. 337-348.
99. Harvey, PJ, et al., *Persistent Sodium Currents and Repetitive Firing in Motoneurons of the Sacrocaudal Spinal Cord of Adult Rats.* J Neurophysiol, 2006. **96**(3): p. 1141-1157.
100. Henneman, E, *The size-principle: a deterministic output emerges from a set of probabilistic connections.* J Exp Biol, 1985. **115**(1): p. 105-112.
101. Hicks, GA, et al., *Excitation of rat colonic afferent fibres by 5-HT3 receptors.* The Journal of Physiology, 2002. **544**(3): p. 861-869.
102. Hochman, S, et al., *Presynaptic inhibition of primary afferents by depolarization: observations supporting nontraditional mechanisms.* Annals of the New York Academy of Sciences, 2010. **1198**(1): p. 140-152.
103. Holets, V and Elde, R, *The differential distribution and relationship of serotoninergic and peptidergic fibers to sympathoadrenal neurons in the intermediolateral cell column of the rat: A combined retrograde axonal transport and immunofluorescence study.* Neuroscience, 1982. **7**(5): p. 1155-1174.
104. Holohean, AM, Hackman, JC, and Davidoff, RA, *Changes in membrane potential of frog motoneurons induced by activation of serotonin receptor subtypes.* Neuroscience, 1990. **34**(3): p. 555-564.
105. Holstege, JC, et al., *Distribution of dopamine immunoreactivity in the rat, cat, and monkey spinal cord.* The Journal of Comparative Neurology, 1996. **376**(4): p. 631-652.
106. Holzer, P, *Neurogenic vasodilatation and plasma leakage in the skin.* General Pharmacology: The Vascular System, 1998. **30**(1): p. 5-11.
107. Hounsgaard, J and Kiehn, O, *Serotonin-induced bistability of turtle motoneurones caused by a nifedipine-sensitive calcium plateau potential.* The Journal of Physiology, 1989. **414**(1): p. 265-282.
108. Inokuchi, H, et al., *Membrane properties and dendritic arborization of the intermediolateral nucleus neurons in the guinea-pig thoracic spinal cord in vitro.* Journal of the Autonomic Nervous System, 1993. **43**(2): p. 97-106.
109. Inokuchi H, YM, Polosa C, Nishi S, *Adrenergic receptors (alpha 1 and alpha 2) modulate different potassium conductances in sympathetic preganglionic neurons.* Can J Physiol Pharmacol, 1992. **70**(Supplement): p. S92-97.
110. J. M. Petras, JFC, *Autonomic neurons in the spinal cord of the rhesus monkey: A correlation of the findings of cytoarchitectonics and sympathectomy with fiber degeneration following dorsal rhizotomy.* The Journal of Comparative Neurology, 1972. **146**(2): p. 189-218.

111. Jacobs, BL and Fornal, CA, *5-HT and motor control: a hypothesis.* Trends in Neurosciences, 1993. **16**(9): p. 346-352.
112. Jänig, W, *Neurobiology of visceral afferent neurons: neuroanatomy, functions, organ regulations and sensations.* Biological Psychology, 1996. **42**(1-2): p. 29-51.
113. Jänig, W, *The integrative action of the autonomic nervous system: neurobiology of homeostasis*. 2006: Cambridge University Press.
114. Jänig, W and Häbler, H-J, *Visceral-Autonomic Integration*, in *Visceral Pain*, G.F. Gebhart, Editor. 1995, IASP Press: Seattle, WA. p. 311-350.
115. Jänig, W and Häbler, HJ, *Neurophysiological analysis of target-related sympathetic pathways- from animal to human: similarities and differences*.* Acta Physiologica Scandinavica, 2003. **177**(3): p. 255-274.
116. Jänig, W and Lisney, SJ, *Small diameter myelinated afferents produce vasodilatation but not plasma extravasation in rat skin.* The Journal of Physiology, 1989. **415**(1): p. 477-486.
117. Janig, W and Mclachlan, EM, *Organization of lumbar spinal outflow to distal colon and pelvic organs.* Physiological Reviews, 1987. **67**(4): p. 1332-1404.
118. Jänig, W and Szulczyk, P, *The organization of lumbar preganglionic neurons.* Journal of the Autonomic Nervous System, 1981. **3**(2-4): p. 177-191.
119. Jankowska, E, et al., *Effects of monoamines on interneurons in four spinal reflex pathways from group I and/or group II muscle afferents.* European Journal of Neuroscience, 2000. **12**(2): p. 701-714.
120. Jankowska, E and Riddell, J, *Neuronal systems involved in modulating synaptic transmission from group II muscle afferents*. 1998, Presynaptic inhibition and neural control. Editors: Rudomin, P.,Romo, R. Mendell, L. Oxford University Press.
121. Jankowska, E and Riddell, JS, *Interneurones mediating presynaptic inhibition of group II muscle afferents in the cat spinal cord.* The Journal of Physiology, 1995. **483**(Pt 2): p. 461-471.
122. Jiménez, I, Rudomin, P, and Solodkin, M, *PAD patterns of physiologically identified afferent fibres from the medial gastrocnemius muscle.* Experimental Brain Research, 1988. **71**(3): p. 643-657.
123. Jonas, P, Bischofberger, J, and Sandkuhler, J, *Corelease of two fast neurotransmitters at a central synapse [see comments]*. Science, 1998. **281**(5375): p. 419-424.
124. Kaczmarek, LK and Levitan, IB, *Neuromodulation: the biochemical control of neuronal excitability*. 1987: Oxford University Press.
125. Kandel, ER, Schwartz, JH, and Jessell, TM, *Principles of neural science*. 4th ed. 2000: McGraw-Hill, Health Professions Division.
126. Kangrga, I, Larew, JSA, and Randic, M, *The effects of substance P and calcitonin gene-related peptide on the efflux of endogenous glutamate and aspartate from the rat spinal dorsal horn in vitro.* Neuroscience Letters, 1990. **108**(1-2): p. 155-160.
127. Kashiba, H, et al., *Cell size and cell type analysis of calcitonin gene-related peptide-containing cutaneous and splanchnic sensory neurons in the rat.* Peptides. **12**(1): p. 101-106.

128. Kaufman, L and Rousseeuw, PJ, *Finding groups in data: An introduction to cluster analysis*. Applied Probability and Statistics. 1990, New York: Wiley-Interscience.
129. Khasabov, SG, et al., *Modulation of afferent-evoked neurotransmission by 5-HT3 receptors in young rat dorsal horn neurones in vitro: a putative mechanism of 5-HT3 induced anti-nociception.* British Journal of Pharmacology, 1999. **127**(4): p. 843-852.
130. King, BF and Szurszewski, JH, *Peripheral reflex pathways involving abdominal viscera: transmission of impulses through prevertebral ganglia.* American Journal of Physiology - Gastrointestinal and Liver Physiology, 1989. **256**(3): p. G581-G588.
131. Knuepfer, MM, Akeyson, EW, and Schramm, LP, *Spinal projections of renal afferent nerves in the rat.* Brain Research, 1988. **446**(1): p. 17-25.
132. Krasowski, MD and Harrison, NL, *The actions of ether, alcohol and alkane general anaesthetics on GABAA and glycine receptors and the effects of TM2 and TM3 mutations.* British Journal of Pharmacology, 2000. **129**(4): p. 731-743.
133. Kubasak, MD, et al., *Developmental distribution of reelin-positive cells and their secreted product in the rodent spinal cord.* The Journal of Comparative Neurology, 2004. **468**(2): p. 165-178.
134. Kuo, DC, et al., *A wide field electron microscopic analysis of the fiber constituents of the major splanchnic nerve in cat.* The Journal of Comparative Neurology, 1982. **210**(1): p. 49-58.
135. Kuo, JJ, et al., *Essential role of the persistent sodium current in spike initiation during slowly rising inputs in mouse spinal neurones.* The Journal of Physiology, 2006. **574**(3): p. 819-834.
136. Laird, AS, Carrive, P, and Waite, PME, *Cardiovascular and temperature changes in spinal cord injured rats at rest and during autonomic dysreflexia.* J Physiol, 2006. **577**(2): p. 539-548.
137. Laitinen, JT, *Dopamine Stimulates K+ Efflux in the Chick Retina via D1 Receptors Independently of Adenylyl Cyclase Activation.* Journal of Neurochemistry, 1993. **61**(4): p. 1461-1469.
138. Lanuza, GM, et al., *Genetic Identification of Spinal Interneurons that Coordinate Left-Right Locomotor Activity Necessary for Walking Movements.* Neuron, 2004. **42**(3): p. 375-386.
139. Lee, RH and Heckman, CJ, *Bistability in Spinal Motoneurons In Vivo: Systematic Variations in Persistent Inward Currents.* J Neurophysiol, 1998. **80**(2): p. 583-593.
140. Lee, RH and Heckman, CJ, *Enhancement of Bistability in Spinal Motoneurons In Vivo by the Noradrenergic alpha 1 Agonist Methoxamine.* J Neurophysiol, 1999. **81**(5): p. 2164-2174.
141. Léna, I, et al., *Variations in extracellular levels of dopamine, noradrenaline, glutamate, and aspartate across the sleep–wake cycle in the medial prefrontal cortex and nucleus accumbens of freely moving rats.* Journal of Neuroscience Research, 2005. **81**(6): p. 891-899.

142. Levant, B and Mccarson, KE, *D3 dopamine receptors in rat spinal cord: implications for sensory and motor function.* Neuroscience Letters, 2001. **303**(1): p. 9-12.
143. Lew, WY and Longhurst, JC, *Substance P, 5-hydroxytryptamine, and bradykinin stimulate abdominal visceral afferents.* American Journal of Physiology - Regulatory, Integrative and Comparative Physiology, 1986. **250**(3): p. R465-R473.
144. Lewis, DI and Coote, JH, *Excitation and inhibition of rat sympathetic preganglionic neurones by catecholamines.* Brain Research, 1990. **530**(2): p. 229-234.
145. Lewis, DI, Sermasi, E, and Coote, JH, *Excitatory and indirect inhibitory actions of 5-hydroxytryptamine on sympathetic preganglionic neurones in the neonate rat spinal cord in vitro.* Brain Research, 1993. **610**(2): p. 267-275.
146. Lidierth, M, *Local and diffuse mechanisms of primary afferent depolarization and presynaptic inhibition in the rat spinal cord.* The Journal of Physiology, 2006. **576**(1): p. 309-327.
147. Lindh, B, Hökfelt, T, and Elfvin, LG, *Distribution and origin of peptide-containing nerve fibers in the celiac superior mesenteric ganglion of the guinea-pig.* Neuroscience, 1988. **26**(3): p. 1037-1071.
148. Lindvall, OL, Björklund, AB, and Skagerberg, G, *Dopamine-containing neurons in the spinal cord: Anatomy and some functional aspects.* Annals of Neurology, 1983. **14**(3): p. 255-260.
149. Liu, Y and Ma, Q, *Generation of somatic sensory neuron diversity and implications on sensory coding.* Current Opinion in Neurobiology, 2011. **21**(1): p. 52-60.
150. Loewy, AD, *Raphe pallidus and raphe obscurus projections to the intermediolateral cell column in the rat.* Brain Research, 1981. **222**(1): p. 129-133.
151. Logan, SD, et al., *Electrotonic coupling between rat sympathetic preganglionic neurones in vitro.* J Physiol, 1996. **495**(Pt_2): p. 491-502.
152. Lopez-Garcia, JA and King, AE, *Pre- and Post-synaptic Actions of 5-Hydroxytryptamine in the Rat Lumbar Dorsal Horn In Vitro: Implications for Somatosensory Transmission.* European Journal of Neuroscience, 1996. **8**(10): p. 2188-2197.
153. Low, A and Westerman, RA, *Neurogenic vasodilation in the rat hairy skin measured using a laser Doppler flowmeter.* Life Sciences, 1989. **45**(1): p. 49-57.
154. Low, PA and Dyck, PJ, *Splanchnic preganglionic neurons in man: II. Morphometry of myelinated fibers of T7 ventral spinal root.* Acta Neuropathologica, 1977. **40**(3): p. 219-225.
155. Ma, RC and Dun, NJ, *Excitation of lateral horn neurons of the neonatal rat spinal cord by 5-hydroxytryptamine.* Developmental Brain Research, 1986. **24**(1-2): p. 89-98.
156. Machacek, DW, et al., *Serotonin 5-HT2 receptor activation induces a long-lasting amplification of spinal reflex actions in the rat.* The Journal of Physiology, 2001. **537**(1): p. 201-207.

157. Maclachlan, EM, *An analysis of the release of acetylcholine from preganglionic nerve terminals.* The Journal of Physiology, 1975. **245**(2): p. 447-466.
158. Maclean, JN, Schmidt, BJ, and Hochman, S, *NMDA Receptor Activation Triggers Voltage Oscillations, Plateau Potentials and Burstinq in Neonatal Rat Lumbar Motoneurons ln Vitro*. European Journal of Neuroscience, 1997. **9**(12): p. 2702-2711.
159. Madden, CJ and Morrison, SF, *Brown adipose tissue sympathetic nerve activity is potentiated by activation of 5-hydroxytryptamine (5-HT)1A/5-HT7 receptors in the rat spinal cord.* Neuropharmacology, 2008. **54**(3): p. 487-496.
160. Madriaga, MA, et al., *Modulation of Locomotor Activity by Multiple 5-HT and Dopaminergic Receptor Subtypes in the Neonatal Mouse Spinal Cord.* Journal of Neurophysiology, 2004. **92**(3): p. 1566-1576.
161. Maggi, CA, et al., *Neuropeptides as regulators of airway function: vasoactive intestinal peptide and the tachykinins.* Physiological Reviews, 1995. **75**(2): p. 277-322.
162. Major, G, et al., *Detailed passive cable models of whole-cell recorded CA3 pyramidal neurons in rat hippocampal slices.* J. Neurosci., 1994. **14**(8): p. 4613-4638.
163. Marina, N, Taheri, M, and Gilbey, MP, *Generation of a physiological sympathetic motor rhythm in the rat following spinal application of 5-HT.* The Journal of Physiology, 2006. **571**(2): p. 441-450.
164. Markham, JA, Phelps, PE, and Vaughn, JE, *Development of rostrocaudal dendritic bundles in rat thoracic spinal cord: analysis of cholinergic sympathetic preganglionic neurons.* Developmental Brain Research, 1991. **61**(2): p. 229-236.
165. Marks, SA, et al., *[3H]Prazosin binding in the intermediolateral cell column and the effects of iontophoresed methoxamine on sympathetic preganglionic neuronal activity in the anaesthetized cat and rat.* Brain Research, 1990. **530**(2): p. 321-324.
166. Massari, VJ, et al., *Norepinephrine throughout the spinal cord of the cat: I. Normal quantitative laminar and segmental distribution.* Synapse, 1988. **2**(3): p. 258-265.
167. Maxwell, DJ, et al., *Characterisation of axon terminals in the rat dorsal horn that are immunoreactive for serotonin 5-HT₃A receptor subunits.* Experimental Brain Research, 2003. **149**(1): p. 114-124.
168. Mccall, RB, *Serotonergic excitation of sympathetic preganglionic neurons: a microiontophoretic study.* Brain Research, 1983. **289**(1-2): p. 121-127.
169. Mccorry, LK, *Physiology of the Autonomic Nervous System.* American Journal of Pharmaceutical Education, 2007. **71**(4): p. 1-11.
170. Mckenna, KE and Schramm, LP, *Sympathetic preganglionic neurons in the isolated spinal cord of the neonatal rat.* Brain Research, 1983. **269**(2): p. 201-210.
171. Mckenna, KE and Schramm, LP, *Mechanisms mediating the sympathetic silent period: Studies in the isolated spinal cord of the neonatal rat.* Brain Research, 1985. **329**(1-2): p. 233-240.

172. Mclachlan, EM, *Transmission of signals through sympathetic ganglia: modulation, integration or simply distribution?* Acta Physiologica Scandinavica, 2003. **177**(3): p. 227-235.
173. Mclachlan, EM and Oldfield, BJ, *Some observation on the catecholaminergic innervation of the intermediate zone of the thoracolumbar spinal cord of the cat.* The Journal of Comparative Neurology, 1981. **200**(4): p. 529-544.
174. Miles, GB, Dai, Y, and Brownstone, RM, *Mechanisms underlying the early phase of spike frequency adaptation in mouse spinal motoneurones.* The Journal of Physiology, 2005. **566**(2): p. 519-532.
175. Millan, MJ, *Descending control of pain.* Progress in Neurobiology, 2002. **66**(6): p. 355-474.
176. Millan, MJ, et al., *Signaling at G-protein-coupled serotonin receptors: recent advances and future research directions.* Trends in Pharmacological Sciences, 2008. **29**(9): p. 454-464.
177. Milner, TA, et al., *Phenylethanolamine N-methyltransferase-containing terminals synapse directly on sympathetic preganglionic neurons in the rat.* Brain Research, 1988. **448**(2): p. 205-222.
178. Missale, C, et al., *Dopamine Receptors: From Structure to Function.* Physiological Reviews, 1998. **78**(1): p. 189-225.
179. Miyazaki, T, Coote, JH, and Dun, NJ, *Excitatory and inhibitory effects of epinephrine on neonatal rat sympathetic preganglionic neurons in vitro.* Brain Research, 1989. **497**(1): p. 108-116.
180. Miyazaki, T, et al., *Voltage-dependent potassium currents of sympathetic preganglionic neurons in neonatal rat spinal cord thin slices.* Brain Research, 1996. **743**(1-2): p. 1-10.
181. Mizumura, K, Tadaki, E, and Kumazawa, T, *Respiratory changes induced by activation of testicular afferents in dogs.* Pflügers Archiv European Journal of Physiology, 1988. **411**(1): p. 27-33.
182. Molander, C, Ygge, J, and Dalsgaard, CJ, *Substance P-, somatostatin- and calcitonin gene-related peptide-like immunoreactivity and fluoride resistant acid phosphatase-activity in relation to retrogradely labeled cutaneous, muscular and visceral primary sensory neurons in the rat.* Neuroscience Letters, 1987. **74**(1): p. 37-42.
183. Morilak, DA, et al., *Role of brain norepinephrine in the behavioral response to stress.* Progress in Neuro-Psychopharmacology and Biological Psychiatry, 2005. **29**(8): p. 1214-1224.
184. Murase, K, et al., *Serotonin suppresses N-methyl-d-aspartate responses in acutely isolated spinal dorsal horn neurons of the rat.* Brain Research, 1990. **525**(1): p. 84-91.
185. Nagatsu, T, Levitt, M, and Udenfriend, S, *Tyrosine Hydroxylase.* Journal of Biological Chemistry, 1964. **239**(9): p. 2910-2917.
186. Ness, TJ and Gebhart, GF, *Colorectal distension as a noxious visceral stimulus: physiologic and pharmacologic characterization of pseudaffective reflexes in the rat.* Brain Research, 1988. **450**(1-2): p. 153-169.
187. Ness, TJ and Gebhart, GF, *Visceral pain: a review of experimental studies.* Pain, 1990. **41**(2): p. 167-234.

188. Neuhuber, WL, Sandoz, PA, and Fryscak, T, *The central projections of primary afferent neurons of greater splanchnic and intercostal nerves in the rat.* Anatomy and Embryology, 1986. **174**(1): p. 123-144.
189. Noga, BR, et al., *Locomotor-Activated Neurons of the Cat. I. Serotonergic Innervation and Co-Localization of 5-HT7, 5-HT2A, and 5-HT1A Receptors in the Thoraco-Lumbar Spinal Cord.* J Neurophysiol, 2009. **102**(3): p. 1560-1576.
190. O'dowd, DK, Ribera, AB, and Spitzer, NC, *Development of voltage-dependent calcium, sodium, and potassium currents in Xenopus spinal neurons.* J. Neurosci., 1988. **8**(3): p. 792-805.
191. Ootsuka, Y, et al., *Dopamine D2 receptor stimulation inhibits cold-initiated thermogenesis in brown adipose tissue in conscious rats.* Neuroscience, 2007. **147**(1): p. 127-135.
192. Paulus, W and Trenkwalder, C, *Less is more: pathophysiology of dopaminergic-therapy-related augmentation in restless legs syndrome.* The Lancet Neurology, 2006. **5**(10): p. 878-886.
193. Pertovaara, A, *Antinociception induced by alpha-2-adrenoceptor agonists, with special emphasis on medetomidine studies.* Progress in Neurobiology, 1993. **40**(6): p. 691-709.
194. Petras, JM and Cummings, JF, *Autonomic neurons in the spinal cord of the rhesus monkey: A correlation of the findings of cytoarchitectonics and sympathectomy with fiber degeneration following dorsal rhizotomy.* The Journal of Comparative Neurology, 1972. **146**(2): p. 189-218.
195. Phelps, PE, et al., *Postnatal development of neurons containing choline acetyltransferase in rat spinal cord: An immunocytochemical study.* The Journal of Comparative Neurology, 1984. **229**(3): p. 347-361.
196. Phelps, PE, Barber, RP, and Vaughn, JE, *Embryonic development of rat sympathetic preganglionic neurons: Possible migratory substrates.* The Journal of Comparative Neurology, 1993. **330**(1): p. 1-14.
197. Pickering, AE, Spanswick, D, and Logan, SD, *Whole-cell recordings from sympathetic preganglionic neurons in rat spinal cord slices.* Neuroscience Letters, 1991. **130**(2): p. 237-242.
198. Pickering, AE, Spanswick, D, and Logan, SD, *5-Hydoxytryptamine evokes depolarizations and membrane potential oscillations in rat sympathetic preganglionic neurones.* The Journal of Physiology, 1994. **480**(Pt 1): p. 109-121.
199. Pierce, ML, Deuchars, J, and Deuchars, SA, *Spontaneous rhythmogenic capabilities of sympathetic neuronal assemblies in the rat spinal cord slice.* Neuroscience. **170**(3): p. 827-838.
200. Polosa, C, *THE SILENT PERIOD OF SYMPATHETIC PREGANGLIONIC NEURONS.* Canadian Journal of Physiology and Pharmacology, 1967. **45**(6): p. 1033-1045.
201. Pomeranz, B, Wall, PD, and Weber, WV, *Cord cells responding to fine myelinated afferents from viscera, muscle and skin.* The Journal of Physiology, 1968. **199**(3): p. 511-532.
202. Poulat, P, et al., *5-Hydroxytryptamine, substance P and thyrotropin-releasing hormone synapses in the intermediolateral cell column of the rat thoracic spinal cord.* Neuroscience Letters, 1992. **136**(1): p. 19-22.

203. Purves, D, et al., *Relation of animal size to convergence, divergence, and neuronal number in peripheral sympathetic pathways.* The Journal of Neuroscience, 1986. **6**(1): p. 158-163.
204. Pyner, S and Coote, JH, *A comparison between the adult rat and neonate rat of the architecture of sympathetic preganglionic neurones projecting to the superior cervical ganglion, stellate ganglion and adrenal medulla.* Journal of the Autonomic Nervous System, 1994. **48**(2): p. 153-166.
205. Qu, S, et al., *Projections of diencephalic dopamine neurons into the spinal cord in mice.* Experimental Brain Research, 2006. **168**(1): p. 152-156.
206. Quevedo, J, Calvo, J, and Hochman, S, *Monoamine transmitters adjust actions of muscle and cutaneous afferents via modulation of presynaptic inhibition in the mouse spinal cord* In Review, Journal of Neuroscience, 2011.
207. Quevedo, J, et al., *Raphe magnus and reticulospinal actions on primary afferent depolarization of group I muscle afferents in the cat.* The Journal of Physiology, 1995. **482**(Pt 3): p. 623-640.
208. Quigg, M, Elfvin, L-G, and Aldskogius, H, *Anterograde transsynaptic transport of WGA-HRP from spinal afferents to postganglionic sympathetic cells of the stellate ganglion of the guinea pig.* Brain Research, 1990. **518**(1-2): p. 173-178.
209. Rall, W, *Time Constants and Electrotonic Length of Membrane Cylinders and Neurons.* 1969. **9**(12): p. 1483-1508.
210. Rando, TA, Bowers, CW, and Zigmond, RE, *Localization of neurons in the rat spinal cord which project to the superior cervical ganglion.* The Journal of Comparative Neurology, 1981. **196**(1): p. 73-83.
211. Rekling, JC, et al., *Synaptic Control of Motoneuronal Excitability.* Physiol. Rev., 2000. **80**(2): p. 767-852.
212. Richter, DW, et al., *Presynaptic depolarization in myelinated vagal afferent fibres terminating in the nucleus of the tractus solitarius in the cat.* Pflügers Archiv European Journal of Physiology, 1986. **406**(1): p. 12-19.
213. Riddell, JS, Jankowska, E, and Huber, J, *Organization of neuronal systems mediating presynaptic inhibition of group II muscle afferents in the cat.* The Journal of Physiology, 1995. **483**(Pt 2): p. 443-460.
214. Ridet, J-L, et al., *Spinal dopaminergic system of the rat: light and electron microscopic study using an antiserum against dopamine, with particular emphasis on synaptic incidence.* Brain Research, 1992. **598**(1-2): p. 233-241.
215. Roerig, SC and Howse, KM, *[omega]-Agatoxin IVA blocks spinal morphine/clonidine antinociceptive synergism.* European Journal of Pharmacology, 1996. **314**(3): p. 293-300.
216. Ross, CA, et al., *Adrenaline neurons in the rostral ventrolateral medulla innervate thoracic spinal cord: A combined immunocytochemical and retrograde transport demonstration.* Neuroscience Letters, 1981. **25**(3): p. 257-262.
217. Rudomin, P, *Presynaptic inhibition induced by vagal afferent volleys.* Journal of Neurophysiology, 1967. **30**(5): p. 964-981.
218. Rudomin, P, *Excitability changes of superior laryngeal, vagal and depressor afferent terminals produced by stimulation of the solitary tract nucleus.* Experimental Brain Research, 1968. **6**(2): p. 156-170.

219. Rudomin, P and Schmidt, RF, *Presynaptic inhibition in the vertebrate spinal cord revisited.* Experimental Brain Research, 1999. **129**(1): p. 1-37.
220. Sah, P and Mclachlan, EM, *Membrane properties and synaptic potentials in rat sympathetic preganglionic neurons studied in horizontal spinal cord slices in vitro.* Journal of the Autonomic Nervous System, 1995. **53**(1): p. 1-15.
221. Sandkühler, J, et al., *Low-Frequency Stimulation of Afferent Aδ-Fibers Induces Long-Term Depression at Primary Afferent Synapses with Substantia Gelatinosa Neurons in the Rat.* The Journal of Neuroscience, 1997. **17**(16): p. 6483-6491.
222. Sapru, HN, Gonzalez, ER, and Krieger, AJ, *Greater splanchnic nerve activity in the rat.* Brain Research Bulletin, 1982. **8**(3): p. 267-272.
223. Schmidt, BJ and Jordan, LM, *The role of serotonin in reflex modulation and locomotor rhythm production in the mammalian spinal cord.* Brain Research Bulletin, 2000. **53**(5): p. 689-710.
224. Schramm, LP and Barton, GN, *Diminished sympathetic silent period in spontaneously hypertensive rats.* American Journal of Physiology - Regulatory, Integrative and Comparative Physiology, 1979. **236**(3): p. R147-R152.
225. Schramm, LP, et al., *Spinal pathways mediating splanchnic sympathetic excitation and sympathetic silent periods in the rat.* Brain Research, 1979. **167**(2): p. 396-401.
226. Sekerli, M, et al., *Estimating action potential thresholds from neuronal time-series: new metrics and evaluation of methodologies.* Biomedical Engineering, IEEE Transactions on, 2004. **51**(9): p. 1665-1672.
227. Selzer, M and Alden Spencer, W, *Convergence of visceral and cutaneous afferent pathways in the lumbar spinal cord.* Brain Research, 1969. **14**(2): p. 331-348.
228. Selzer, M and Spencer, WA, *Interactions between visceral and cutaneous afferents in the spinal cord: Reciprocal primary afferent fiber depolarization.* Brain Research, 1969. **14**(2): p. 349-366.
229. Sengupta, J and Gebhart, GF, *Mechanosensitive afferent fibers in the gastrointestinal and lower urinary tracts*, in *Visceral Pain*, G.F. Gebhart, Editor. 1995, IASP Press: Seattle, WA. p. 75-98.
230. Seybold, V and Elde, R, *Receptor autoradiography in thoracic spinal cord: correlation of neurotransmitter binding sites with sympathoadrenal neurons.* The Journal of Neuroscience, 1984. **4**(10): p. 2533-2542.
231. Shen, E, Wu, SY, and Dun, NJ, *Spontaneous and transmitter-induced rhythmic activity in neonatal rat sympathetic preganglionic neurons in vitro.* J Neurophysiol, 1994. **71**(3): p. 1197-1205.
232. Simon, OR and Schramm, LP, *Spinal superfusion of dopamine excites renal sympathetic nerve activity.* Neuropharmacology, 1983. **22**(3, Part 1): p. 287-293.
233. Skoog, B and Noga, BR, *Dopaminergic control of transmission from group II muscle afferents to spinal neurones in the cat and guinea-pig.* Experimental Brain Research, 1995. **105**(1): p. 39-47.
234. Smith, P, Slotkin, TA, and Mills, E, *Development of sympathetic ganglionic neurotransmission in the neonatal rat. Pre- and postganglionic nerve response to asphyxia and 2-deoxyglucose.* Neuroscience, 1982. **7**(2): p. 501-507.

235. Spanswick, D and Logan, SD, *Spontaneous rhythmic activity in the intermediolateral cell nucleus of the neonate rat thoracolumbar spinal cord in vitro.* Neuroscience, 1990. **39**(2): p. 395-403.
236. Spanswick, D and Logan, SD, *Sympathetic preganglionic neurones in neonatal rat spinal cord in vitro: electrophysiological characteristics and the effects of selective excitatory amino acid receptor agonists.* Brain Research, 1990. **525**(2): p. 181-188.
237. Staley, KJ, Otis, TS, and Mody, I, *Membrane properties of dentate gyrus granule cells: comparison of sharp microelectrode and whole-cell recordings.* J Neurophysiol, 1992. **67**(5): p. 1346-1358.
238. Stanford, IM and Lacey, MG, *Differential Actions of Serotonin, Mediated by 5-HT1Band 5-HT2C Receptors, on GABA-Mediated Synaptic Input to Rat Substantia Nigra Pars Reticulata Neurons In Vitro.* The Journal of Neuroscience, 1996. **16**(23): p. 7566-7573.
239. Stein, RB and Parmiggiani, F, *Optimal motor patterns for activating mammalian muscle.* Brain Research, 1979. **175**(2): p. 372-376.
240. Stéphane Doly, et al., *The 5-HT2A receptor is widely distributed in the rat spinal cord and mainly localized at the plasma membrane of postsynaptic neurons.* The Journal of Comparative Neurology, 2004. **472**(4): p. 496-511.
241. Stéphane Doly, JFM-JBDVMC, *5-HT5A receptor localization in the rat spinal cord suggests a role in nociception and control of pelvic floor musculature.* The Journal of Comparative Neurology, 2004. **476**(4): p. 316-329.
242. Stepien, AE, Tripodi, M, and Arber, S, *Monosynaptic rabies virus reveals premotor network organization and synaptic specificity of cholinergic partition cells.* Neuron, 2010. **68**(3): p. 456-72.
243. Stone, LS, et al., *Differential Distribution of alpha 2A and alpha 2C Adrenergic Receptor Immunoreactivity in the Rat Spinal Cord.* J. Neurosci., 1998. **18**(15): p. 5928-5937.
244. Strack, AM, et al., *Spinal origin of sympathetic preganglionic neurons in the rat.* Brain Research, 1988. **455**(1): p. 187-191.
245. Su, C-K, *Rhythmic sympathetic nerve discharges in an in vitro neonatal rat brain stem-spinal cord preparation.* J Appl Physiol, 1999. **87**(3): p. 1066-1074.
246. Sugiura, Y, Terui, N, and Hosoya, Y, *Difference in distribution of central terminals between visceral and somatic unmyelinated (C) primary afferent fibers.* Journal of Neurophysiology, 1989. **62**(4): p. 834-840.
247. Sugiura, Y, et al., *Quantitative analysis of central terminal projections of visceral and somatic unmyelinated (C) primary afferent fibers in the guinea pig.* The Journal of Comparative Neurology, 1993. **332**(3): p. 315-325.
248. Sugiura, Y and Tonosaki, Y, *Spinal organization of unmyelinated visceral afferent fibers in comparison with somatic afferent fibers*, in *Visceral pain*, G.F. Gebhart, Editor. 1995, IASP Press: Seattle, WA. p. 41-62.
249. Takano, M, Takano, Y, and Yaksh, TL, *Release of calcitonin gene-related peptide (CGRP), substance P (SP), and vasoactive intestinal polypeptide (VIP) from rat spinal cord: Modulation by [alpha]2 agonists.* Peptides. **14**(2): p. 371-378.

250. Tamae, A, et al., *Direct inhibition of substantia gelatinosa neurones in the rat spinal cord by activation of dopamine D2-like receptors.* The Journal of Physiology, 2005. **568**(1): p. 243-253.
251. Tattersall, JE, Cervero, F, and Lumb, BM, *Viscerosomatic neurons in the lower thoracic spinal cord of the cat: excitations and inhibitions evoked by splanchnic and somatic nerve volleys and by stimulation of brain stem nuclei.* Journal of Neurophysiology, 1986. **56**(5): p. 1411-1423.
252. Thaler, J, et al., *Active Suppression of Interneuron Programs within Developing Motor Neurons Revealed by Analysis of Homeodomain Factor HB9.* Neuron, 1999. **23**(4): p. 675-687.
253. Thurbon, D, et al., *Passive Electrical Properties of Ventral Horn Neurons in Rat Spinal Cord Slices.* J Neurophysiol, 1998. **79**(5): p. 2485-2502.
254. Trantham-Davidson, H, et al., *Mechanisms Underlying Differential D1 versus D2 Dopamine Receptor Regulation of Inhibition in Prefrontal Cortex.* The Journal of Neuroscience, 2004. **24**(47): p. 10652-10659.
255. Ursin, R, *Serotonin and sleep.* Sleep Medicine Reviews, 2002. **6**(1): p. 55-67.
256. Van Dijken, H, et al., *Localization of Dopamine D2 Receptor in Rat Spinal Cord Identified with Immunocytochemistry and In Situ Hybridization.* European Journal of Neuroscience, 1996. **8**(3): p. 621-628.
257. Van Wijngaarden, I, Tulp, MTM, and Soudijn, W, *The concept of selectivity in 5-HT receptor research.* European Journal of Pharmacology: Molecular Pharmacology, 1990. **188**(6): p. 301-312.
258. Varro, A, et al., *Calcitonin gene-related peptide in visceral afferent nerve fibres: Quantification by radioimmunoassay and determination of axonal transport rates.* Neuroscience, 1988. **26**(3): p. 927-932.
259. Venda, LL, et al., *[alpha]-Synuclein and dopamine at the crossroads of Parkinson's disease.* Trends in Neurosciences, 2010. **33**(12): p. 559-568.
260. Vera, PL and Nadelhaft, I, *Anatomical evidence for two spinal 'afferent-interneuron-efferent' reflex pathways involved in micturition in the rat: a 'pelvic nerve' reflex pathway and a 'sacrolumbar intersegmental' reflex pathway.* Brain Research, 2000. **883**(1): p. 107-118.
261. Viana, F, Bayliss, DA, and Berger, AJ, *Postnatal changes in rat hypoglossal motoneuron membrane properties.* Neuroscience, 1994. **59**(1): p. 131-148.
262. Wallis, DI, *5-HT receptors involved in initiation or modulation of motor patterns: Opportunities for drug development.* Trends in Pharmacological Sciences, 1994. **15**(8): p. 288-292.
263. Walmsley, B, Graham, B, and Nicol, MJ, *Serial E-M and simulation study of presynaptic inhibition along a group Ia collateral in the spinal cord.* Journal of Neurophysiology, 1995. **74**(2): p. 616-623.
264. Wang, C, et al., *Clonidine Has Comparable Effects on Spontaneous Sympathetic Activity and Afferent A[delta]- and C-Fiber-mediated Somatosympathetic Reflexes in Dogs.* Anesthesiology, 1994. **81**(3): p. 710-717.
265. Wei, ZY, Karim, F, and Roerig, SC, *Spinal morphine/clonidine antinociceptive synergism: involvement of G proteins and N-type voltage-dependent calcium channels.* Journal of Pharmacology and Experimental Therapeutics, 1996. **278**(3): p. 1392-407.

266. Westlund, KN, et al., *Noradrenergic projections to the spinal cord of the rat.* Brain Research, 1983. **263**(1): p. 15-31.
267. Wichterle, H, et al., *Directed Differentiation of Embryonic Stem Cells into Motor Neurons.* Cell, 2002. **110**(3): p. 385-397.
268. Willis Jr, WD, *Dorsal root potentials and dorsal root reflexes: a double-edged sword.* Experimental Brain Research, 1999. **124**(4): p. 395-421.
269. Wilson, JM, et al., *Conditional Rhythmicity of Ventral Spinal Interneurons Defined by Expression of the Hb9 Homeodomain Protein.* J. Neurosci., 2005. **25**(24): p. 5710-5719.
270. Wilson, JMM, et al., *Active and passive membrane properties of rat sympathetic preganglionic neurones innervating the adrenal medulla.* J Physiol, 2002. **545**(3): p. 945-960.
271. Wu, H-C, et al., *Dopaminergic D2 receptors activate PKA to inhibit spinal pelvic-urethra reflex in rats.* American Journal of Physiology - Renal Physiology, 2010. **299**(3): p. F681-F686.
272. Yamamoto, S, Araki, K, and Kikuchi, M, *Abdominal muscle reflexes of pelvic nerve origin in cats.* Experimental Neurology, 1961. **4**(4): p. 345-357.
273. Yoshimura, M and Nishi, S, *Intracellular recordings from lateral horn cells of the spinal cord in vitro.* Journal of the Autonomic Nervous System, 1982. **6**(1): p. 5-11.
274. Yoshimura, M, Polosa, C, and Nishi, S, *Afterhyperpolarization mechanisms in cat sympathetic preganglionic neuron in vitro.* J Neurophysiol, 1986. **55**(6): p. 1234-1246.
275. Yoshimura, M, Polosa, C, and Nishi, S, *Noradrenaline-induced afterdepolarization in cat sympathetic preganglionic neurons in vitro.* J Neurophysiol, 1987. **57**(5): p. 1314-1324.
276. Yoshimura, M, Polosa, C, and Nishi, S, *Noradrenaline induces rhythmic bursting in sympathetic preganglionic neurons.* Brain Research, 1987. **420**(1): p. 147-151.
277. Yoshimura, M, Polosa, C, and Nishi, S, *Slow EPSP and the depolarizing action of noradrenaline on sympathetic preganglionic neurons.* Brain Research, 1987. **414**(1): p. 138-142.
278. Yoshimura, M, Polosa, C, and Nishi, S, *Slow IPSP and the noradrenaline-induced inhibition of the cat sympathetic preganglionic neuron in vitro.* Brain Research, 1987. **419**(1-2): p. 383-386.
279. Zhang, Y-Q, et al., *The role of 5-hydroxytryptamine1A and 5-hydroxytryptamine1B receptors in modulating spinal nociceptive transmission in normal and carrageenan-injected rats.* Pain, 2001. **92**(1-2): p. 201-211.
280. Zheng, P, et al., *Opposite modulation of cortical N-methyl--aspartate receptor-mediated responses by low and high concentrations of dopamine.* Neuroscience, 1999. **91**(2): p. 527-535.
281. Zhu, H, et al., *Expression and distribution of all dopamine receptor subtypes (D1-D5) in the mouse lumbar spinal cord: A real-time polymerase chain reaction and non-autoradiographic in situ hybridization study.* Neuroscience, 2007. **149**(4): p. 885-897.
282. Zimmerman, AL and Hochman, S, *Heterogeneity of membrane properties in sympathetic preganglionic neurons of neonatal mice: Evidence of four*

subpopulations in the intermediolateral nucleus. Journal of Neurophysiology, 2009.